Title
Characterization of Biological Effects of Computed Tomography by Assessing the DNA Damage Response

Author
Elgart, Shona Robin

Publication Date
2014

Peer reviewed|Thesis/dissertation

UNIVERSITY OF CALIFORNIA

Los Angeles

Characterization of Biological Effects of Computed Tomography by Assessing the DNA Damage Response

A dissertation submitted in partial satisfaction of the requirements for the degree Doctor of Philosophy in Biomedical Physics

by

Shona Robin Elgart

2014

ABSTRACT OF THE DISSERTATION

Characterization of Biological Effects
of Computed Tomography by Assessing the
DNA Damage Response

By

Shona Robin Elgart
Doctor of Philosophy in Biomedical Physics
University of California, Los Angeles, 2014
Professor Michael McNitt-Gray

The purpose of this work is to characterize the biological response of clinically relevant low doses of ionizing radiation (IR) to inform risk assessment for diagnostic radiographic procedures. Computed tomography (CT) exams provide a non-invasive, fast and extremely detailed diagnostic tool for physicians. Despite the immense impact diagnostic radiology has had on the advancement of healthcare, recent incidents and retrospective studies have focused attention on radiation dose and potential risks from diagnostic exams, especially CT. Because CT exams are often necessary and very commonly employed to provide standard and life-saving medical care, it is crucial to understand the potential risks and avoid adverse health effects. As current risk estimate are based on population statistics and the “average patient” is rarely average, determining the risk for an individual scenario based on specific patient parameters could revolutionize diagnostic medicine. The lack of scientific evidence for specific biological

mechanisms in response to low doses of IR makes even defining risk particularly imprecise. Furthermore, the relationship between physical and biological dose following IR is especially unclear for low dose modalities such as CT. Due to the dynamic nature of cellular damage repair, it is clear that accurate and reproducible kinetic analysis is essential to properly assess the gammaH2AX response. For this reason, this work focuses on 1) developing and evaluating a technique to be applied to kinetic analysis of DNA damage in patient blood samples for clinical application, 2) investigating the differences in DNA damage repair kinetics between dose levels and the effects of short-interval fractionated low-dose irradiation schemes on phosphorylation of H2AX, and 3) applying the previously developed technique to characterize the response to CT examinations in patients.

It is important to control variables which may have unrelated and unintended effects on biological endpoints. Standard procedures of blood sample collection followed by ill-defined storage at room temperature or on ice before laboratory analysis is suboptimal when analyzing highly dynamic systems such as the DNA damage response. The developed rapid fixation protocol that uses immediate exposure to formaldehyde after treatment was superior to the standard practice for isolation and fixation of whole blood as well as cell culture samples. Comparison of different sample handling protocols indicates that whole blood samples are especially sensitive to changes in their environment.

Dose-response kinetics to IR were established in both cultured and whole blood human lymphocytes. The biological response to IR was measured by immunofluorescent analysis of gammaH2AX by flow cytometry at different time points To understand the response to doses from CT exams fractionated exposures were employed. Both the kinetics and extent of H2AX

phosphorylation appear to be dose-dependent. For the first time, differences in DNA repair kinetics of both cultured and whole blood lymphocytes are characterized. Moreover, using a modified split-dose *in vitro* experiment, it is shown that phosphorylation of H2AX is significantly reduced following exposure to CT doses fractionated over a few minutes compared to the same total dose delivered as a single exposure. The possibility of an altered H2AX phosphorylation response to split-dose irradiations could have marked implications for current diagnostic procedures and thus underscores the importance of understanding how imaging protocols may affect the biological response in order to accurately assess risk estimates and biological dose. Though the consequences on late effects and other related risks are unclear, these findings suggest that risk may be a function of not only total dose delivered, but also other contributing factors such as scan and patient parameters.

Here, the complexity of the biological response to a variety of CT protocols and the relation to patient and CT exam parameters is described. Blood from 21 adult patients undergoing clinically-indicated CT exams was analyzed to assess the effects of CTs *in vivo*. Varying biological responses are observed after irradiation. While no clear dose response is evident, three distinct biological responses to CT examinations: fast, slow and none are suggested. Additionally, age and average dose-rate are significant factors in the biological response. Interestingly, *ex vivo* and *in vivo* samples differ in biological response to CT exams. These effects suggests distinct DNA damage responses depending on exam conditions that may not necessarily be reflected solely by dose metrics like dose length product (DLP) or CT dose index (CTDI) which only quantify scanner output. Even though this study only had a small population size, two patients were identified who exhibited aberrant responses compared to

the rest of the population indicating that this application could provide a useful tool to identify putative radiation sensitive individuals who may require further testing to ensure the least risk to the patient.

This work provides compelling evidence supporting differential biological responses not only between high and low doses, but also between single and multiple exposures of low doses of ionizing radiation. Moreover, individual patient factors may further modulate the response to radiographic procedures. Although the radio-protector experiments provide some interesting insight into the possible mechanisms by which these responses are controlled, it is clear that this work has instigated more questions than it has answered. Future work needs to further probe the responsible mechanisms involved in the damage response at different dose levels and schemes as well as those involved in carcinogenesis and other late effects. In addition to understanding the response at a cellular level, it is imperative to also examine the systemic response as well as how repeated exposures over an individual's lifetime may affect lifetime risk. Once it is possible to integrate both cellular and systemic knowledge then it may be possible to accurately forecast individual risk.

The dissertation of Shona Robin Elgart is approved.

William McBride

Stephen Smale

Keisuke S. Iwamoto

Michael McNitt-Gray, Committee Chair

University of California, Los Angeles

2014

This work is dedicated to Zachary,

for never doubting me,

even when I did.

Table of Contents

List of Figures and Tables

Acknowledgements

The work included in this dissertation was possible because of the generosity of others. Much of this work would have been impossible without the immortalized wild-type human lymphocyte cell line, ESW-WT3 provided by Dr. Richard Gatti and the excellent discussions we have had over the years. Acquisition of blood from healthy donors was only made possible by the willingness of Dr. Andrew Saxon to help and donate his expertise. Acquiring patient samples was only possible thanks to the incredible UCLA Radiology staff including the CT technologists and nurses. I am forever your debt for allowing us to intrude upon your already busy schedule. And thank you to the patients who gave us part of themselves in the name of science.

My committee, especially my co-chairs Dr. Iwamoto and Dr. McNitt-Gray, has been an invaluable resource. They have guided me to success but have also let me fail which I now understand to be just as important. They have pushed me to discover my limits, academically and personally, and when I got there, they pushed me further. Thank you for teaching me how to question the world around me.

Life as a graduate student is similar to what I image being addicted to methamphetamines is like. There are brief (very brief) moments of unbelievable highs when something works and then the rest of your time is spend scrambling in destitution for your next fix, because most things don't work the way you planned. Fortunately, research doesn't come with most of the pitfalls of drug addiction, but similarly, to get through it, I needed a support system. I have been extremely fortunate to be surrounded by not only highly intelligent people but also the most caring. Dorthë, Ewa, and Josephine always made time to answer my never ending questions and your companionship has been a light down in the depths of CHS and

Factor. Terry Moore, the rock of the Biomedical Physics IDP, is many things to me: a mentor, a friend, a mother and a coach. You gave me strength when I was weak, hope when I was lost, hugs when I was sad, and hi-fives when I was proud. My life is brighter and the world is a better place having you in it. It has been my pleasure to know all of the students within and without BMP that I have shared this time with. I couldn't have asked for a better group of scientists to share my first year with: Meral, Maryam, Matt and Gilmer. I owe you so much for helping me through our classes and for your friendship, which has meant more to me than you know. I owe a sincere thank you to Graham Cole, who I consider to be my big brother. If I had a problem – big or small – you'd fix it, or nearly die trying.

Sometimes people come into your life and when you think back to before you knew them, it doesn't seem to make any sense. They've made such an impact on you that they must have always been there. The Pusey-Martins are these kind of people. Nate, Ciara, Brit and Drew, there are no word to describe how much you all mean to me. I can't imagine what these past six years would have been like without your friendship. You make bad times good and good times better.

My family has been a great source of strength for me and for that I am eternally grateful. Without the constant haranguing of my Auntie Shona, I would have never become interested in medical physics in the first place. So you can all blame her for bringing me into your lives. My moms – biological and otherwise – never stopped telling me I could when I thought I couldn't. And to my dad, thank you for knowing what to say when it really mattered. Thank you for sharing your wisdom and understanding and for being proud of me.

Lastly, I owe everything to my husband, Zachary. Your unflagging faith in me has been the most important brick in my foundation. Without you I would crumble. With you I am strong. You make me my best self and help me at my worst.

Chapter four is a version of "Evaluation of a rapid protocol for time sensitive kinetic assessment of DNA damage response following ionization radiation using whole blood samples," by Shona Robin Elgart, A. Adibi, M. Bostani, S. Ruehm, D. Enzmann, M. McNitt-Gray and K. S. Iwamoto currently under review in BMC Clinical Pathology.

Chapter five is a version of "Investigation of DNA damage dose-response kinetics after ionizing radiation schemes similar to CT protocols," by Shona Robin Elgart, M. Bostani, K. C. Mok, A. Adibi, S. Ruehm, D. Enzmann, M. McNitt-Gray and K. S. Iwamoto currently under review in Radiation Research.

Chapter six is based on a manuscript in progress by Shona Robin Elgart, A. Adibi, M. Bostani, S. Ruehm, D. Enzmann, M. McNitt-Gray and K. S. Iwamoto entitled, "Characterizing in vivo biological response of individual patients to ionizing radiation from CT Scans: it's not the size of the dose that matters; it's how you use it."

This work was supported by Siemens Healthcare through the Master Research Agreement with UCLA Radiological Sciences.

Vita

Shona Robin Elgart attended Santa Monica High School, California. In 2002 she entered the University of California at Santa Barbara, and graduated with highest honors with a Bachelor of Science degree in Microbiology emphasizing in Genetic Engineering in June 2006. In September 2008, she was started the Biomedical Physics Interdepartmental Program at the University of California at Los Angeles. In October 2010, she received the degree of Master of Science from the University of California at Los Angeles in Biomedical Physics. She successfully passed part 1 of the American Board of Radiology Medical Physics board examination in 2012. Robin has presented research findings at eight scientific conferences and submitted two original manuscripts to peer-reviewed journals. In 2013, she was awarded a Dissertation Year Fellowship from UCLA's Graduate Division.

Chapter 1: Introduction

It is no secret that the number of prescribed computed tomography (CT) protocols has increased dramatically since their introduction in the 1970s. CTs provide a non-invasive, fast and extremely detailed diagnostic tool for physicians. From 1980 to 2006 the number of CT examinations exploded, and their contribution to the population's radiation dose more than doubled, (**Figure 1.1**) (1). Despite the immense impact diagnostic radiology has had on the

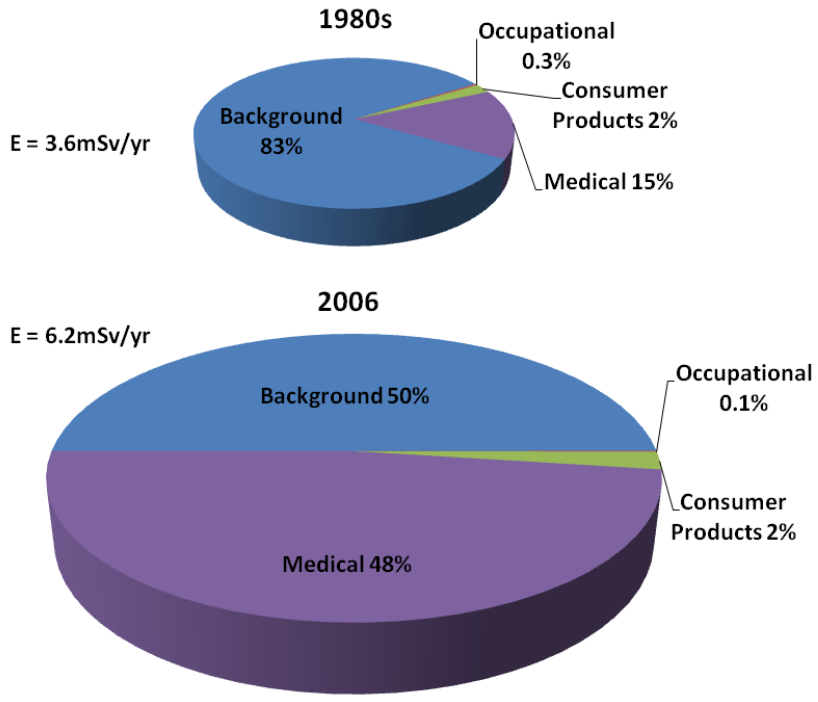

Figure1.1. Population ionizing radiation (IR) exposure of the United States from NCRP report 160. Included sources of IR are attributable to background, occupational, consumer products and medical exposures. Total effective dose (E) from all sources per individual is presented with the percentage each source contributes to the total. The major contributor to increased population dose from 1980 to 2006 was dose from medical examinations. Adapted from NCPR report 160.

advancement of healthcare (2), recent incidents and retrospective studies have focused attention on radiation dose and potential risks from diagnostic exams, especially CT (3-7). Over the last decade the debate over the safety of CT has played out like a poorly-watched soap opera. Public fear is fueled by a mix of tragic incidences (6), scientific reports on the mass loss

of life which CT exams will inevitably cause (3, 5, 7), media sensationalism and the appearance that the scientific community has no understanding of the long term effects of routine medical examinations. The root of the problem lies with the lack of empirical evidence showing a direct link to increased cancer incidence and mortality after CT examinations. Because CT exams are often necessary and very commonly employed to provide standard and life-saving medical care, it is crucial to understand the potential risks and avoid adverse health effects. Protection standards, designed using a Linear No-Threshold (LNT) model, aim to ensure conservative risk estimates for individuals exposed to ionizing radiation (IR) (8). These estimates were defined primarily using the Life Span Study (LSS) of atomic bomb survivors in Japan which contains a large cohort that received IR doses in the 5-150mSv range. Although these doses are within the range of typical CT scans (9), the doses are not delivered in the same manner. Individuals in the LSS received whole body doses that were delivered relatively homogeneously in a single exposure which may not accurately reflect or describe the risks of protocols typically encountered in diagnostic radiology procedures. CT, by its very nature, exposes patients heterogeneously, typically over multiple exposures in a short time period. Though the consequences on late effects and other related risks are unclear, making direct assumptions from the LSS may not prove as useful as previously thought (4). Furthermore, the uncertainties associated with the low-dose risk estimates remain large.

Risk reduction is a major focus of medical imaging research. As risk estimates are based on a no threshold model, current methods to reduce risk primarily concentrate on the reduction of scan and exam dose. Radiologic techniques that require IR, such as CT, walk a line between achieving acceptable diagnostic image quality and lowering dose. Better quality

images require more photons and thus more dose to the patient and limiting the dose will degrade image quality. While the development of automatic tube current modulation (or automated exposure control – AEC) (10), automated tube potential selection (11) and iterative reconstruction techniques (12) have promised significant decreases in scan dose while retaining diagnostic image quality, these techniques are widely underused in the radiology community (13). The use of magnetic resonance imaging (MRI), when applicable, can also be used to decrease radiation dose. MRI is considered to be a safer option because it does not expose patients to IR, however not all exams can be recreated with MRI due to imaging or logistical reasons.

The interest in using biological markers for clinical diagnostics is growing. The emergence of medical treatments based on individual genetics has spawned an age of personalized medicine. Because current risk estimate are based on population statistics and the "average patient" is rarely average, determining the risk for an individual scenario based on specific patient parameters could revolutionize diagnostic medicine. However, unlike radiation therapy, where specific deterministic effects have been characterized (14), the lack of scientific evidence for specific biological mechanisms in response to low doses of IR makes even defining risk particularly imprecise. Furthermore, the relationship between physical and biological dose following IR is especially unclear for low dose modalities such as CT (15-18). It is essential to define the biological mechanisms of damage and repair of low doses of IR to assess its risks and avoid potential adverse health effects. Characterization of biological changes resulting from doses of radiation in the range of CT protocols is often limited to a few, if not a single, time point evaluated for gammaH2AX foci by fluorescent microscopy. Although H2AX

phosphorylation is an attractive marker for DNA double strand breaks (DSB) it is only surrogate marker and detects an early step in the DNA damage response. Even so, evaluation of gammaH2AX foci is quickly becoming the standard method to describe the biological response to a variety of external forces; however, sample handling practices often vary or are unreported, offering little standardization not only between studies but also between samples. Recently, it has been suggested that magnetic resonance imaging (MRI) may induce the formation of gammaH2AX foci (19) and thus, the safety of MRI has been thrown into question. However, these studies may be interpreting the effects of sample handling as biological effects of MRI. Due to the dynamic nature of cellular damage repair, it is clear that accurate and reproducible kinetic analysis is essential to properly assess the gammaH2AX response. For this reason, this work focuses on 1) developing and evaluating a technique to be applied to kinetic analysis of DNA damage in patient blood samples for clinical application, 2) investigating the differences in DNA damage repair kinetics between dose levels and the effects of short-interval fractionated low-dose irradiation schemes on phosphorylation of gammaH2AX, and 3) applying the previously developed technique to characterize the response to CT examinations in patients.

The purpose of this study is to characterize the biological response of clinically relevant low doses of ionizing radiation to inform risk assessment for diagnostic radiographic procedures.

1.1 Specific Research Aim 1: Develop a rapid and accurate handing and fixation protocol for *in vivo* and *in vitro* experiments

In this aim it is hypothesized that development of a rapid fixation protocol will allow for precise kinetic assessment of biological markers of DNA damage even at very short time-points. Sample handling prior to fixation will be minimized to achieve analysis as close to physiological conditions as possible, especially for patient blood analysis. The developed protocol will be compared to standard handling and fixation practices and the DNA damage kinetics following different sample handling practices is compared by flow cytometry analysis of H2AX phosphorylation after ionizing radiation exposure. From this analysis, damage kinetics will be established to provide guidance for further *in vitro* and *in vivo* experiments.

1.2 Specific Research Aim 2: Characterize the effects of CT-relevant doses and protocols on cellular radiation response *in vitro* using immortalized human lymphocytes

In this aim it is hypothesized that low doses of IR and dosing schemes that mimic CT exam protocols will alter the biological response to IR compared to higher doses or single exposure irradiations. Baseline dose-response kinetics for the DNA damage response are defined for both cultured and whole blood lymphocytes for a range of doses covering the low (relevant to CT protocols) and high dose spectrum by H2AX phosphorylation analysis. Temporal differences in RNA expression between low and high doses are characterized in cultured lymphocytes by whole genome shotgun sequencing (RNASeq). The effects of multi-pass clinical CT protocols on the DNA damage response are probed by exposing cultured lymphocytes to 20mGy fractionated exposures separated by two minutes or single exposures of the equivalent

total dose. The effects of pre and post-exposure to radio-protectors on the cellular radiation response are examined.

1.3 Specific Research Aim 3: Describe the effects of CT protocols on whole blood patient samples and compare the cellular radiation response between *in vivo* and *ex vivo* conditions

In this aim it is hypothesized that the previously developed protocol can be used to successfully illustrate the complexity of the biological response to a variety of CT protocols and its relation to patient and CT exam parameters. Instead of examining DNA repair at a single point in time, which is common, short-term kinetics are evaluated to better understand the effects of exam and patient parameters on the biological response to CT examinations.

1.4 Definitions

For the purposes of this work we define the following:

Low dose – radiation doses below 150mGy or mSv

CT scan or scan: a single exposure or pass of an anatomical region during a CT exam.

CT exam or exam: a complete CT study that may contain multiple CT scans.

1.5 Significance

Individualized biological dosimetry is an intriguing possibility to improve dose estimates and risk assessment as well as allow for personalized and evidence-based medical care and longitudinal dose tracking. Unfortunately, in the low dose range, assay sensitivity must be extremely high to distinguish any changes that may occur. Development of a sensitive and accurate assay to analyze the biological response at low doses of IR for clinical application will not only advance the understanding of the consequences of diagnostic radiological procedures but also has the potential to improve patient care. Radiation damage analysis techniques for

low doses rely heavily on fluorescent microscopy which is not only labor intensive but also time consuming. Coupling rapid fixation with flow cytometry offers accurate timing and a more streamline protocol which is essential for clinical applications. Furthermore, due to its rapid analysis, flow cytometry offers the opportunity to examine multiple time points to assess kinetic variation at low dose levels. While others have investigated gammaH2AX under similar circumstance, many have used techniques which question the validity of results (20). Without the need for blood separation, our protocol allows for virtually immediate fixation of patient samples and thus precise kinetic analysis of the damage response. Understanding the biological response at low dose levels will create a deeper appreciation of the unique risks involved in diagnostic radiology procedures, better characterize the possible role of external agents in protection against radiation damage and offer a more thorough understanding of the safety for diagnostic radiology.

1.6 References

1. Thurston J. NCRP Report No. 160: Ionizing Radiation Exposure of the Population of the United States. Physics in Medicine and Biology 2010; 55:6327.

2. Amis ES, Butler PF, Applegate KE, et al. American College of Radiology White Paper on Radiation Dose in Medicine. Journal of the American College of Radiology : JACR 2007; 4:272-284.

3. Pearce MS, Salotti JA, Little MP, et al. Radiation exposure from CT scans in childhood and subsequent risk of leukaemia and brain tumours: a retrospective cohort study. The Lancet 2012; 380:499-505.

4. Brenner DJ, Hall EJ. Computed Tomography - An Increasing Source of Radiation Exposure. New England Journal of Medicine 2007; 357:2277-2284.

5. Berrington de Gonzalez A, Darby S. Risk of cancer from diagnostic X-rays: estimates for the UK and 14 other countries. The Lancet 2004; 363:345-351.

6. Smith-Bindman R. Is Computed Tomography Safe? New England Journal of Medicine 2010; 363:1-4.

7. Berrington de Gonzalez A, Mahesh M, Kim K, et al. Projected cancer risks from computed tomographic scans performed in the united states in 2007. Archives of Internal Medicine 2009; 169:2071-2077.

8. Health Risks from Exposure to Low Levels of Ionizing Radiation: BEIR VII Phase 2: The National Academies Press, 2006.

9. What's NEXT? Nationwide Evaluation of X-ray Trends: Computed Tomography 2005 – 06 Preliminary Summary. In: Conference of Radiation Control Program Directors, Inc., U.S. Department of Health and Human Services, 2012.

10. Lee HY, Choi CS, Birkenfeld AL, Alves TC, Jornayvaz FR, Jurczak MJ. Targeted expression of catalase to mitochondria prevents age-associated reductions in mitochondrial function and insulin resistance. Cell Metab 2010; 12:668-674.

11. Gnannt R, Winklehner A, Eberli D, Knuth A, Frauenfelder T, Alkadhi H. Automated tube potential selection for standard chest and abdominal CT in follow-up patients with testicular cancer: comparison with fixed tube potential. European Radiology 2012; 22:1937-1945.

12. Xu J, Mahesh M, Tsui BMW. Is Iterative Reconstruction Ready for MDCT? Journal of the American College of Radiology : JACR 2009; 6:274-276.

13. Raman SP, Johnson PT, Deshmukh S, Mahesh M, Grant KL, Fishman EK. CT Dose Reduction Applications: Available Tools on the Latest Generation of CT Scanners. Journal of the American College of Radiology : JACR 2013; 10:37-41.

14. Hall EJ, Giaccia AJ. Radiobiology for the Radiologist. Philidelphia, PA USA: Lippincott Williams & Wilkins, 2006.

15. Geisel D, Zimmermann E, Rief M, et al. DNA double-strand breaks as potential indicators for the biological effects of ionising radiation exposure from cardiac CT and conventional coronary angiography: a randomised, controlled study. European Radiology 2012; 22:1641-1650.

16. Brand M, Sommer M, Achenbach S, et al. X-ray induced DNA double-strand breaks in coronary CT angiography: Comparison of sequential, low-pitch helical and high-pitch helical data acquisition. European journal of radiology 2012; 81:e357-e362.

17. Kuefner MA, Hinkmann FM, Alibek S, et al. Reduction of X-Ray Induced DNA Double-Strand Breaks in Blood Lymphocytes During Coronary CT Angiography Using High-Pitch

Spiral Data Acquisition With Prospective ECG-Triggering. Investigative Radiology 2010; 45:182-187 110.1097/RLI.1090b1013e3181d1093eddf.

18. Kuefner MA, Grudzenski S, Hamann J, et al. Effect of CT scan protocols on x-ray-induced DNA double strand breaks in blood lymphocytes of patients undergoing coronary CT angiography. Eur Radiol 2010; 20:2917 - 2924.

19. Fiechter M, Stehli J, Fuchs TA, Dougoud S, Gaemperli O, Kaufmann PA. Impact of cardiac magnetic resonance imaging on human lymphocyte DNA integrity. European Heart Journal 2013.

20. Elgart SR, Bostani M, Adibi A, et al. Evaluation of a rapid protocol for time sensitive kinetic assessment of DNA damage response following ionization radiation using whole blood samples. PLoS ONE: Submitted May 7, 2014.

Chapter 2: Literature Review

2.1 The Development of Risk Estimates from Low-Level Radiation Exposure

In 1972 the National Academy of Science – National Research Council published its first report which reviewed and evaluated epidemiological and laboratory research related to the long term effects of low levels of IR (Biological Effects of Ionizing Radiation – BEIR I) (21). The most recent edition of this report (BEIR VII – phase 2) was released in 2006 (22). These reports are instrumental in defining the scientific foundation of radiation protection standards and the development of public health policy related to low doses of IR. However, since (and even during) their inception, controversy has reined in the health physics community. Because the epidemiological and mechanistic data for low dose IR exposure is minimal and inconclusive, and it would be unethical to conduct full scale Nazi-esque longitudinal studies on human subjects (23), the uncertainties of current risk estimates remain a major hindrance in clearly defining the safe use of low levels of IR, especially in medical diagnostics. Although other data is available to provide a more robust estimation of risks, these studies have been largely dismissed due to their large uncertainties and inconsistencies. Importantly, the scientist who battled over which studies to omit and which sources of uncertainty to include in the 95% subjective confidence interval (22), emphasized the great many assumptions made in their analysis of the relevant and available data. It is these assumptions that continue to fuel the debate over the safety of medical imaging (24). Despite the uncertainties and controversy, risk estimates have been calculated and have become a popular way to generate frightening news for public consumption (25-27).

2.2 Computed Tomography and Medical Radiation Exposure

Exposure to ionizing radiation is unavoidable; it is in the air we breathe, the champagne we drink and the bananas we eat. Beyond everyday background radiation, scientists have developed devices and techniques to utilize IR for medical imaging and treatment. The impact of advancements in radiology on healthcare is clearly seen in the incredible growth in the field and the increase in medical exposure to radiation that has mirrored this development (28). Diagnostic examinations range in effective dose (**Table 2.1**). Effective dose is a sex and age averaged value which describes the approximate whole body dose from a partial body irradiation (29). While the effective dose should not be used to imply specific risk, it is useful to compare the potential risks between radiographic techniques (30). CT doses are relatively high compared to other procedures and new advancements, such as brain perfusion studies are even higher. Doses are now within a range where risk no longer has to be extrapolated from higher dose data (31). However, irradiation schemes for CT exams do not exactly fit with the BEIR VII/LSS model of homogenous whole-body exposure. So, although there is direct epidemiological evidence for increased cancer risk after doses experienced from CT examinations, the effects of CT protocols still remain unclear. A recent large-scale retrospective study of risk related to childhood CT exposure concluded that there exists an age-related increased risk of leukemia and brain tumors following CT exams (32). Despite the limitations of this study, it provides valuable evidence for the risk assessment of children. Similar studies in adult subjects have yet to be undertaken. Further retrospective and prospective studies combined with characterization of the biological response to diagnostic imaging protocols will

aid in defining more robust risk estimates and allow the medical community to objectively reassess the safety of this vitally useful technology.

Table 2.1. Effective Doses for Common Radiographic Techniques	
Examination	**Average Effective Dose (mSv) (30, 33)**
Dental radiography	0.005
Posterior-anterior chest radiography	0.02
Hip radiography	0.1
Mammography	0.4
Routine head CT	2
Routine chest CT	7
Barium enema	8
Virtual colonoscopy	10
Brain perfusion CT	16
Pelvic vein embolization	60

An unfortunate string of incidents involving radiation overexposures due to CT has shown the public and the medical community the dangers of medical imaging with IR (34). These types of incidents are more an indicator of the lack of awareness in the medical community regarding CT and IR (35) rather than a reflection on the dangers of medical radiation exposure. It may be that the public should fear their medical providers rather than the radiation itself. IR has granted the medical community a great power and "with great power there must also come – great responsibility (36)." Increased awareness in both the medical and patient communities, along with standardization, regulation and monitoring is necessary to reduce these errors and increase the safety of CT.

2.3 Biological Dosimetry

The first attempt of any physicist to answer a problem involving a physical object undoubtedly includes the phrase, "assume the object is a sphere," followed by the phrases "infinitesimally small" and "infinitely far away" if the problem involves a beam of radiation

(ionizing or otherwise) (29, 37). Unfortunately, the rest of us do not live in a world made of spheres or beams of light that are emitting isotropically from a point source infinitely far away. The rest of us live on Earth, where humans fail to act like cylinders of water (or water equivalent material), patients get emergency CT examinations and there is the always present fear of imminent nuclear war. Physical dose estimates are vitally important to ensure the safe operation of both therapeutic and diagnostic devices and while these estimates are exquisitely accurate in terms of the physical energy deposited into a unit of mass, the response of that unit of mass or the living breathing being of which it is a part, is not taken into account. Thus, biological – rather than physical – dosimetry has emerged in an effort to supplement dose assessment for both medical exposures and radiation emergencies. A nuclear explosion or any other large-scale radiation emergency requires rapid estimates of exposures in order to triage individuals for appropriate medical care. Analytical systems which require only limited resources and are easily deployable are a necessity (38). In contrast, assessing biological dosimetry for routine medical exposures (for therapeutic or diagnostic purposes) does not require such stringent criteria. However, similar improvements to ease of use and resource requirements will make achieving large-scale monitoring of biological dose more attainable. An important aspect of recording and monitoring individual biological dosimetry is the variation in radiation sensitivity within the population (39). Due to genetic variability, some individuals are more sensitive to IR than others (40) and awareness of personal sensitivity may justify alteration of imaging and treatment strategies to avoid potential health detriment.

2.4 The DNA-Damage Response

Genomes everywhere are under constant attack from physiological and environmental assailants that induce DNA lesions (41). A variety of highly evolved systems – known collectively as the DNA-damage response (DDR) – monitor and maintain genetic material by neutralizing lesions to ensure the biological imperative of transmitting genetic material to future generations. Two primary mechanisms are available for the detection, signaling and repair of double strand breaks (DSBs) – which are considered the most important lesions induced by IR as they are most likely to induce carcinogenesis: non-homologous end joining (NHEJ) (42) and homologous recombination (HR) (43). While NHEJ can be used in all phases of the cell cycle, HR is limited to S or G2 phase when a sister chromatid is available for sequence homology. If both mechanisms are available the choice between which pathway is selected appears to be associated with the complexity of the break (44) and end resection. There is mounting evidence that NHEJ is the first mechanism to attempt repair, but if unsuccessful or suppressed, a switch to HR is made (44). While HR is considered to be error-free repair due to the availability of a template, NHEJ is relatively error-prone. Regardless of pathway, DNA damage is detected by sensor proteins, response mediators are recruited to the damage site, and the damage signal is amplified to transducers and effectors that stimulate a response to the break. Responses range from cell cycle arrest, chromatin remodeling, repair and – if repair is unsuccessful or unachievable – apoptosis (45) or senescence (46).

2.5 gammaH2AX

Core histones make up the protein scaffolding which allows approximately six feet of human DNA to be compacted into the nucleus of a microscopic cell. The variant histone H2AX

makes up approximately 2-20% of the native H2A core histones in humans (47). gammaH2AX is produced over large regions of chromatin flanking a DNA DSB (48) when H2A is rapidly phosphorylated at Serine 139 following induction of a break (49, 50). gammaH2AX promotes the recruitment of necessary DDR factors, ubiquitin-adduct formation and other modifications to chromatin (51). Upon induction of a DSB, a focus forms around the break which includes not only gammaH2AX but other detectable response factors and are readily detectable by antibodies for specific DDR factors. If the break is induced by IR these foci are referred to as ionizing radiation induced foci (IRIF). gammaH2AX IRIF can be detected quickly following IR exposure and increase swiftly to maximum levels then begin to decrease following kinetics consistent with both fast and slow components (52). By using gammaH2AX IRIF detection, it has been established that most breaks are repaired quickly in an ATM-independent fashion (fast component) and approximately 15% of breaks (those with higher chromatin complexity) are repaired more slowly and require both ATM and Artemis (slow component) (53). Foci first appear faint but over time, increase in intensity as H2AX phosphorylation continues if a DSB remains unrepaired (54). Phosphorylation kinetics closely follow those of DNA DSB repair, at least at high doses (52, 55-58). Due to the natural large-scale amplification of signal, detection of gammaH2AX foci has become a popular method to monitor the damage response following exposure to DNA damaging agents. However, while this technique provides both extreme sensitivity and reliability in assessing DDR, there are limitations that must be appreciated, namely analysis of gammaH2AX indirectly measures DSB formation and H2AX phosphorylation does not always correlated with induced DSB formation (59). Provided these limitations are

respected, it is clear that analysis of gammaH2AX IRIF can provide a useful biomarker for DDR following IR even at low doses (54, 60).

2.6 Radio-protection

Different classes of agents which protect and/or mitigate the detrimental effects of IR are currently under investigation mainly to aid in the event of a radiation emergency. However, in light of the increases in medical IR exposure, these agents are being investigated for their efficacy in a clinical setting. Radio-protectors such as antioxidants are attractive agents as they are typically well tolerated and are already used clinically (61, 62). Although antioxidants indicate protection on a cellular level, as measured by gammaH2AX IRIF, survival is unaffected after high doses of IR. However, if the repair machinery is compromised survival is improved with the treatment of an antioxidant following similar doses (63). If an insult of low dose IR promotes a similar environment in terms of the available repair mechanisms to that of repair-deficient conditions, the use of antioxidants may be more applicable to providing protection at low doses of IR. Nevertheless, caution must be taken when implementing the use of anti-oxidant radio-protectors clinically; As ROS may act as a signal for repair pathways, hindering that signal may have detrimental effects on effective repair of DNA damage or cellular function (64-66) and thus may be counterproductive in the prevention injury or disease.

Because radical scavengers are only effective if given before a radiation insult (67), and those that demonstrate the most effective protection have poor toxicity profiles (68), the investigation for better tolerated agents and those that can be administered after a radiation insult (radio-mitigators) continues. Recently, two classes of antibiotics have been discovered to be radio-protective: tetracylines and fluoroquinones (69). Additionally, tetracycline exhibited

both radio-protective and radio-mitigative properties. Investigation into the protective mechanism indicates not a classical radical scavenging action like most protective agents, but rather alteration in chromatin structure. Although inducing the rampant spread of an antibiotic-resistant super-bug within the global population is a possibility, saving as many lives following a WWIII nuclear crisis may have to take precedence. In the meantime, if the action of protection/mitigation can be determined, it could be possible to develop well-tolerated agents that provide robust protection and mitigation but lack the antibiotic properties that would contribute to problematic bacterial resistance.

2.7 Analysis of gammaH2AX in Patients Following CT Studies

In vivo studies show relatively good correlation with *in vitro* results with respect to IRIF formation and initial repair (70, 71). Dose enhancement effects of contrast media also show similar trends between *in vitro* and *in vivo* irradiations (72). There have been reports of low-dose hypersensitivity seen in pediatric cardiac catheterization patients (73) as well as in low-dose exposed areas of radiation therapy patients (74). This corroborating evidence has led many to claim *in vitro* analysis sufficiently predicts *in vivo* radiation response behavior. However, there is conflicting evidence with respect to resolution of DNA damage repair following low doses of IR. *In vitro* studies present a model where damage is repaired to a threshold level which may persist indefinitely (57), whereas *in vivo* studies show little evidence for this phenomenon with spiral CT (75), cardiac CT and conventional coronary angiography (76). Clearly, *in vitro* analysis may not model the *in vivo* radiation response in its entirety. Because approximately 2% of lymphocytes reside within the bloodstream, while the rest are contained within lymphatic tissues any resolution of damage indicated by a reduction in signal

may not relate to repair of DNA DSBs in damaged cells but the result of cells being sequestered out of the peripheral blood stream (77) or committed to senescence (78). This mechanism may partially explain why there is a low level of persistent DSB seen *in vitro* but not *in vivo*. The persistence of conflicting evidence indicates that a more thorough understanding is necessary to accurately estimate biological dose with biomarkers like gammaH2AX.

Lobrich *et al.* were able to uncover a radiation sensitive patient within their patient cohort who previously responded poorly to radiation therapy (75). Although, it would be difficult to identify every radiation sensitive patient, an analysis technique which could indicate potential increased radiation sensitivity in patients would be valuable for assessing personal excess radiation risk and biological dose. Genetically determined radiation sensitive patients exist as two populations: homozygotes, the most radiation sensitive, and heterozygotes typically have intermediate radiation sensitivity as one gene encodes functional protein. The homozygote population is relatively easy to distinguish due to hallmark symptomatic disorders that result (40). However, the heterozygote population is typically unknown due to the lack of symptoms and makes up a larger portion of the population. Furthermore, radiation sensitivity is expected to vary between individuals in the “non-radiation sensitive” population. Determining individual patient radiation sensitivity will promote more evidenced-based medicine and provide a way to prevent harmful levels of exposure.

2.8 RNASeq

IR induces changes in gene expression and protein levels. Traditionally, microarray technologies have been used to assess these changes (79). A large panel of genes can be profiled efficiently; however, the number of genes assessed is finite and requires prior

knowledge of sequence information and specific probe selection. Until recently, high throughput RNA sequencing was infeasible due to limitations in sequencing technology and prohibitive cost. RNA sequencing has the distinct advantage of profiling all mRNA transcripts that are present in cells without sequence information a priori. Thus, it is possible to analyze global changes in gene expression with whole transcriptome shotgun sequencing (RNASeq) with great sensitivity. Analysis of transcriptional changes following low doses or IR has been performed with traditional microarray methods but no data has been published using RNASeq for transcriptome analysis following low or high doses of IR. Because the mechanism(s) that may be activated after low doses of IR are still unclear, it is possible that genes currently not thought of as typical radiation response genes are activated or suppressed. Thus, analysis that does not require prior knowledge of sequence or gene activation and examines the global transcriptome would be advantageous. RNASeq also offers very high sensitivity to low transcript levels which could be necessary for examining the transcriptional response to low doses of IR. Microarray studies indicate that there are changes in the transcriptome following low doses of IR and these changes differ from those at high doses. Different genes within the same DNA damage response pathways are regulated at low doses compared to high doses and although the same genes may be regulated they may be regulated differentially and thus alter the kinetic response to radiation (80). Interestingly, at low doses the major ATM dependent pathway seems to be only transiently activated, if at all. However, a novel pathway involving a chromatin modifying complex has been identified to respond to both low and high doses (80).

2.9 Overall Summary and Conclusions

It is taken for granted that the biological response to lower doses of IR will mimic that of higher doses. Without an evidenced-based model for low-dose radiation sensitivity however, a description of the biological response to low dose IR will continue to be circumstantial and phenomenological. This work will provide substantial data to support a kinetic-based model for radiation sensitivity to allow for a more evidence-based medical approach. Implementation of a whole blood protocol coupled with optimized flow cytometry analysis could make personalized excess risk assessment a reality. Additionally, the effects of short-interval additive irradiation on radiation sensitivity at low doses may elucidate more subtle features of the radiation response pathways which could be utilized to promote radiation protection. How new research in molecular biology and genetics should be integrated to providing better risk estimations still remains unclear. It is imperative that risk estimates be based not solely on epidemiological assumptions, but also on empirical evidence of biological repercussions, especially in the light of increasing radiation exposure due to medical examinations, particularly CT.

2.10 References

21. The effects on populations of exposure to low levels of ionizing radiation. Washington, DC: National Academy of Sciences, United States National Research Council Division of Medical Sciences Advisory Committee on the Biological Effects of Ionizing Radiations, 1972.

22. Health Risks from Exposure to Low Levels of Ionizing Radiation: BEIR VII Phase 2: The National Academies Press, 2006.

23. Friedman LM, Furberg CD, DeMets DL. Fundamentals of clinical trials: Springer, 2010.

24. Fabrikant JI. The BEIR III Controversy. Radiation Research 1980; 84:361-368.

25. Berrington de Gonzalez A, Mahesh M, Kim K, et al. Projected cancer risks from computed tomographic scans performed in the united states in 2007. Archives of Internal Medicine 2009; 169:2071-2077.

26. Smith-Bindman R. Is Computed Tomography Safe? New England Journal of Medicine 2010; 363:1-4.

27. Berrington de Gonzalez A, Darby S. Risk of cancer from diagnostic X-rays: estimates for the UK and 14 other countries. The Lancet 2004; 363:345-351.

28. Thurston J. NCRP Report No. 160: Ionizing Radiation Exposure of the Population of the United States. Physics in Medicine and Biology 2010; 55:6327.

29. Bushberg JT, Seibert JA, Leidholdt Jr EM, Boone JM, Goldschmidt Jr EJ. The essential physics of medical imaging. Medical Physics 2003; 30:1936.

30. Mettler FA, Huda W, Yoshizumi TT, Mahesh M. Effective Doses in Radiology and Diagnostic Nuclear Medicine: A Catalog. Radiology 2008; 248:254-263.

31. Hall EJ, Brenner DJ. Cancer risks from diagnostic radiology. British Journal of Radiology 2008; 81:362-378.

32. Pearce MS, Salotti JA, Little MP, et al. Radiation exposure from CT scans in childhood and subsequent risk of leukaemia and brain tumours: a retrospective cohort study. The Lancet 2012; 380:499-505.

33. Mnyusiwalla A, Aviv R, Symons S. Radiation dose from multidetector row CT imaging for acute stroke. Neuroradiology 2009; 51:635-640.

34. USFDA. Safety Investigation of CT Brain Perfusion Scans: Update 11/9/2010. 2010.

35. Lee CI, Haims AH, Monico EP, Brink JA, Forman HP. Diagnostic CT Scans: Assessment of Patient, Physician, and Radiologist Awareness of Radiation Dose and Possible Risks. Radiology 2004; 231:393-398.

36. Lee S, Ditko S. Spiderman, Amazing Fantasy# 15. New York: Marvel 1962.

37. Attix FH. Introduction to radiological physics and radiation dosimetry: Wiley. com, 2008.

38. Blakely WF, Salter CA, Prasanna PGS. Early-response biological dosimetry-recommended countermeasure enhancements for mass-casualty radiological incidents and terrorism. Health Physics 2005; 89:494-504.

39. Nahas SA, Gatti RA. DNA double strand break repair defects, primary immunodeficiency disorders, and 'radiosensitivity'. Current Opinion in Allergy and Clinical Immunology 2009; 9:510-516 510.1097/ACI.1090b1013e328332be328317.

40. Pollard JM, Gatti RA. Clinical Radiation Sensitivity With DNA Repair Disorders: An Overview. International Journal of Radiation Oncology*Biology*Physics 2009; 74:1323-1331.

41. Hall EJ, Giaccia AJ. Radiobiology for the Radiologist. Philidelphia, PA USA: Lippincott Williams & Wilkins, 2006.

42. Lieber MR. The mechanism of double-strand DNA break repair by the nonhomologous DNA end joining pathway. Annual review of biochemistry 2010; 79:181.

43. San Filippo J, Sung P, Klein H. Mechanism of Eukaryotic Homologous Recombination. Annual review of biochemistry 2008; 77:229-257.

44. Shibata A, Conrad S, Birraux J, et al. Factors determining DNA double-strand break repair pathway choice in G2 phase. EMBO J 2011; 30:1079-1092.

45. Ellis RE, Yuan JY, Horvitz HR. Mechanisms and functions of cell death. Annu. Rev. Cell Biol. 1991; 7:663.

46. Campisi J, d'Adda di Fagagna F. Cellular senescence: when bad things happen to good cells. Nat Rev Mol Cell Biol 2007; 8:729-740.

47. Takahashi A, Ohnishi T. Does [gamma]H2AX foci formation depend on the presence of DNA double strand breaks? Cancer Letters 2005; 229:171-179.

48. Costes SV, Boissiere A, Ravani S, Romano R, Parvin B, Barcellos-Hoff MH. Imaging Features that Discriminate between Foci Induced by High- and Low-LET Radiation in Human Fibroblasts. Radiation Research 2006; 165:505-515.

49. Rogakou EP, Pilch DR, Orr AH, Ivanova VS, Bonner WM. DNA double-stranded breaks induce histone H2AX phosphorylation on serine 139. J Biol Chem 1998; 273:5858 - 5868.

50. Rogakou EP, Boon C, Redon C, Bonner WM. Megabase Chromatin Domains Involved in DNA Double-Strand Breaks in Vivo. The Journal of Cell Biology 1999; 146:905-916.

51. Huen MSY, Chen J. The DNA damage response pathways: at the crossroad of protein modifications. Cell research 2007; 18:8-16.

52. Wang H, Zeng Z-C, Bui T-A, et al. Efficient rejoining of radiation-induced DNA double-strand breaks in vertebrate cells deficient in genes of the RAD52 epistasis group. Oncogene 2001; 20.

53. Goodarzi AA, Jeggo P, Lobrich M. The influence of heterochromatin on DNA double strand break repair: Getting the strong, silent type to relax. DNA Repair 2010; 9:1273-1282.

54. Rothkamm K, Horn S. gamma-H2AX as protein biomarker for radiation exposure. Annali dell'Istituto superiore di sanità 2009; 45:265-271.

55. Sedelnikova OA, Rogakou EP, Panyutin IG, Bonner WM. Quantitative detection of (125) IdU-induced DNA double-strand breaks with gamma-H2AX antibody. Radiation Research 2002; 158:486-492.

56. Rothkamm K, Kruger I, Thompson LH, Lobrich M. Pathways of DNA double-strand break repair during the mammalian cell cycle. Molecular and Cellular Biology 2003; 23:5706-5715.

57. Kuhne M, Riballo E, Rief N, Rothkamm K, Jeggo PA, Lobrich M. A double-strand break repair defect in ATM-deficient cells contributes to radiosensitivity. Cancer Research 2004; 64:500-508.

58. Li S, Takeda Y, Wragg S, Barrett J, Phillips A, Dynan WS. Modification of the ionizing radiation response in living cells by an scFv against the DNA-dependent protein kinase. Nucleic Acids Research 2003; 31:5848-5857.

59. Lobrich M, Shibata A, Beucher A, et al. gammaH2AX foci analysis for monitoring DNA double-strand break repair: strengths, limitations and optimization. Cell Cycle 2010; 9:662-669.

60. Rothkamm K, Lobrich M. Evidence for a lack of DNA double-strand break repair in human cells exposed to very low x-ray doses. Proceedings of the National Academy of Sciences of the United States of America 2003; 100:5057-5062.

61. Miller LF, Rumack BH. Clinical safety of high oral doses of acetylcysteine. In:Seminars in Onco/ogy, 1983.

62. Kelly GS. Clinical applications of N-acetylcysteine. Alternative medicine review: a journal of clinical therapeutic 1998; 3:114-127.

63. Ito K, Takubo K, Arai F, Satoh H, Matsuoka S, Ohmura M. Regulation of reactive oxygen species by Atm is essential for proper response to DNA double-strand breaks in lymphocytes. J Immunol 2007; 178:103-110.

64. Kerksick C, Willoughby D. The Antioxidant Role of Glutathione and N-Acetyl-Cysteine Supplements and Exercise-Induced Oxidative Stress. Journal of the International Society of Sports Nutrition 2005; 2:38 - 44.

65. Ditch S, Paull TT. The ATM protein kinase and cellular redox signaling: beyond the DNA damage response. Trends Biochem Sci 2012; 37:15-22.

66. Guo Z, Kozlov S, Lavin MF, Person MD, Paull TT. ATM activation by oxidative stress. Science 2010; 330:517-521.

67. Greenberger JS. Radioprotection. In Vivo 2009; 23:323-336.

68. Seed TM. Radiation protectants: current status and future prospects. Health Physics 2005; 89:531-545.

69. Kim K, Pollard JM, Norris AJ, et al. High-throughput screening identifies two classes of antibiotics as radioprotectors: tetracyclines and fluoroquinolones. Clinical Cancer Research 2009; 15:7238-7245.

70. Rothkamm K, Balroop S, Shekhdar J, Fernie P, Goh V. Leukocyte DNA Damage after Multi-Detector Row CT: A Quantitative Biomarker of Low-Level Radiation Exposure. Radiology 2007; 242:244-251.

71. Beels L, Werbrouck J, Thierens H. Dose response and repair kinetics of gH2AX foci induced by in vitro irradiation of whole blood and T-lymphocytes with X- and gamma-radiation. International Journal of Radiation Biology 2010; 86:760-768.

72. Grudzenski S, Kuefner MA, Heckmann MB, Uder M, Lobrich M. Contrast Medium-enhanced Radiation Damage Caused by CT Examinations. Radiology 2009; 253:706-714.

73. Beels L, Bacher K, De Wolf Dl, Werbrouck J, Thierens H. gH2AX Foci as a Biomarker for Patient X-Ray Exposure in Pediatric Cardiac Catheterization. Circulation 2009; 120:1903-1909.

74. Simonsson M, Qvarnstram F, Nyman J, Johansson K-A, Garmo H, Turesson I. Low-dose hypersensitive gH2AX response and infrequent apoptosis in epidermis from radiotherapy patients. Radiotherapy and oncology : journal of the European Society for Therapeutic Radiology and Oncology 2008; 88:388-397.

75. Lobrich M, Rief N, Kuhne M, et al. In vivo formation and repair of DNA double-strand breaks after computed tomography examinations. Proceedings of the National Academy of Sciences of the United States of America 2005; 102:8984-8989.

76. Geisel D, Zimmermann E, Rief M, et al. DNA double-strand breaks as potential indicators for the biological effects of ionising radiation exposure from cardiac CT and conventional coronary angiography: a randomised, controlled study. European Radiology 2012; 22:1641-1650.

77. Neff RD, Cassen B. Relative Radiation Sensitivity of Circulating Small and Large Lymphocytes. Journal of Nuclear Medicine 1968; 9:402-405.

78. Di Leonardo A, Linke SP, Clarkin K, Wahl GM. DNA damage triggers a prolonged p53-dependent G1 arrest and long-term induction of Cip1 in normal human fibroblasts. Genes & Development 1994; 8:2540-2551.

79. Marioni JC, Mason CE, Mane SM, Stephens M, Gilad Y. RNA-seq: An assessment of technical reproducibility and comparison with gene expression arrays. Genome Research 2008; 18:1509-1517.

80. Albrecht H, Blythe D-J, Yunis R, et al. Transcriptional Response of Ex Vivo Human Skin to Ionizing Radiation: Comparison Between Low- and High-Dose Effects. Radiation Research 2012; 177:69-83.

Chapter 3: Materials and Methods

This work seeks to characterize the biological response of low doses of ionizing radiation clinically relevant to CT examinations to inform risk assessment for diagnostic radiographic procedures. To accomplish this objective a sensitive and accurate protocol is developed and evaluated (Chapter 4) and analysis of the biological response to relevant radiation doses and schemes is performed for both *in vitro* (Chapter 5) and *in vivo* (Chapter 6) experiments. Materials and methods specific to each research aim are described in the corresponding chapters. Common materials and methods are described here.

3.1 Cell lines

A previously established murine tumor infiltrating lymphocyte (TIL) cell line and the Epstein-Barr Virus-immortalized wild-type human lymphocyte cell line, ESW-WT3, were cultured in complete media (RPMI with 10%FBS) and incubated in a humidified incubator at 37°C with 5% CO_2.

3.2 *In Vitro* Blood Samples

For consistency, blood from a single healthy donor (female, 29 years) was used for all experiments involving *in vitro* whole blood analysis. Following consent, blood samples were collected into 4mL K2 EDTA (7.2 mg) tubes. Samples were immediately placed in a light proof container and kept in the dark at room temperature until treatment. All blood samples were collected in accordance with the UCLA IRB (#10-001571).

3.3 Irradiators

In vitro irradiations were performed with an RS320 Irradiation System (Gulmay Medical, Bethel, CT, USA) with 3mm inherent aluminum filtration and 1.5mm added copper filtration at

150kVp with 20mA. This irradiation setup has a dose rate of 0.72Gy/min and HVL of 21.07mmAl. This irradiator is capable of delivering doses ranging from 1mGy to over 10,000mGy. Additional irradiations to determine sensitivity were performed with a multidetector row CT scanner at 120kVp (Sensation 64, Siemens Healthcare, Forchheim, Germany). For this irradiation setup, blood samples were placed in a plastic 500mL tube which was in turn placed in the center chamber of a 16cm CTDI head phantom. This setup allows samples to be irradiated with doses that range from 1 to 1000mGy.

3.4 Immunofluorescent Staining for gammaH2AX

Following fixation, samples were pelleted and supernatant removed. 0.02ug Ab (FITC conjugated goat antiHu-gammaH2AX, Millipore Catalogue #:16-202A) in 50uL of permeablization buffer (5% Saponin, 100mM HEPES, 1.4M NaCl, 25mM CaCl2 in ddH_20) was added to each sample, mixed well and incubated on ice for 20 minutes with agitation. 100uL of antibody wash solution (1% BSA, 0.2% Triton-X-100 in PBS) was added following antibody incubation. Samples were then centrifuged at 400g for 5min and re-suspended in isotone for analysis by flow cytometry.

3.5 Statistical Analyses

Statistical significance between treatments was determined by t-test analysis and ANOVA where indicated. P-values less than 0.05 ($p<0.05$) were considered significant.

Chapter 4: Protocol Development

4.1 Introduction

The evaluation of gammaH2AX foci is quickly becoming the standard method to describe the biological response to a variety of external forces, especially IR. H2AX is a variant of the histone protein H2A. H2AX becomes phosphorylated for thousands of base-pairs at sites flanking a DNA DSB very quickly after damage is incurred. DSB are considered to be the most important DNA lesions when considering DNA damage as they are the most detrimental and hardest to repair. This phosphorylated form (gammaH2AX) can be detected by specific antibodies. H2AX phosphorylation is an attractive marker for DNA DSB as it has high sensitivity due to the natural expansion and amplification of the signal. However, gammaH2AX is only surrogate marker for DSBs as it detects an early step in the DNA damage response not the breaks directly.

Analysis of the biological changes after low doses of IR is very limited due to the requirement for extreme sensitivity. Using 50DSB/human cell/Gy, it can be estimated that 20mGy is required to achieve an average of 1DSB/human cell. 1mGy will induce an average of 1DSB/20 human cells. Thus, gammaH2AX foci evaluation has superseded most other assays in assessing the biological response to low doses of IR due to its excellent sensitivity. However, the characterization of the biological changes resulting from doses of IR in the range of CT protocols is often limited to a few, if not a single, time point evaluated for gammaH2AX foci by fluorescent microscopy. Furthermore, sample handling practices often vary or are unreported, offering little standardization not only between studies but also between samples. Due to the

dynamic nature of cellular damage repair, it is clear that accurate and reproducible kinetic analysis is essential to properly assess the gammaH2AX response, especially at low doses.

The goal of this work is to develop and evaluate a highly efficient technique that can be readily applied to kinetic analysis of DNA damage in patient blood samples for clinical application. Development of a rapid fixation technique of whole blood will provide precise kinetic analysis of biomarkers for DNA damage repair compared to standard handling and fixation techniques, especially at short time points. Current methods require blood samples to be separated before fixation (81-85) which may introduce artifacts and prolongs analysis time. Results may not reflect physiological cellular conditions at the time of extraction for cells are likely to activate damage repair or other mechanisms during the time lag. Additionally, samples are routinely incubated on ice or at room temperature for transport to laboratory facilities where the samples are processed. It is unknown what effects these practices have on the assessment of DNA damage or the artifacts that may be introduced. We have developed a method to examine whole blood without separation that offers rapid and standardized analysis. Here, the efficacy of the developed method's fixation protocol is compared to standard fixation protocols. The analysis of the DNA damage response after IR following standard practices for sample handling is explored to understand the effects of these practices on biological endpoints.

Additionally, this work provides fundamental analysis for further *in vitro* and *in vivo* experiments

4.2 Materials and Methods

4.2.1 Protocol Design

For analysis of either white blood cells (WBCs) extracted from whole blood, or cell lines following irradiation, fixation is an important step to 'freeze' cells at a given moment to characterize the temporal dynamics of cellular responses. Therefore, the fixation protocol and its timing should be swift and standardized to maximize accuracy and minimize variance in estimating the rapid DNA repair response. The over-abundance of red blood cells (RBCs) in whole blood can affect reagent uptake and skew results, thus WBCs are isolated for assessment of DNA damage and other biological endpoints. It is standard practice to either physically separate WBCs with gradient medium or lyse RBCs with lysis buffer prior or fixation. As both these procedures take valuable time and can be rather unstandardized especially if samples need to be transported back to the laboratory before fixation, the aim of this work is to develop an alternative method to standardize the pre-analytical procedures as much as possible.

Due to the relative sensitivity of RBCs to changes in osmolality, different volumes (0-500uL) of standard fixation buffer (2.3% formaldehyde: 1:16 dilution of 37% formaldehyde solution stabilized with methanol in ddH_20) was added to 100uL samples of whole blood, to determine if it would successfully lyse RBCs and fix WBCs simultaneously, and if so what volume would be required for adequate lysis. After addition of fixation buffer, samples were mixed by pipetting and incubated on ice for 20min. Samples were centrifuged at 500g for 5 min and the supernatant was discarded. 600uL of 2% SDS was added to the remaining pellet to lyse any remaining RBC and mixed by inversion. 100uL samples were aliquoted into each of four separate wells of a 96well clear bottom plate and analyzed for absorbance at 541, 555, 577nm to score the amount of hemoglobin left in the sample after fixation and provide an estimate of un-lysed cells remaining in the sample. Four samples of2% SDS were included for comparison.

Averaged blank absorbance values were subtracted from each sample absorbance reading for each wavelength tested. Sample absorbance readings were then averaged and presented with the standard deviation. Once successful lysis and fixation was established, standard wash procedures were followed. Samples were washed twice – with three times the amount of fixation buffer – with wash buffer (1% BSA-PBS). 300uL of fixation buffer was selected for further whole blood fixation experiments.

4.2.2 Adaptation of Fixation Protocol for Cell Lines

For standardization across experiments, the rapid fixation protocol (RFP) described above was adapted for use with cultured cell line samples. Cells were first harvested by centrifugation and aliquoted into treatment tubes at a cellular concentration of 2,000 cells/uL to mimic the peripheral blood mononuclear cell (PBMC) concentration in the blood (~1,000-2,000cells/uL). For fixation, 100uL of cells were added to 200uL of ice-cold fixation buffer, mixed and incubated on ice for 20 min. Samples were washed twice with wash buffer as before (with three times the amount of fixation buffer). As RBC lysis is unnecessary in culture cell line samples, a reduced volume of fixation buffer was still provided an environment of excess buffer, but reduced the amount of reagents required.

4.2.3 Standard Fixation Protocol for Cultured Cell Line Samples or Isolated PBMCs

In the standard fixation protocol (SFP), cells are centrifuged after treatment at 250g for 5 min. Supernatant is discarded and 50uL of ice-cold fixation buffer is added per 10^5cells, mixed and incubated on ice for 20min. Samples were washed twice – with three times the amount of fixation buffer – with wash buffer. Results from cell-line analysis indicated that fixation using 50uL per 10^5cells may not be as complete as using 100uL per 10^5cells. For a more similar

comparison we altered the protocol for whole blood samples so cells fixed by the standard fixation protocol received 200uL of fixation buffer per $2x10^5$cells.

4.2.4 Standard Lymphocyte Isolation from Whole Blood Samples

Blood was separated using standard gradient separation. Briefly, blood samples were diluted 1:1 with PBS and gently layered on to Ficoll-Paque Premium (GE Healthcare Life Sciences, Pittsburgh, PA, USA) and centrifuged at 500g for 30 min at room temperature (~22-25°C) to maintain integrity of gradient separation medium. The interface was collected, washed twice with media and centrifuged at 500g for 10min to attain PBMCs.

4.2.5 Trypan Blue Staining

To investigate any adverse effects the greater amount of fixation buffer used in the RFP may have on further analysis, membrane integrity of fixed and non-fixed cells was evaluated by trypan blue staining. Cultured lymphocytes were fixed using the RFP. Two samples were treated with PBS to serve as non-fixed controls; one sample was kept at 37°C and one sample was kept on ice for the same time as the fixed sample. Since cells are incubated on ice during the fixation process a sample of non-fixed cells was kept on ice to control for any effects due to ice-cold incubation. Samples were diluted 1:1 with trypan blue reagent and the numbers of unstained and stained cells were enumerated to assess membrane integrity. The average value of intact cells after each treatment from three independent experiments is reported with the standard error of the mean (SEM).

4.2.6 Cellular Metabolism

The CellTiter-Glo® assay (Promega Corporation, Madison, WI, USA) was used to determine the effectiveness of the different fixation protocols to arrest metabolic activity. In

this assay, cells are exposed to a lytic solution, which reacts with any intact ATP to produce a bioluminescent signal that can be detected and measured by a luminometer. The amount of ATP present is an indicator of metabolic activity. Cultured lymphocytes were fixed by either the RFP or SFP. Non-fixed cultured lymphocytes treated with PBS were incubated on ice for the same amount of time as fixed sample. Whole blood samples were fixed by either the RFP or separated by standard separation and then fixed by the SFP. Non-fixed whole blood samples, treated with PBS, were incubated on ice for the same time as fixed samples. 70uL of each sample was aliquoted into four separate wells of a 96-well plate and allowed to equilibrate to room temperature. PBS or supernatant from fixed whole blood samples was used for blank samples for cultured lymphocytes of whole blood samples respectively. 70uL of room temperature CellTiter-Glo® reagent was added to each well. Plates were placed on an orbital shaker for 2 min and then incubated at room temperature for an additional 8 min. Luminescence was measured using a SpectraMax M5 plate reader with SoftMax Pro software (Molecular Devices, Sunnyvale, California, USA). Blank values were averaged and subtracted from treatment samples. Cellular concentration was recorded for each treatment and luminescence values were adjusted to account for differences in cell count. The average values of three independent experiments are reported with the SEM.

4.2.7 Irradiation Treatments

The kinetics of the DNA damage response following IR were analyze to examine the effects of sample handling practices on the measurement of biological endpoints. Irradiations were performed with the RS320 Irradiation System described in the Material and Methods chapter. Cell culture or whole blood samples were irradiated to 1Gy with 150kVp at 20mA with

a dose rate of 0.72Gy/min. Samples were either fixed immediately using the developed RFP at 1, 2, 3, 5 or 30 min following the start of irradiation (RFP samples) or placed on ice at the same times (ICE and ICE/RT samples) (**Figure 4.1A**). Samples were incubated on ice

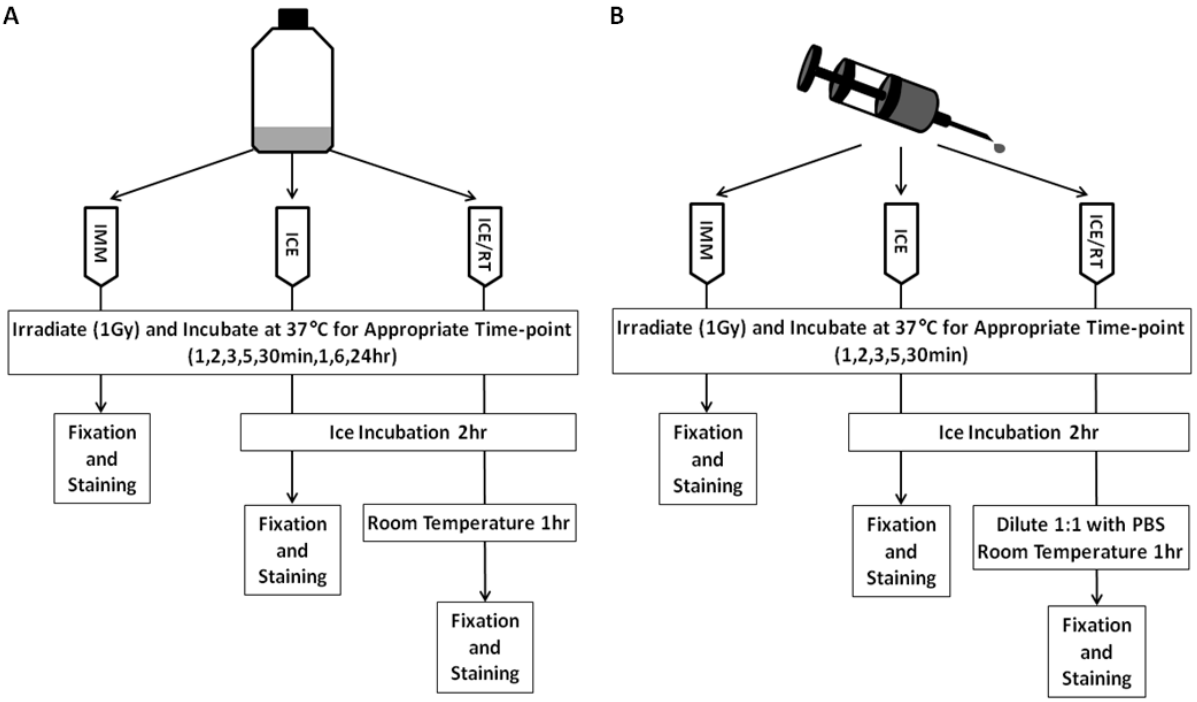

Figure 4.1. Schematic of experimental design to compare sample handling practices. Cultured lymphocyte (**A**) or whole blood (**B**) samples were fixed immediately (IMM), after incubation on ice for 2 hours (ICE), or after incubation on ice for 2 hours plus and additional hour at room temperature (ICE/RT) to simulate various handling practices following irradiation. Blood samples were diluted 1:1 with PBS for room temperature incubation. Samples were then assessed for DNA damage by antibody staining for gH2AX. Additionally, cell culture samples were assessed at 15min, 1hr, 6hr and 24hr.

for 2 hr and then fixed using the RFP (ICE samples) or incubated at room temperature for and additional hour (ICE/RT samples) before fixation to mimic standard sample handling and preparation practices. Blood samples were diluted 1:1 with PBS for room temperature incubation (**Figure 4.1B**). Samples were then assessed for DNA damage by antibody staining for gammaH2AX. Additionally, cell culture samples were assessed at 15 min, 1 hr, 6 hr and 24 hr for more complete kinetic assessment. To minimize the effects of changes in background

fluorescence for flow cytometry non-irradiated control samples were included for each time point and each treatment for comparison with irradiated samples.

To determine if flow cytometry would be acceptable for gammaH2AX analysis of low dose irradiations and correlate with microscopic analysis, cell culture samples were irradiated to 20, 40 and 170mGy and incubated at 37°C for 15 min. These samples were assessed by flow cytometry and fluorescent microscopy following antibody staining.

4.2.8 gammaH2AX Foci Analysis

To ensure samples could be analyzed by fluorescent microscopy using the RFP, we assessed gammaH2AX foci in cell culture samples after low dose IR exposure. For microscopy, cells were fixed using the RFP, aliquoted on to L-lysine coated cover slips and allowed to adhere for 15 min at room temperature. Samples were permeablized with 0.5% Triton X-100 for 5min, washed 3 x 5 min with PBS and blocked in 10%FBS-PBS for 1hr at room temperature. Cover slips were incubated with anti-gammaH2AX primary antibody (Millipore, Billerica, MA, USA) for 1 hr at room temperature, incubated with 0.1% Triton X-100 for 5 min, washed 3 x 5 min with PBS and blocked in 10%FBS-PBS for 1 hr at room temperature. Samples were then incubated with Alexa Fluor 488 anti-mouse secondary antibody (Invitrogen, Carlsbad, CA, USA) for 45 min at room temperature, washed 3 times with PBS and mounted to slides with Vectashield containing DAPI. Cells were enumerated by fluorescent microscopy. Percent positive cells and foci per cell were calculated. Cells were scored as positive if nuclei contained 4 or more foci. Relative median fluorescence data from flow cytometry was correlated to foci per cell and percent positive cells data from fluorescent microscopy. The average values of three independent experiments are reported with the SEM.

4.2.9 Determination of Isolated Cell Populations from Fixed Blood Samples

Isolated PBMCs and whole blood samples were fixed by the SFP or RFP respectively and samples were analyzed by flow cytometry using forward and side scatter gating to determine cell sub-populations. Average population percentage values of four independent experiments are reported with the SEM.

4.2.10 gammaH2AX Analysis by Flow Cytometry

Following fixation by the RFP and immunofluorescent staining for gammaH2AX as described in the Materials and Methods chapter, H2AX phosphorylation after IR exposure was assessed by flow cytometry to compare relative levels of measured DNA damage following different sample handling practices. Samples were analyzed on a BD LSRFortessa flow cytometer with FACSDIVA 6 software package. (Becton, Dickinson and Company, Franklin Lakes, New Jersey, USA). Forward and side scatter gating was used to isolate healthy cells and 20,000 events were collected for each sample. The average median fluorescence from three independent experiments is reported with the SEM.

4.3 Results

4.3.1 Immediate fixation effectively arrests cellular metabolism and preserves cell populations in whole blood without degrading cellular integrity

Clearly, adding excess fixation buffer on the order of 200uL and above lyses most RBCs in a 100uL sample of whole blood as indicated by the dramatic drop in absorbance seen at all three wavelengths for hemoglobin ($p >> 0.001$; **Figure 4.2**). Additionally, it was visually apparent that few RBCs remained in these samples as the pellets only contained a small amount of red coloration (200uL) or none at all (300 and 400uL) upon inspection. Samples receiving either 50

or 100uL both contained large pellets, clearly dominated by intact RBCs. As a driving purpose of this work is to develop an efficient assay for wide-spread clinical use, both empirical and

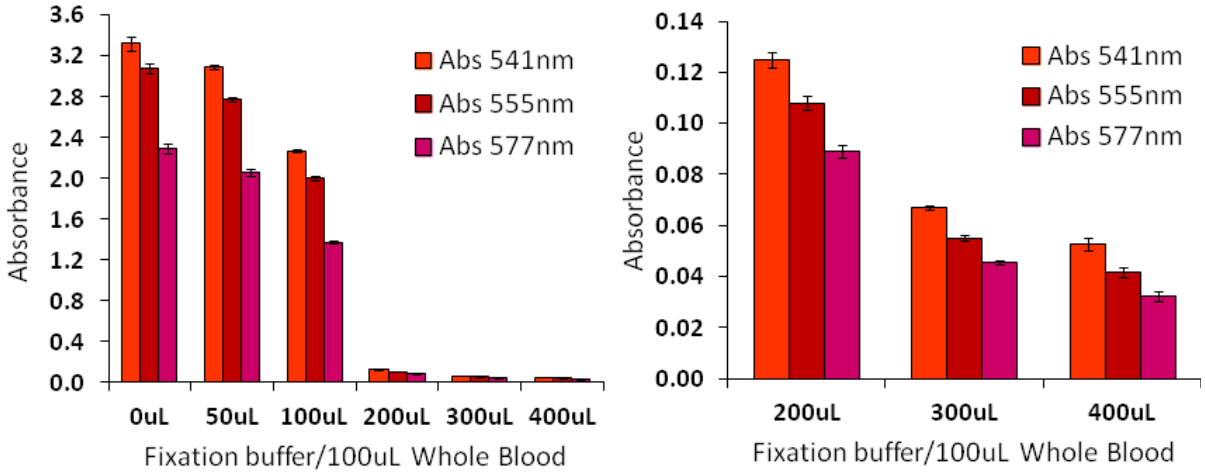

Figure 4.2. Fixation buffer efficacy in red blood cell lysis. Different amounts of fixative were added per 100uL of whole blood. Supernatant was discarded and remaining red blood cells (RBCs) were lysed with 2%SDS. Intact RBCs remaining after initial fixation were quantified by measuring absorbance at 541, 555 and 577nm (Hemoglobin). A sharp decrease in absorbance was apparent following 200uL fixative. The right panel is an enlarged plot illustrating the fixation efficacy at the larger quantities of fixation buffer.

logistical factors were taken in to account to select the appropriate amount of fixation buffer to be used in further analysis of whole blood. Due to the requirement of adding three times the amount of wash solution in subsequent steps, 300uL of fixation buffer was selected for further whole blood analysis. This amount adequately lyses RBCs and allows for the use of 1.5mL tubes which are easily attainable and useable in commonplace laboratory bench-top centrifuges.

The addition of excess fixation solution (as opposed to the standard 50uL/10^5cells) does not interfere with membrane permeability to an extent that would affect permeabilization and antibody staining. The percentage of cells which exclude trypan blue stain following fixation – 82.10 ± 5.67% – is not significantly different from the percentage of non-fixed cells which exclude trypan blue stain after incubation at 37°C or on ice – 81.70% ± 9.28% and 85.97% ±

4.60% respectively (**Table 4.1**). Incubation on ice does not have a significant effect on stain exclusion in non-fixed cells. Comparison between cells fixed by the rapid fixation protocol (RFP) and non-fixed samples indicates that this fixation protocol does not significantly alter membrane integrity.

Table 4.1. Intact cell following fixation	
Treatment	% Intact
Non-Fixed Cells at 37˚C	81.70% ± 9.28%
Non-Fixed Cells on Ice	85.97% ± 4.60%
Fixed Cells	82.10 ± 5.67%

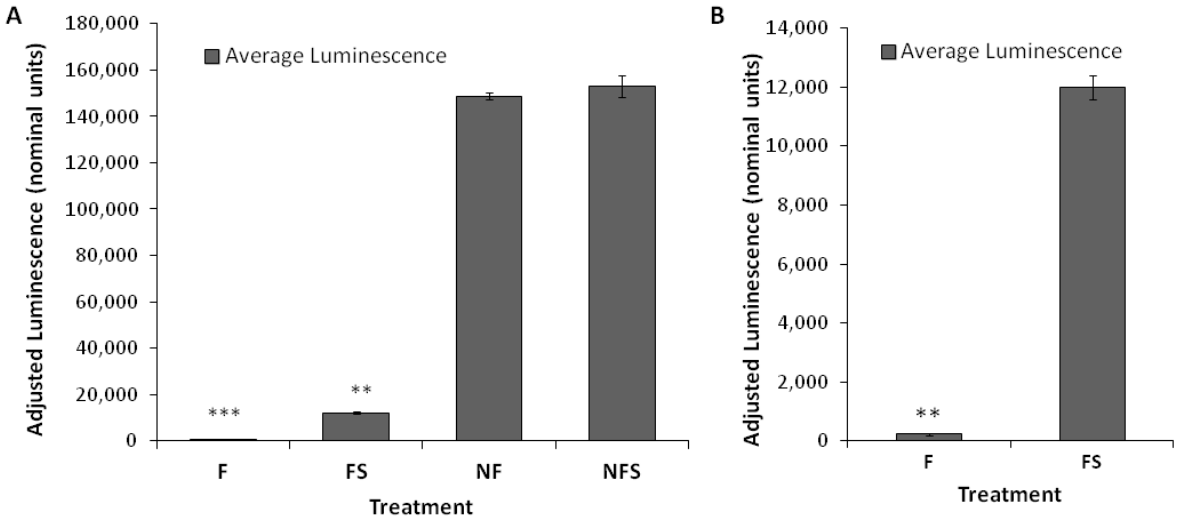

Figure 4.3. Effectiveness of the different fixation protocols to arrest metabolic activity of cultured lymphocytes. Samples were fixed by either the RFP (F) or SFP (FS). Non-fixed samples treated with PBS were incubated on ice (NF/NFS). Metabolic activity was measured using the Cell-Titer Glo® Assay for cellular viability. Cellular concentration was recorded for each treatment and luminescence values were adjusted to account for differences in cell count. ATP levels are dramatically reduced compared to non-fixed samples following both standard ($p<0.01$) and rapid fixation ($p<0.001$) protocols (A), indicating successful arrest of metabolism. Luminescence is reduced to a greater extent following the RFP ($p<0.01$) compared to the SFP (B). The average values of three independent experiments are reported with the SEM.

The ATP levels following both standard (FS) and rapid (F) fixation protocols in cultured lymphocytes are dramatically reduced compared to non-fixed samples (NFS/NF) (**Figure 4.3A**), indicating successful arrest of metabolism. However, metabolism is reduced to a greater extent following the RFP – F=0.15% $\pm$ 0.06% compared to FS=7.83% $\pm$ 1.22% by the SFP ($p<0.01$; **Figure 4.3B**). Both fixation protocols also dramatically reduce luminescence (surrogate for cell viability) in whole blood samples compared to non-fixed samples (**Figure 4.4A**). Metabolism is reduced to a greater extent following the RFP – F=0.11% $\pm$ 0.13%, compared to FS=0.31% $\pm$ 0.10% after separation and SFP ($p<0.05$) – even following the addition of 200uL of fixation buffer (**Figure 4.4B**). The reduction in luminescence seen in whole blood samples treated by standard gradient separation and fixation compared to cultured lymphocytes is likely due to the increase in fixation solution volume from 50uL to 200uL.

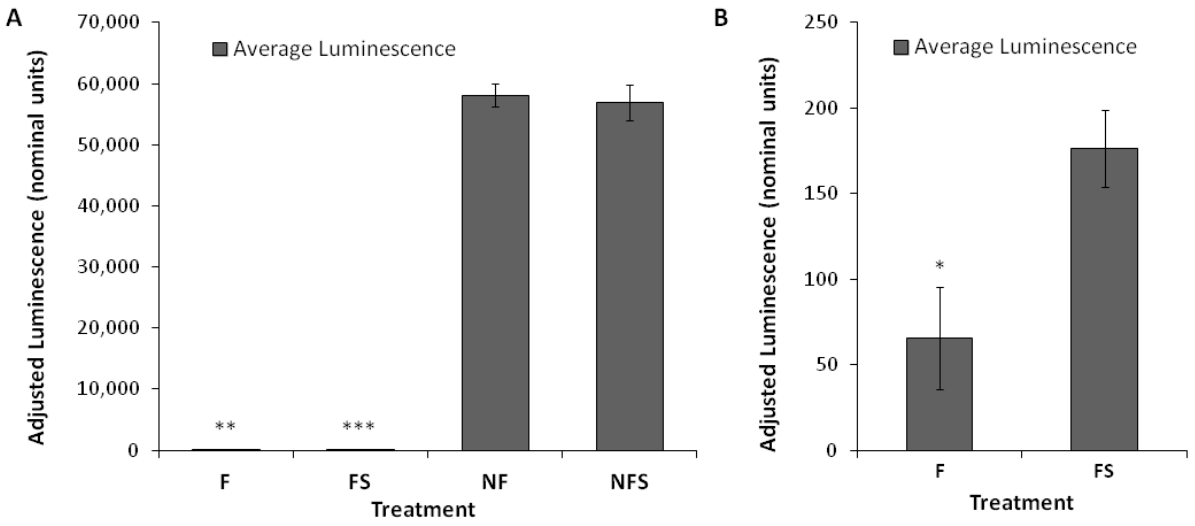

Figure 4.4. Effectiveness of the different fixation protocols to arrest metabolic activity of whole blood samples. Samples were fixed by either the RFP (**F**) or separated by standard separation and then fixed by the SFP (**FS**). Non-fixed samples treated with PBS were incubated on ice (**NF/NFS**). Metabolic activity was measured using the Cell-Titer Glo® Assay for cellular viability. Cellular concentration was recorded for each treatment and luminescence values were adjusted to account for differences in cell count. Luminescence is dramatically reduced compared to non-fixed samples following both standard ($p<0.001$) and rapid fixation ($p<0.01$) protocols (**A**). Luminescence is reduced to a greater extent following the rapid fixation protocol compared to separation and SFP ($p<0.05$) (**B**). The average values of three independent experiments are reported with the SEM.

Only mononuclear cells, including lymphocytes (82.3% $\pm$ 1.8%) and monocytes (4.7% $\pm$ 0.4%) were obtained following standard gradient separation of whole blood samples (**Figure 4.5 left panel**). Whole blood fixation with the RFP yielded lymphocytes (28.1% $\pm$ 1.3%), monocytes (3.5% $\pm$ 0.4%) and granulocytes (55.9% $\pm$ 2.2%) (**Figure 4.5 right panel**).

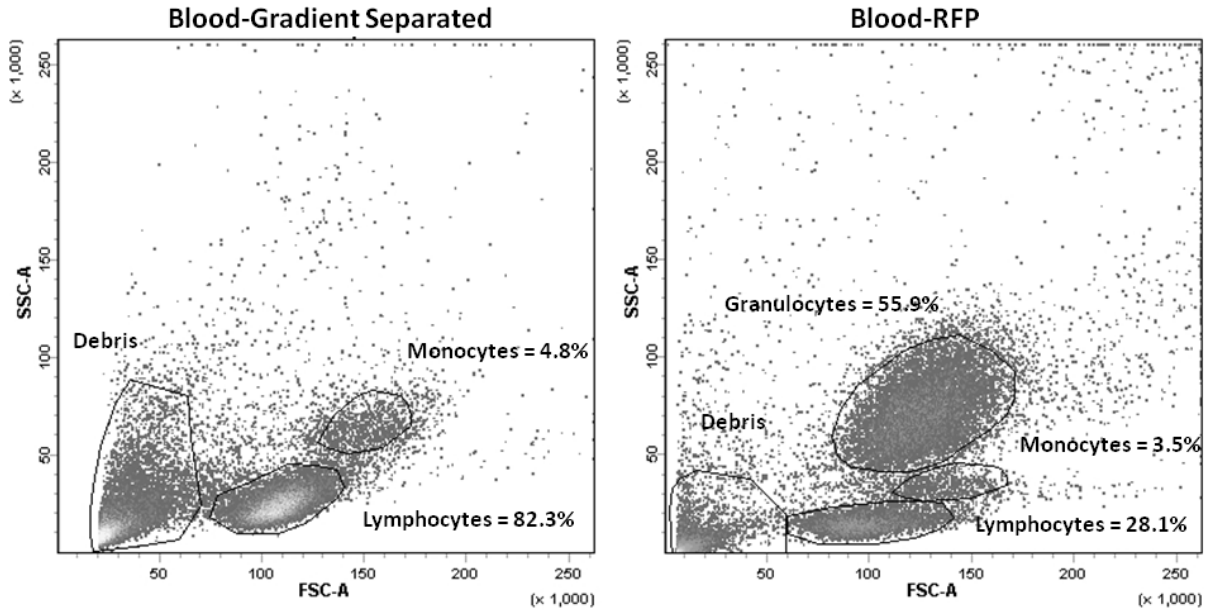

Figure 4.5. Determination of isolated cell populations from fixed blood samples. Isolated PBMCs (left panel) and whole blood (right panel) were fixed by the SFP or RFP respectively. Both samples were analyzed by flow cytometry using forward and side scatter gating to determine cell sub-populations. Average population percentage values of four independent experiments are reported with the SEM.

4.3.2 Immediate fixation allows for sensitive kinetic analysis of DNA repair following ionizing radiation

gammaH2AX foci detection (**Figure 4.6A**) and the clear dose response seen for both average foci per cell and percent positive cells (**Figure 4.6B**) demonstrates successful gammaH2AX analysis by fluorescent microscopy using the RFP. gammaH2AX levels show an average of 1.2 foci per cell and 12.0% positive cells in unirradiated samples and show a

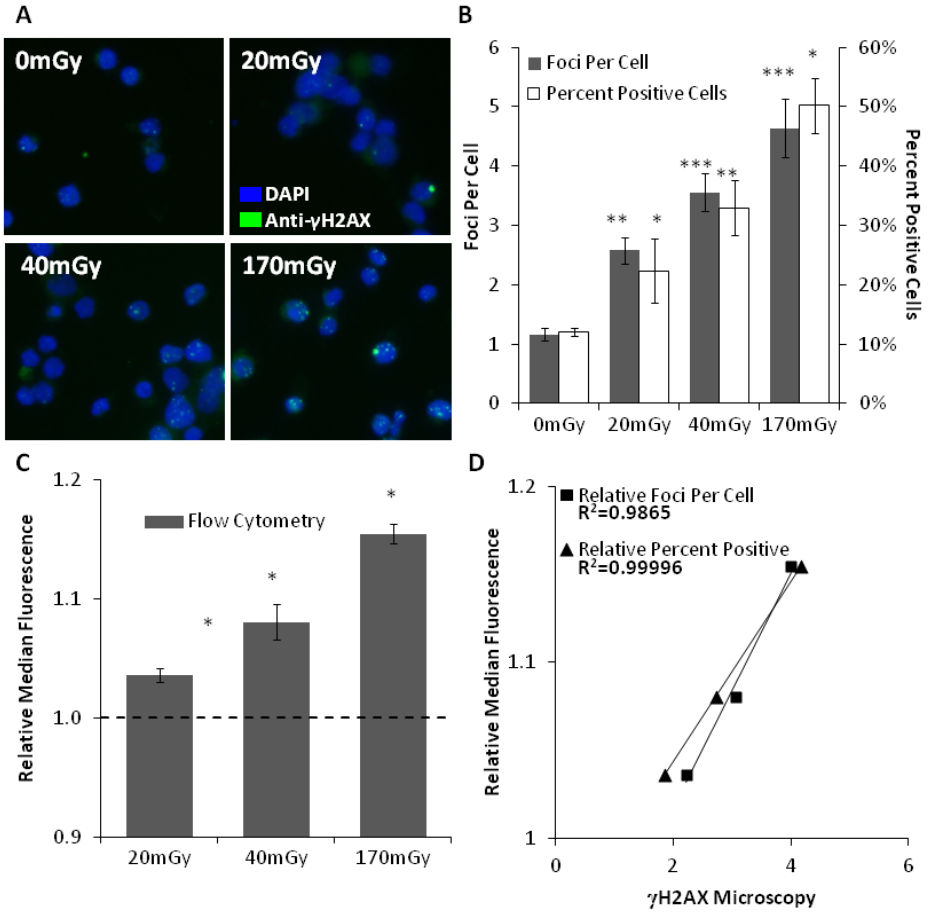

Figure 4.6. Comparison of gammaH2AX immunofluorescent analysis by flow cytometry and fluorescent microscopy. Cell culture samples were irradiated to 20, 40 and 170mGy and incubated at 37°C for 15min, fixed by the RFP and assessed by flow cytometry and fluorescent microscopy. Cells were enumerated by fluorescent microscopy (**A**) and percent positive cells and foci per cell were calculated (**B**). Cells were scored as positive if nuclei contained 4 or more foci. Cells were stained with DAPI (blue) to highlight the nucleus while distinct γH2AX foci appear in green (FITC). γH2AX median fluorescence was evaluated by flow cytometry and the relative median fluorescence was calculated (**C**). Analysis by flow cytometry shows a significant increase in γH2AX fluorescence for all doses evaluated ($p<0.05$). Relative median fluorescence data from flow cytometry was correlated to foci per cell and percent positive cells data from fluorescent microscopy (**D**). Relative γH2AX fluorescence correlates well with both relative foci per cell ($R^2=0.9865$) and relative percent positive cells ($R^2=0.99996$) as measured by fluorescent microscopy. The average values of three independent experiments are reported with the SEM.

significant dose dependent increase to 2.6 ($p<0.01$), 3.6 ($p<0.001$) and 4.6 ($p<0.001$) foci per cell and 22.35% ($p<0.05$), 33.0% ($p<0.01$) and 50.3% ($p<0.05$) positive cells following 20, 40 and 170mGy respectively (**Figure 4.6B**). The obvious dose response seen for gammaH2AX

fluorescence indicates successful analysis of low dose irradiations by flow cytometry (**Figure 4.6C**). Analysis by flow cytometry shows a significant increase in gammaH2AX fluorescence for all doses evaluated ($p<0.05$). Furthermore, relative gammaH2AX fluorescence correlates well with both relative foci per cell ($R^2=0.9865$) and relative percent positive cells ($R^2=0.99996$) as measured by fluorescent microscopy (**Figure 4.6D**). The strong correlation between flow cytometry and microscopy data and the demonstrated sensitivity indicates that flow cytometry is an acceptable method for quantifying gammaH2AX phosphorylation even at low doses of IR.

Samples fixed with the RFP following IR, show a steep increase in relative gammaH2AX median fluorescence after short incubation times for both cultured lymphocytes (**Figure 4.7A insert**) and whole blood samples (**Figure 4.7B**). Even after 1 min (approximately 17 sec after the cessation of radiation), there is a significant increase in relative median fluorescence ($p<0.001$) for cultured lymphocytes. The increase in fluorescence for whole blood reaches a significance at 2 min ($p<0.001$). For cultured lymphocytes, peak gammaH2AX signal is seen between 30 and 60 min after irradiation. By 6 hr gammaH2AX fluorescence is reduced drastically but is still significantly higher than background levels ($p<0.05$). At 24 hr, gammaH2AX fluorescence returns to background levels. When plotted together it is clear that samples fixed following standard incubation practices show different H2AX phosphorylation patterns compared to those fixed immediately with the RFP for both cultured lymphocytes (**Figure 4.7A**) and whole blood (**Figure 4.7B**). Cultured lymphocyte samples incubated on ice show similar results to those fixed immediately at short time points (1-15 min) (**Figure 4.7A insert**); however, at 30 and 60 min, relative gammaH2AX median fluorescence is lower and significantly so at 60 min ($p<0.05$). The peak gammaH2AX signal appears to be between 30 and 60 minutes after

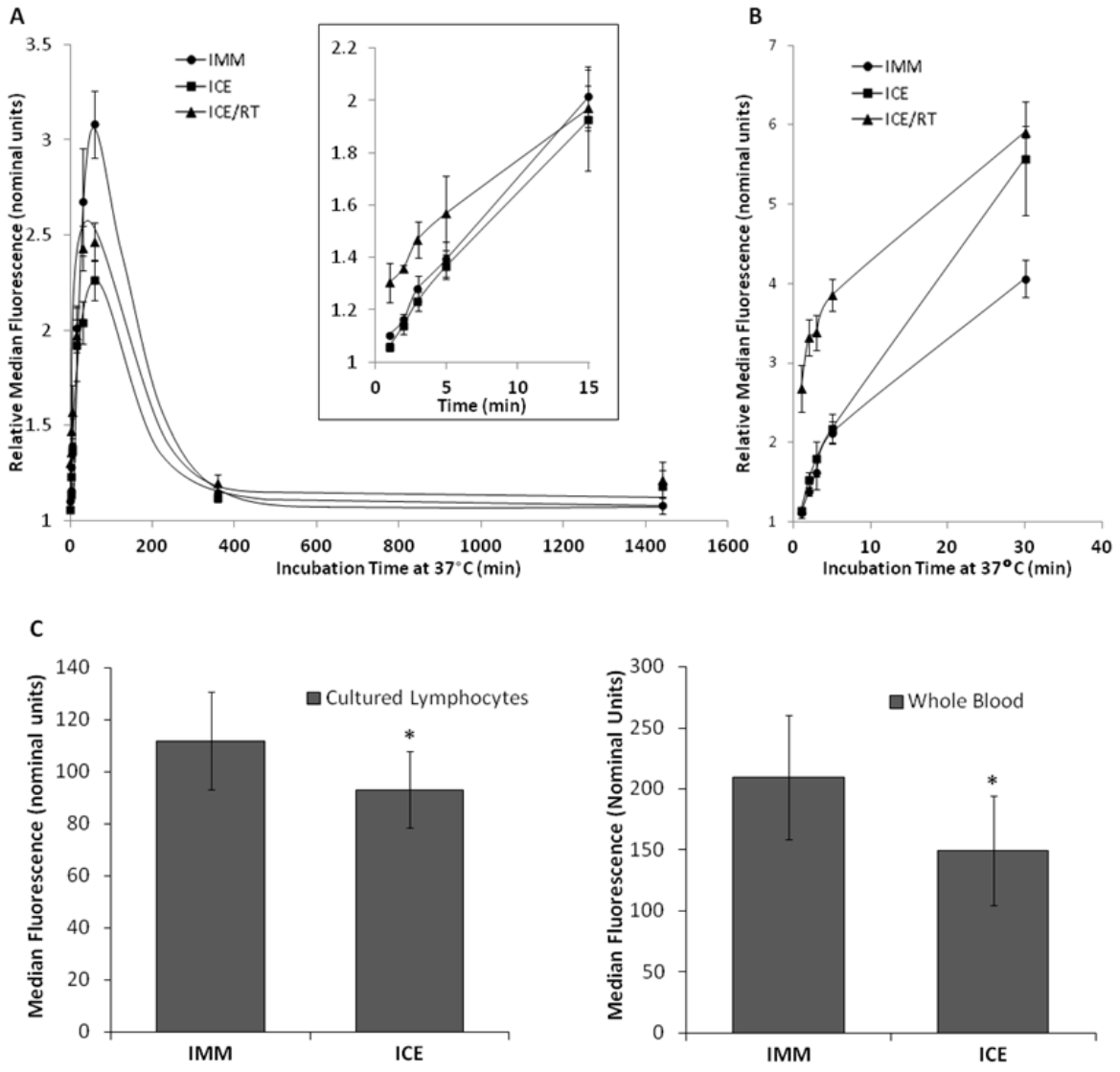

Figure 4.7. Effects of sample handling on the DNA damage response. Cell culture (**A**) or whole blood samples (**B**) were irradiated to 1Gy and fixed immediately using the rapid fixation protocol (RFP) at 1, 2, 3, 5 or 30min following the start of irradiation (**IMM – closed circles**) or placed on ice at the same times. Samples were incubated on ice for 2hr and then fixed using the RFP (**ICE – closed squares**) or incubated at room temperature for and additional hour (**ICE/RT – closed triangles**) before fixation to mimic standard handling practices. Additionally, cell culture samples were assessed at 15min, 1hr, 6hr and 24hr.Samples were assessed for DNA damage by antibody staining for gammaH2AX Standard incubation practices alter the gammaH2AX phosphorylation patterns compared to immediate fixation for both cultured lymphocytes and whole blood. A significant difference in gammaH2AX profiles between immediate, ice and ice/room temperature treatments in cultured lymophocytes is seen (ANOVA $p<0.001$). Unirradiated samples incubated on ice for both cultured lymphocyte (**C – left panel**) and whole blood (**C – right panel**) show a significant decrease in median fluorescence compared to samples fixed immediately ($p<0.05$). The average median fluorescence from three independent experiments is reported with the SEM.

irradiation. By 6 hr gammaH2AX fluorescence is reduced drastically but is still significantly higher than background levels ($p<0.02$). At 24 hr, gammaH2AX fluorescence returns to background levels. Comparison between immediate and ice treatments by ANOVA indicates a significant difference in gammaH2AX profiles ($p<0.001$). Whole blood samples incubated on ice show similar results to those fixed immediately at all measured time points. While at 30 min, the relative gammaH2AX fluorescence is higher for whole blood samples incubated on ice, this difference is not significant (**Figure 4.7B**). Interestingly, unirradiated samples incubated on ice for both cultured lymphocyte and whole blood show a significant decrease ($p<0.05$) in median fluorescence compared to samples fixed immediately (**Figure 4.7C**). Cultured lymphocyte samples incubated an additional hour at room temperature to mimic the time delay and temperature conditions of gradient separation show an increase in relative gammaH2AX median fluorescence at early time points (1-5 min) compared to those fixed immediately following irradiation (**Figure 4.7A insert**). Room temperature incubation increased fluorescence significantly at 1-3 min ($p<0.05$). At 30 and 60 min, relative gammaH2AX median fluorescence is lower, significantly at 60 min ($p<0.01$). Peak gammaH2AX signal is seen between 30 and 60 min after irradiation. By 6 hr, gammaH2AX fluorescence is reduced drastically but is still significantly higher than background levels ($p<0.05$). At 24 hr, gammaH2AX fluorescence returns to background levels. For whole blood samples, room temperature incubation increased fluorescence significantly at all time-points ($p<0.02$) (**Figure 4.7B**).

4.4 Conclusions

When investigating DNA damage repair – which is dynamic in nature – timing is essential. A single snapshot in time fails to provide insight into the total amount of damage

incurred or the rate at which damage is detected and repaired. If biological dose is to be estimated to assess possible risk from radio-diagnostic procedures, these factors have to be taken into account. The results presented here show peak gammaH2AX signal to be between 30 and 60 min following irradiation with 1Gy. Previously, peak H2AX phosphorylation has been seen as quickly as 3min but also as late as 60 (86-89). Differences in irradiation time (which can be on the order of tens of minutes (87) and fixation protocols may account for these discrepancies as well as inherent cell-line characteristics. As indicated here as well as by others (86, 89-91), H2AX phosphorylation is initiated rapidly following irradiation, thus lengthy irradiations, sample handling and fixation procedures may alter the perceived time of maximum signal. Additionally, gammaH2AX foci intensity may follow slower kinetics compared to physical foci formation as the number of H2AX molecules that are phosphorylated increases over time if DSBs are unrepaired (89). Comparison of different treatment protocols and sample handling indicates that whole blood samples are especially sensitive to changes in the environment and thus, it is important to control variables which may have unrelated effects on biological endpoints.

The overall shape of the curves for cultured lymphocytes and whole blood samples are similar. However, it appears that damage detection and repair happen faster in whole blood as indicated by the steeper initial increase in gammaH2AX signal. The relative median fluorescence levels for blood samples are higher than for cultured cells line samples. Fresh WBCs from whole blood may be more radiation sensitive than cultured lymphocytes, or background levels of gammaH2AX may be higher for cultured immortalized lymphocytes than for blood lymphocytes, minimizing the measured effect of radiation on overall gammaH2AX levels.

Samples incubated on ice after incubation at 37°C show similar gammaH2AX profiles to those fixed immediately following 37°C incubation at short time-points (1-15 min), but show significant differences in peak signal, namely, incubation on ice lowers peak gammaH2AX signal. It is possible that multiple mechanisms are activated following IR exposure and some are more temperature sensitive than others. Mechanisms activated within the first 15 min appear to be arrested by ice-cold temperatures. However, mechanisms activated after 15 min appear to be less sensitive to ice-cold temperatures and may continue to either process the DSB themselves, or affect the phosphorylation of H2AX in some way unrelated to the repair process. We have also shown that incubation on ice significantly lowers gammaH2AX signal in unirradiated control samples. This result may explain a recent finding that MRI may induce gammaH2AX foci formation (92). The researchers in this study use the same standard separation method mentioned above with no discussion of sample handling prior to analysis. Control samples are most likely kept on ice until treatment samples are ready. The apparent increase in gammaH2AX signal in samples taken after cardiac MR (CMR) exams may in fact be a reduction in background signal due to the longer incubation on ice, rather than an increase in signal after CMR. Incubation at room temperature following incubation on ice has a dramatic effect on H2AX phosphorylation and de-phosphorylation indicating that gradient separation of blood may not only affect cellular viability and function (93-97), but also allow for processing of DSBs to occur during this unmeasured time before fixation. Furthermore, some studies separate blood samples at 37°C (81-84, 98, 99). If samples continue to process DSBs at room temperature it is likely that they will continue to process damage at 37°C and possibly to a greater extent. Continuation of the repair processes during these incubations may mislead conclusions about

repair kinetics. The higher peak signal observed when using the RFP indicates greater sensitivity which affords the opportunity to examine DNA damage at dose levels below 100mGy with flow cytometry, especially with whole blood samples, which show greater overall gammaH2AX signal. Successful examination of these dose levels provides the ability to assess DNA damage following CT studies *in vivo* with the added benefit of utilizing flow cytometry for analysis, which was previously only used for doses above 100mGy due to lack of sensitivity (89).

Our rapid fixation protocol has features that make it superior to the standard practice for isolation and fixation of whole blood as well as cell culture samples. Membrane integrity is preserved to the same extent of unfixed cells, and not only does the RFP adequately arrest cellular metabolism, it arrests metabolism more fully than the standard fixation protocol. Sample processing by this method allows for immunofluorescent analysis by both microscopy and flow cytometry and offers sensitive assessment of samples irradiated with a range of doses of IR. The RFP provides for the analysis of a population of cells (granulocytes) previously excluded from analysis of whole blood. Although granulocytes are typically excluded from DNA repair kinetics, inclusion of this cell population for assessment of other biological endpoints could prove useful.

Due to logistics with standard fixation protocols, blood samples are stored at various temperatures for various lengths of time after irradiation and procurement. Therefore a data point labeled as “10 minutes post-irradiation” may have come from a sample that incubated on ice for 5 minutes and was separated at room temperature for 30 minutes or from a sample that incubated for 180 minutes on ice and then was separated at 37°C for 30 minutes. Our data raises the question, whether these manipulations perturb accurate measurement of the cellular

response at physiological conditions. While it may not be feasible under certain circumstances to analyze samples immediately after collection, it is important to understand the consequences of such standard practices and how they affect experimental outcomes especially when used for patient analysis. The interest in using biological markers for personalized medicine and clinical diagnostics is growing. To ensure these methods are utilized appropriately it is imperative that the effects of sample handling are minimized. The RFP developed here offers kinetic analysis of H2AX phosphorylation in a practically unperturbed cell system prior to fixation, especially at early time points. Most notably, this protocol eliminates the requirement of cellular separation as well as the need for laboratory equipment for fixation, other than a pipette. Additionally, once fixed and washed, samples can be frozen for storage or transportation. Furthermore, a single sample requires only 300uL of blood for triplicate samples, compared to 6mL needed for current separation techniques. Thus, immediate fixation at the patient site provides convenience, time-savings, resource reduction and more importantly, analysis of a virtually unperturbed cell system, allowing sensitive damage assessment.

4.5 References

81. Kuefner MA, Grudzenski S, Hamann J, et al. Effect of CT scan protocols on x-ray-induced DNA double strand breaks in blood lymphocytes of patients undergoing coronary CT angiography. Eur Radiol 2010; 20:2917 - 2924.

82. Brand M, Sommer M, Achenbach S, et al. X-ray induced DNA double-strand breaks in coronary CT angiography: Comparison of sequential, low-pitch helical and high-pitch helical data acquisition. European journal of radiology 2012; 81:e357-e362.

83. Kuefner MA, Grudzenski S, Schwab SA, et al. X-ray-induced DNA double-strand breaks after angiographic examinations of different anatomic regions. Rofo 2009; 181:374 - 380.

84. Kuefner MA, Grudzenski S, Schwab SA, et al. DNA Double-Strand Breaks and Their Repair in Blood Lymphocytes of Patients Undergoing Angiographic Procedures. Investigative Radiology 2009; 44:440-446.

85. Lobrich M, Rief N, Kuhne M, et al. In vivo formation and repair of DNA double-strand breaks after computed tomography examinations. Proc Natl Acad Sci USA 2005; 102:8984 - 8989.

86. Rogakou EP, Boon C, Redon C, Bonner WM. Megabase Chromatin Domains Involved in DNA Double-Strand Breaks in Vivo. The Journal of Cell Biology 1999; 146:905-916.

87. Rogakou EP, Pilch DR, Orr AH, Ivanova VS, Bonner WM. DNA Double-stranded Breaks Induce Histone H2AX Phosphorylation on Serine 139. Journal of Biological Chemistry 1998; 273:5858-5868.

88. Neumaier T, Swenson J, Pham C, et al. Evidence for formation of DNA repair centers and dose-response nonlinearity in human cells. Proceedings of the National Academy of Sciences of the United States of America 2012; 109:443-448.

89. Rothkamm K, Horn S. gamma-H2AX as protein biomarker for radiation exposure. Annali dell'Istituto superiore di sanità 2009; 45:265-271.

90. Costes SV, Ponomarev A, Chen JL, Nguyen D, Cucinotta FA, Barcellos-Hoff MH. Image-based modeling reveals dynamic redistribution of DNA damage into nuclear sub-domains. Plos Computational Biology 2007; 3:1477-1488.

91. Costes SV, Boissiere A, Ravani S, Romano R, Parvin B, Barcellos-Hoff MH. Imaging Features that Discriminate between Foci Induced by High- and Low-LET Radiation in Human Fibroblasts. Radiation Research 2006; 165:505-515.

92. Fiechter M, Stehli J, Fuchs TA, Dougoud S, Gaemperli O, Kaufmann PA. Impact of cardiac magnetic resonance imaging on human lymphocyte DNA integrity. European Heart Journal 2013.

93. Berger CL, Edelson RL. Comparison of Lymphocyte Function after Isolation by Ficoll-Hypaque Flotation or Elutriation. J Investig Dermatol 1979; 73:231-235.

94. Mita A, Ricordi C, Messinger S, et al. Antiproinflammatory Effects of Iodixanol (OptiPrep)-Based Density Gradient Purification on Human Islet Preparations. Cell Transplantation 2010; 19:1537-1546.

95. Mita A, Ricordi C, Miki A, et al. Purification Method Using Iodixanol (OptiPrep)-Based Density Gradient Significantly Reduces Cytokine Chemokine Production From Human Islet Preparations, Leading to Prolonged Beta-Cell Survival During Pretransplantation Culture. Transplantation proceedings 2009; 41:314-315.

96. Min T, Yi L, Chao Z, et al. Superiority of Visipaque (Iodixanol)-Controlled Density Gradient Over Ficoll-400 in Adult Porcine Islet Purification. Transplantation proceedings 2010; 42:1825-1829.

97. Sroka J, Kordecka A, WÅ‚osiak Pa, Madeja Z, Korohoda Wo. Separation methods for isolation of human polymorphonuclear leukocytes affect their motile activity. European Journal of Cell Biology 2009; 88:531-539.

98. Zwicker F, Swartman B, Sterzing F, et al. Biological in-vivo measurement of dose distribution in patients' lymphocytes by gamma-H2AX immunofluorescence staining: 3D conformal- vs. step-and-shoot IMRT of the prostate gland. Radiation Oncology 2011; 6:62.

99. Kuefner MA, Hinkmann FM, Alibek S, et al. Reduction of X-Ray Induced DNA Double-Strand Breaks in Blood Lymphocytes During Coronary CT Angiography Using High-Pitch Spiral Data Acquisition With Prospective ECG-Triggering. Investigative Radiology 2010; 45:182-187 110.1097/RLI.1090b1013e3181d1093eddf.

Chapter 5: *In vitro* Characterization of the DNA Damage Response

5.1 Introduction

Unlike radiation therapy, where specific deterministic effects of IR have been characterized (100), the lack of scientific evidence for specific biological mechanisms in response to low doses of IR makes defining risk especially imprecise. Furthermore, the relationship between physical and biological dose following IR is especially unclear for low dose modalities such as CT (101-104). It is essential to define the biological mechanisms of damage and repair of low doses of IR to assess its risks and avoid potential adverse health effects.

Current methods for accessing the biological damage of ionizing radiation at diagnostic radiology dose levels have significant variability in both methodology and results (105), and fail to examine irradiation schemes similar to those experienced in many CT exams (106). Instead of a single exposure, many CT exams are comprised of series of scans separated on the order of minutes. Each scan can range from extremely small doses such as CT projection radiographs (0.2 to 1.0mGy) (107) and pre-injection, contrast monitoring scans (1-3mGy) to scans in the range of 6-100mGy. Not only are the biological consequences of these relatively low dose exposures still unclear, but whether doses within an exam protocol are simply additive remains to be determined. Moreover, the dynamic nature of DNA double strand break repair suggests that kinetic analysis may be required for different irradiation protocols. Here, the differences in DNA damage repair kinetics between dose levels are characterized and the effects of short-interval fractionated low-dose irradiation (multi-pass) schemes on phosphorylation of H2AX are examined. Additionally, the effects of two different classes of radio-protective agents on H2AX phosphorylation at different dose levels and radiation schemes are characterized.

Understanding the biological response at low dose levels will create a deeper appreciation of the unique risks involved in diagnostic radiology procedures, better characterize the possible role of external agents in protection against radiation damage and offer a more thorough understanding of the safety for diagnostic radiology.

5.2 Materials and Methods

5.2.1 gammaH2AX Dose-Response Kinetics

To establish baseline dose-response kinetics of DNA repair, both cell culture and whole blood samples were irradiated with the RS320 irradiator to doses ranging from 50-1000mGy (50, 100, 500, 1000mGy) and incubated in a 37°C water bath for 5 min-24 hr (5, 15, 30, 60 min, 2, 6, 24 hr). Whole blood samples degraded when kept at 37°C for longer than 2 hr, making a 24 hr time point unfeasible, thus a shorter kinetic curve was generated for whole blood samples (5, 15, 30, 60 min, 2 hr).

5.2.2 Assay Sensitivity

Once baseline kinetics were established, assay sensitivity at 30 min was tested by irradiating whole blood samples to doses as low as 2 mGy (2, 4, 5, 10, 20, 40mGy) using a CT scanner as described in the Materials and Methods chapter.

5.2.3 Multi-Fraction Low Dose Irradiations

To better understand the damage kinetics induced by typical clinical CT protocols which often include several scans separated in time, ESW-WT3 lymphocytes were exposed to 20, 40, or 60mGy in 20mGy fractionated exposures separated by two minutes or as single exposures. Samples were analyzed at 15-60 min and 24 hr after IR exposure. To account for any possible differences in repair kinetics during the fractionation periods, two timing schemes were

employed: one where time points were measured from the start of radiation exposure (MPS) and a second where time points were measured from the end of radiation exposure (MPE). Additionally, to investigate if the response patterns observed with 20mGy fractions could be extended to fractions with higher doses samples were irradiated with the following schemes: two 40mGy doses separated by two minutes with an equivalent 80mGy single dose control or two 60mGy doses separated by two minutes with an equivalent 120mGy single dose control. These samples were evaluated at 30 min after IR exposure based on the differential response seen for 20mGy fractions.

5.2.4 Sample fixation

Irradiated samples were fixed immediately following incubation, as described previously (6), to ensure analysis as close to physiological conditions as possible. Following fixation and washing samples were stained for immunofluorescent analysis immediately.

5.2.5 Immunofluorescent Analysis

Following immunofluorescent staining for gammaH2AX as described in the Materials and Methods chapter, H2AX phosphorylation after IR exposure was assessed by flow cytometry to measure the biological response to IR. Samples were analyzed on a BD LSRFortessa flow cytometer with FACSDIVA 6 software package. (Becton, Dickinson and Company, Franklin Lakes, New Jersey, USA). Forward and side scatter gating was used to isolate healthy cells and 20,000 events were collected for each sample. Average median fluorescence normalized to non-irradiated controls was determined from three independent experiments and reported with the standard error of the mean (SEM).

5.2.6 Whole Genome Shotgun Sequencing (RNASeq)

To characterize any differential gene transcription between low and high doses, total mRNA content was analyzed by RNASeq. Cultured ESW-WT3 lymphocytes were harvested, irradiated to 20 or 1000mGy and incubated at 37°C for 30 min or 6 hr. Non-irradiated control samples were included for each time point. Following incubation, $2x10^6$ cells of each treatment were concentrated into 1mL ice cold PBS, centrifuged at 300g for 5 min and the supernatant discarded. Cells were lysed with 1mL TRIZOL reagent by repetitive pipetting, incubated at room temperature for 5 min then placed in a -20°C freezer until ready for RNA isolation and purification. Samples were thawed on ice and RNA extraction and purification was carried out with the RNeasy Mini Kit (QIAGEN, Germantown, MD, USA Catalog No. 74104). Samples were placed in a -80°C freezer until ready for RNASeq analysis. Samples were thawed on ice and RNA concentration was quantified by NonoDrop. cDNA libraries were generated for each sample with the Illumina TrueSeq Stranded Total RNA Sample Preparation Kit (Illumina, San Diego, CA, USA Catalog No. RS-122-2101). Once cDNA libraries were generated, a small amount of each sample was run on a 2% agarose gel to confirm quality and DNA concentration was quantified by both NanoDrop and Qubit analysis. Samples were then placed in a -80°C freezer until sequencing at the UCLA BSCRC Sequencing Core facility. Once available, sequencing data was analyzed using Microsoft Excel. Reads per kilobase per million (RPKM) values were generated for each probe and for each treatment by the following equation: RPKM = (Rx1E9)/NL, where R is the number of reads counted for each probe, N is the total number of reads for each treatment and L is the length of the specific probe. RPKM provides a normalization of the number of reads between different RNA species to remove biases due to preparation and sequencing between transcripts of different lengths. Probes were assigned to respective gene

labels. Probes 200kB or less in length were discarded as these are typically small RNAs for which this analysis is inadequate. Probes were selected only if at least one of the treatment RPKM values were equal to or greater than 2. Genes with differential transcription patterns were then selected based on a two-fold difference (increase or decrease) from baseline (non-irradiated) samples from the same time point. Two independent experiments were compared.

5.2.7 Radio-protector Analysis

Cultured lymphocytes were exposed to two different classes of agents known to alter the response to IR. N-acetyl cysteine (NAC) was added either 30 min prior to, or immediately following irradiation to a final concentration of 500uM. Tetracycline (TET) was added 3 hr prior to irradiation to a final concentration of 20uM. Samples were irradiated to 20mGy or 1Gy and incubated at 37°C for 15, 30 or 60 min and 24 hr as indicated and analyzed for gammaH2AX fluorescence as described above. Additional samples were irradiated to 60mGy either as single exposures or three fractions of 20mGy similar to previous multi-pass experiments at 60 min. Control samples treated with PBS were included for comparison.

5.3 Results

5.3.1 Both the kinetics and extent of H2AX phosphorylation are dose dependent

H2AX phosphorylation and de-phosphorylation kinetics are dependent on the magnitude of the radiation dose delivered, as shown in Figures 1 and 3. All doses show a steep increase in relative gammaH2AX median fluorescence after short incubation times for both cultured (**Figure 5.1**) and whole blood lymphocytes (**Figure 5.3**). For cultured lymphocytes, peak gammaH2AX signal is seen between 30 and 60 min after irradiation (**Figure 5.1 insert**). However, the signal from 500mGy and 1Gy irradiations appears to peak earlier than 100mGy.

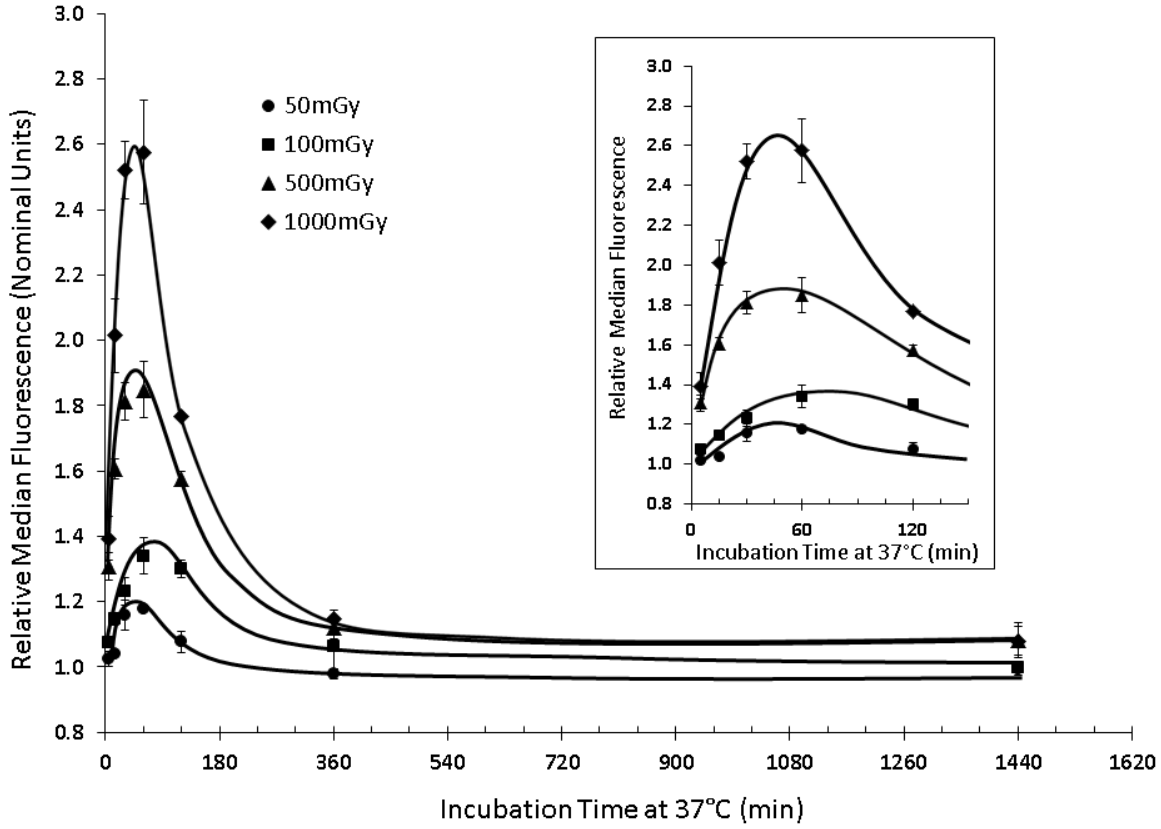

Figure 5.1. Kinetic response to different dose levels in cultured human lymphocytes. Cell culture samples were irradiated to doses ranging from 50-1000mGy and incubated T 37°C for 5min-24hr. Peak gammaH2AX signal is seen between 30 and 60 minutes after irradiation. After 2hrs, gammaH2AX signal is reduced but is still higher than background levels ($p<0.05$) and is reduced further at 6hrs. At 24hrs, gammaH2AX fluorescence returns to background levels.

50mGy shows a similar peak time to that of higher doses. After 2 hr, the gammaH2AX signal is reduced but is still higher than background levels and is reduced further at 6 hr. At 24 hr, gammaH2AX fluorescence returns to background or slightly above background levels.

Damage induction and detection, measured by phosphorylation of H2AX, show a clear dose response, albeit different, at all time-points from 5 min-6 hr for ESW-WT3 lymphocytes (**Figure 5.2**). The most linear response is at 30 min (R^2=0.99995). For whole blood samples, peak gammaH2AX signal is seen between 15 and 60 min after irradiation. Signal after 500mGy

and 1Gy seem to peak earlier than both 50 and 100mGy which appear to peak at similar times between 30 and 60 min after irradiation.

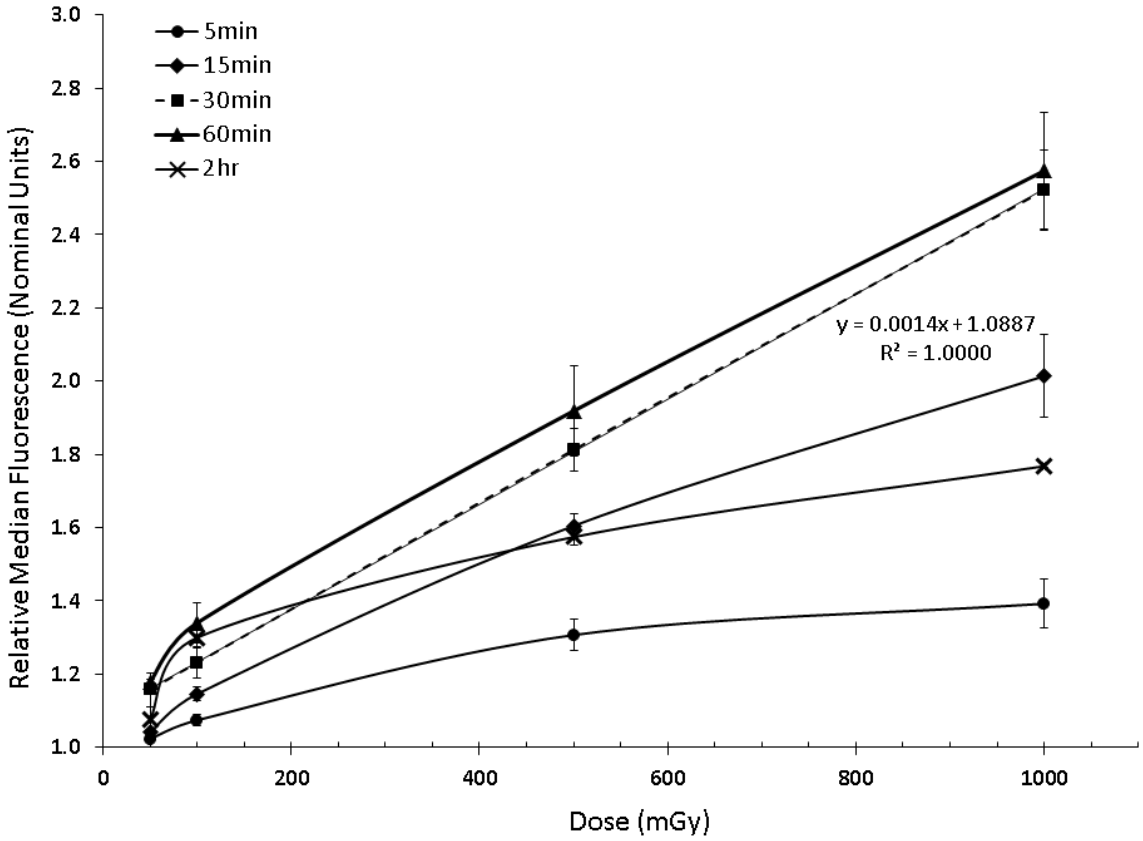

Figure 5.2. Dose response at different time points (5min-2hr) in cultured human lymphocytes. Damage induction and detection, measured by phosphorylation of H2AX, show a clear dose response, albeit different, at all time-points from 5min-6hr for ESW-WT3 lymphocytes. The most linear response is at 30 minutes (R^2=0.99995).

Similar to ESW-WT3 lymphocytes, whole blood lymphocytes show a clear dose response at all time-points evaluated (**Figure 5.4**) and this response ranges in linearity with the most linear occurring at 15 min (R^2=0.9994). For both cultured and whole blood lymphocytes, divergence from a linear dose response is observed after peak H2AX phosphorylation. The absolute signals for whole blood lymphocytes were generally higher than that of ESW-WT3 lymphocytes.

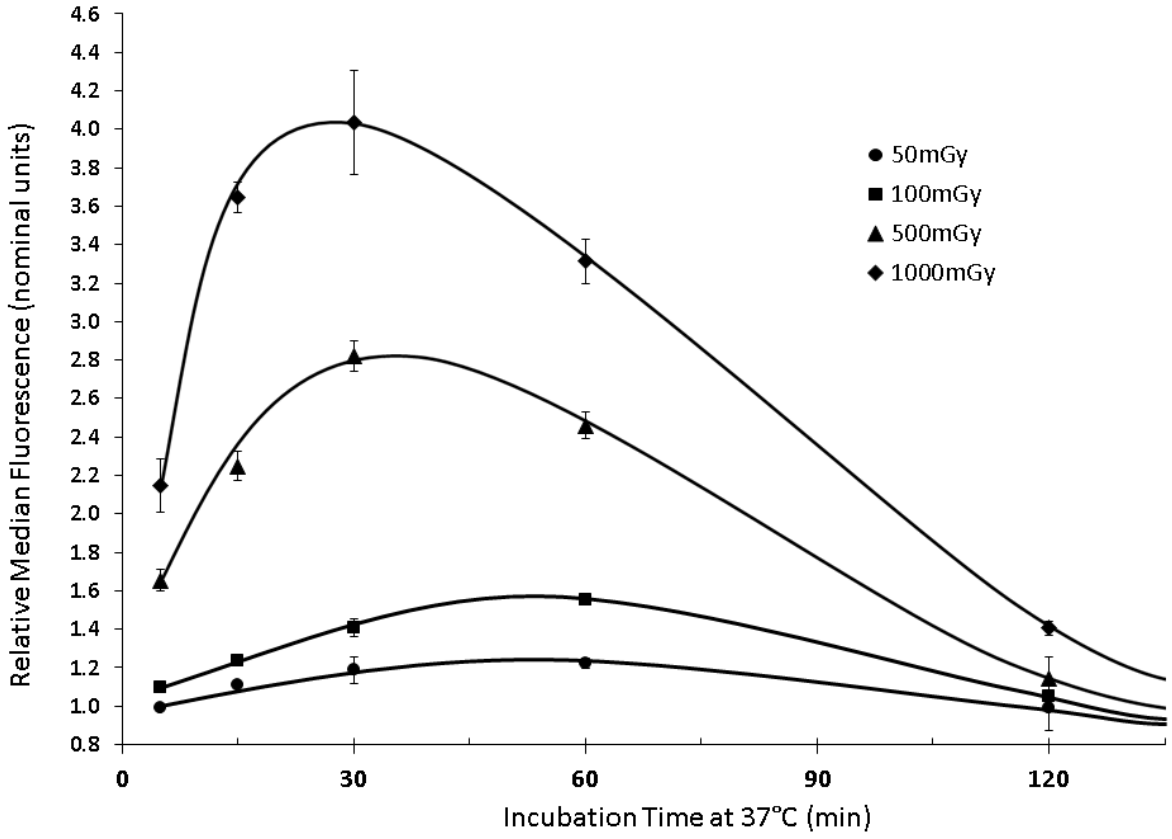

Figure 5.3. Kinetic response to different dose levels in whole blood lymphocytes. Whole blood samples were irradiated to doses ranging from 50-1000mGy and incubated at 37°C for 5min-2hr. Whole blood samples degraded when kept at 37°C longer than 2hr, making a 24hr time point unfeasible, thus a shorter kinetic curve was generated. Peak gammaH2AX signal is seen between 15 and 60 minutes after irradiation.

Assay sensitivity for whole blood was tested at 30 min as this time point was close to peak signal as indicated by the previous kinetic analysis and deemed most feasible for future patient studies. Significant increase in gammaH2AX signal was observed after as little as 5mGy at 30 min (**Figure 5.5A**). Although, an increase was seen after 4mGy, this difference was not statistically significant. This low-dose data correlates well with the quadratic curve fitted to the higher dose data from the same 30 min time-point (R^2=0.9989) (**Figure 5.5B**).

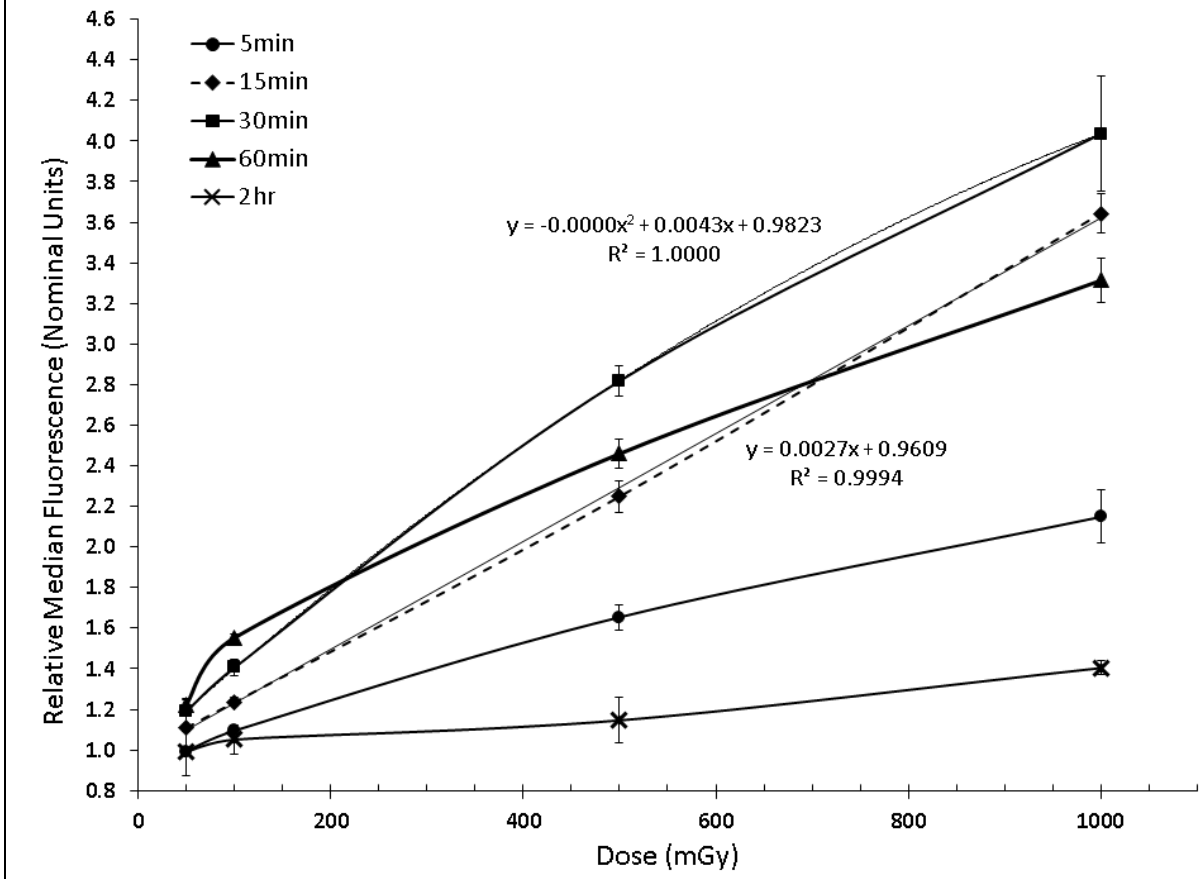

Figure 5.4. Dose response at different time points in whole blood lymphocytes. Whole blood lymphocytes show a clear dose response, albeit different, at all time-points evaluated and this response ranges in linearity but reaches its most linear at 15 minutes (R^2=0.9994).

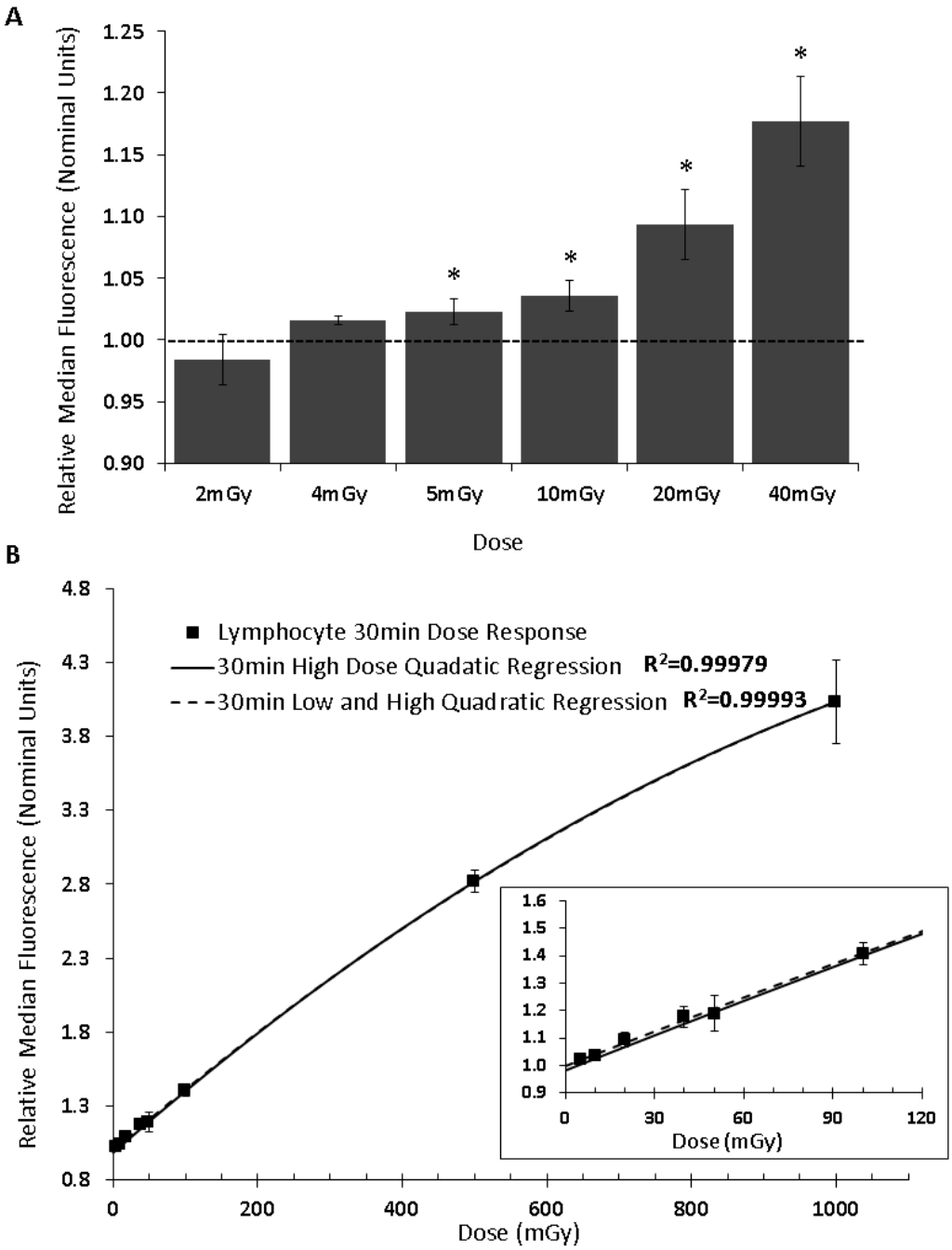

Figure 5.5. gammaH2AX fluorescence analysis sensitivity in whole blood lymphocytes. **A.** Significant increase ($p<0.05$) in gammaH2AX signal was seen after a little as 5mGy at 30min. Although an increase was seen after 4mGy, this difference was not statistically significant. **B.** Low-dose data correlates well with the quadratic curve fitted to the higher dose data from the same 30min time-point (solid line) – R^2=0.9989, demonstrating an acceptable sensitivity down to 5mGy at 30 minutes. However, low dose data was collected using a Siemens Sensation 64-slice CT scanner at 120kVp which varies in IR energy and spectrum from the RS320 Irradiation System used for the higher dose irradiations. Inset shows blow-up of low dose region illustrated in (B).

5.3.2 RNASeq Analysis

There was little overlap in genes that met selection criteria between the two experiments. Of the three genes that did overlap, each showed different expression patterns between experiments. Due to the lack of overlap, each experiment was examined and presented individually. In the first experiment, 30 genes met the selection criteria, of which 12 were up-regulated (**Figure 5.6A**) and 18 were down-regulated at 30min and/or 6hr (**Figure 5.6B**). Complete results for the first experiment are reported in Table 5.1 (up-regulated) and Table 5.2 (down-regulated). One up-regulated gene is classified as a solely low-dose fast

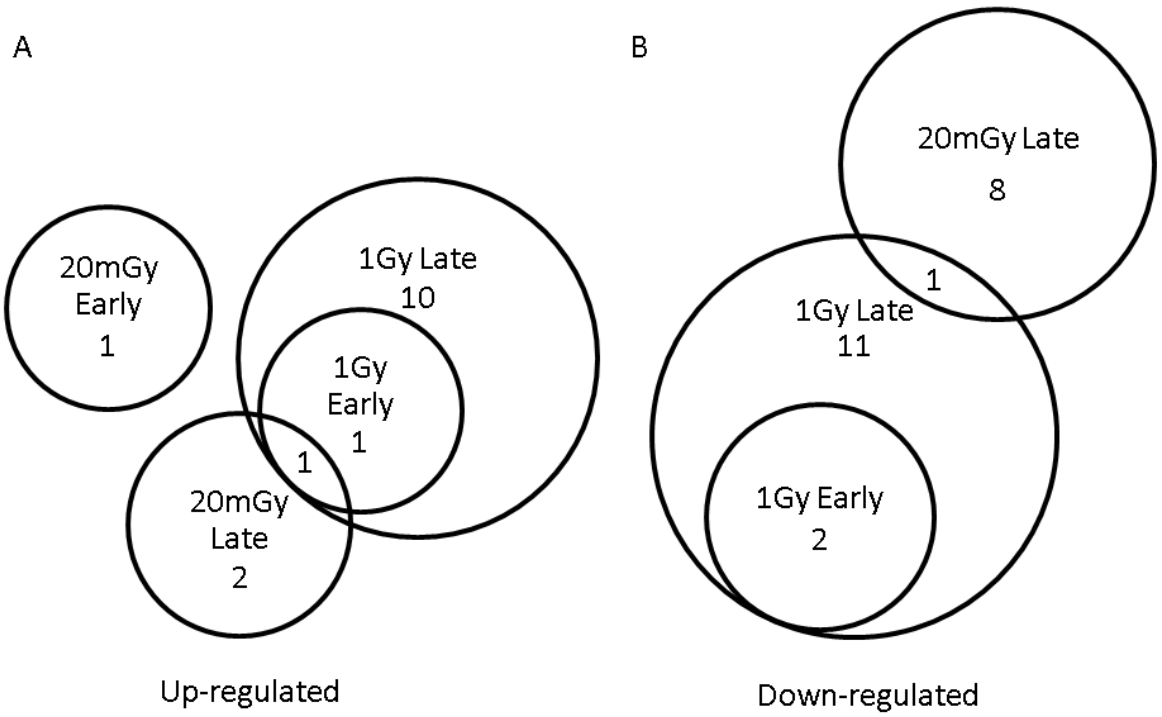

Figure 5.6. Differential regulation of RNA expression for experiment 1 (2012). Cultured lymphocytes were harvested, irradiated to 20 or 1000mGy and incubated at 37°C for 30min or 6hr. RNA transcripts were analyzed by RNASeq. Genes with differential transcription pattern were selected based on a two-fold increase or decrease from baseline (non-irradiated) samples from the same time point. Non-irradiated control samples were included for each time point. 30 genes met the selection criteria, of which 12 were up-regulated and 18 were down-regulated at 30min and/or 6hr.

Table 5.1. RNASeq Experiment 1 Complete Up-regulation Results

Gene Symbol	Length (bp)	Number of Reads						RPKM = (R*1E9)/(LN)						Fold Increase				
		0Gy 30min	0Gy 6hr	20mGy 30min	20mGy 6hr	1Gy 30min	1Gy 6hr	0Gy 30min	0Gy 6hr	20mGy 30min	20mGy 6hr	1Gy 30min	1Gy 6hr	0Gy 6hr	20mGy 30min	20mGy 6hr	1Gy 30min	1Gy 6hr
NOXO1	1132	16	35	39	37	33	27	0.790	2.047	2.028	1.744	1.275	1.363	↑2.592	↑2.567	→0.852	→1.615	→0.666
LOC391322	563	11	8	12	22	15	10	1.092	0.941	1.255	2.085	1.166	1.015	→0.862	→1.149	↑2.216	→1.068	→1.079
fxyd1	547	10	10	16	38	29	24	1.022	1.211	1.722	3.708	2.320	2.507	→1.185	→1.685	↑3.063	↑2.271	↑2.071
RPL23AP7	1231	1	1	2	7	3	44	0.045	0.054	0.096	0.303	0.107	2.042	→1.185	-	-	-	↑37.964
C3orf54	1040	111	28	88	64	114	72	5.965	1.783	4.980	3.284	4.796	3.955	↓0.299	→0.835	→1.842	→0.804	↑2.219
RMRP	268	2	7	1	14	2	86	0.417	1.730	0.220	2.788	0.327	18.334	↑4.147	→0.527	→1.612	→0.783	↑10.600
FHL2	1696	120	53	88	98	99	149	3.954	2.069	3.054	3.084	2.554	5.019	→0.523	→0.772	→1.490	→0.646	↑2.426
ZNF385A	2093	389	240	373	404	538	631	10.386	7.593	10.489	10.301	11.247	17.225	→0.731	→1.010	→1.357	→1.083	↑2.268
LOC253573	2295	108	81	109	119	123	214	2.630	2.337	2.795	2.767	2.345	5.327	→0.889	→1.063	→1.184	→0.892	↑2.280
c1orf183	5838	334	180	289	240	422	476	3.197	2.042	2.914	2.194	3.163	4.658	→0.639	→0.911	→1.075	→0.989	↑2.282
Cmbl	4047	183	165	164	210	238	425	2.527	2.700	2.385	2.769	2.573	6.000	→1.068	→0.944	→1.026	→1.018	↑2.222
SESN1	2681	124	164	174	205	166	381	2.585	4.051	3.820	4.081	2.709	8.119	→1.567	→1.478	→1.007	→1.048	↑2.004

Table 5.2. RNASeq Experiment 1 Complete Down-regulation Results

Gene Symbol	Length (bp)	Number of Reads						RPKM = (R*1E9)/(LN)						Fold Increase				
		0Gy 30min	0Gy 6hr	20mGy 30min	20mGy 6hr	1Gy 30min	1Gy 6hr	0Gy 30min	0Gy 6hr	20mGy 30min	20mGy 6hr	1Gy 30min	1Gy 6hr	0Gy 6hr	20mGy 30min	20mGy 6hr	1Gy 30min	1Gy 6hr
CECR4	340	4	19	9	11	10	12	0.657	3.700	1.558	1.727	1.287	2.016	↑5.628	-	↓0.467	→1.957	→0.545
Kcnip2	907	18	38	17	16	22	24	1.109	2.774	1.103	0.941	1.061	1.512	↑2.501	→0.995	↓0.339	→0.957	→0.545
MTOR-AS1	706	22	23	27	14	41	16	1.741	2.157	2.251	1.058	2.541	1.295	→1.239	→1.293	↓0.491	→1.459	→0.600
Snhg10	275	5	20	4	11	5	14	1.016	4.816	0.856	2.135	0.796	2.909	↑4.740	→0.843	↓0.443	→0.783	→0.604
OR51B5	818	32	47	29	29	43	34	2.186	3.805	2.087	1.892	2.300	2.375	→1.740	→0.954	↓0.497	→1.052	→0.624
LOC284009	576	7	19	5	11	21	21	0.679	2.184	0.511	1.019	1.595	2.083	↑3.216	→0.752	↓0.467	-	→0.954
SCARNA2	420	10	13	5	7	8	24	1.331	2.050	0.701	0.889	0.833	3.265	→1.540	→0.527	↓0.434	→0.626	→1.593
GRIA3	989	21	33	16	20	20	15	1.187	2.209	0.952	1.079	0.885	0.867	→1.862	→0.802	↓0.488	→0.746	↓0.392
UCN	615	7	19	8	17	17	10	0.636	2.046	0.766	1.475	1.209	0.929	↑3.216	→1.204	→0.721	→1.901	↓0.454
LOC100287722	1734	68	99	68	76	82	55	2.192	3.781	2.308	2.339	2.069	1.812	→1.725	→1.053	→0.619	→0.944	↓0.479
TSPAN7	1806	47	60	50	59	52	30	1.454	2.200	1.629	1.743	1.260	0.949	→1.513	→1.120	→0.793	→0.866	↓0.431
CITED4	1291	154	84	94	80	131	45	6.666	4.308	4.285	3.307	4.440	1.991	→0.646	→0.643	→0.768	→0.666	↓0.462
LOC729234	852	37	26	26	23	29	12	2.427	2.021	1.796	1.441	1.489	0.805	→0.833	→0.740	→0.713	→0.614	↓0.398
SAP25	835	101	160	60	148	73	89	6.760	12.688	4.229	9.459	3.825	6.090	→1.877	→0.626	→0.746	→0.566	↓0.480
Ube2s	1191	738	551	575	579	483	264	34.628	30.635	28.416	25.945	17.744	12.664	→0.885	→0.821	→0.847	→0.512	↓0.413
Lrrc26	1195	564	500	432	409	367	259	26.375	27.706	21.277	18.266	13.437	12.383	→1.050	→0.807	→0.659	→0.509	↓0.447
Tmem160	655	724	506	474	452	462	293	61.771	51.154	42.593	36.828	30.861	25.557	→0.828	→0.690	→0.720	↓0.500	↓0.500
MESP1	1162	82	72	47	70	47	37	3.944	4.103	2.381	3.215	1.770	1.819	→1.040	→0.604	→0.784	↓0.449	↓0.443

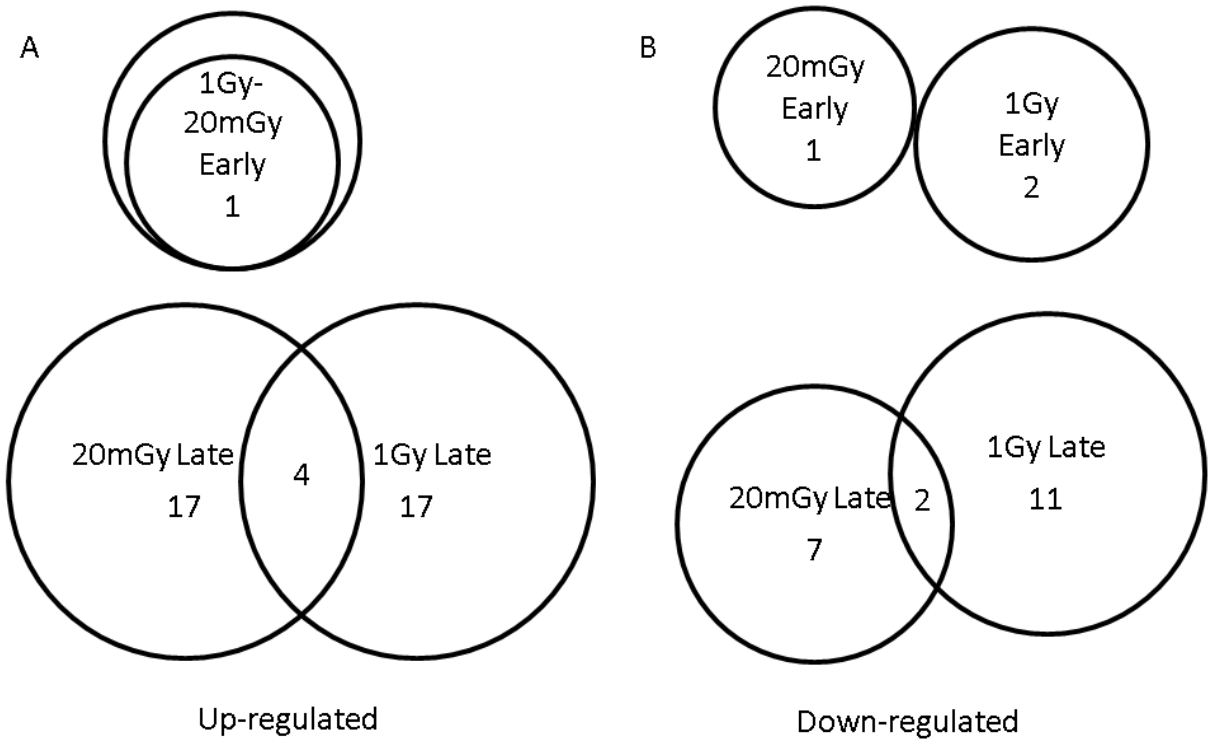

Figure 5.7. Differential regulation of RNA expression for experiment 2 (2013). Cultured lymphocytes were harvested, irradiated to 20 or 1000mGy and incubated at 37°C for 30min or 6hr. RNA transcripts were analyzed by RNASeq. Genes with differential transcription pattern were selected based on a two-fold increase or decrease from baseline (non-irradiated) samples from the same time point. Non-irradiated control samples were included for each time point. 50 genes met the selection criteria, of which 31 were up-regulated and 19 were down-regulated at 30min and/or 6hr.

response gene (NOXO1) as it is up-regulated at 30 min for only 20mGy. 10 up-regulated genes are classified as solely slow response genes as these up-regulated at 6 hr for both 20mGy and 1Gy. One gene is up-regulated at 30 min for 1Gy and remains up-regulated at 6hr for both 20mGy and 1Gy (fxyd1). 16 down-regulated genes are classified as solely slow response genes as these are down-regulated at 6 hr for 20mGy and/or 1Gy. One of these genes is down-regulated at 6 hr for both 20mGy and 1Gy (GRIA3). Two genes are down-regulated at 30 min for 1Gy and remain down-regulated at 6hr.

Table 5.3. RNASeq Experiment 2 Complete Up-regulation Results

Gene Symbol	Length (bp)	Number of Reads						RPKM = (R*1E9)/(LN)						Fold Increase				
		0Gy 30min	0Gy 6hr	20mGy 30min	20mGy 6hr	1Gy 30min	1Gy 6hr	0Gy 30min	0Gy 6hr	20mGy 30min	20mGy 6hr	1Gy 30min	1Gy 6hr	0Gy 6hr	20mGy 30min	20mGy 6hr	1Gy 30min	1Gy 6hr
SNHG9	233	21	57	54	42	65	63	2.628	10.647	5.962	8.587	6.711	10.651	↑ 4.051	↑ 2.268	→ 0.807	↑ 2.554	→ 1.000
HIST1H4B	357	1	7	3	20	3	14	0.082	0.853	0.216	2.669	0.202	1.545	↑ 10.447	-	↑ 3.127	-	→ 1.810
CD9	1314	111	79	136	152	168	126	2.463	2.617	2.663	5.511	3.076	3.777	→ 1.062	→ 1.081	↑ 2.106	→ 1.249	→ 1.444
DHRS4	1278	226	76	293	189	267	159	5.157	2.588	5.898	7.045	5.026	4.901	→ 0.502	→ 1.144	↑ 2.722	→ 0.975	→ 1.894
EGFL7	1302	55	49	70	90	86	29	1.232	1.638	1.383	3.293	1.589	0.877	→ 1.330	→ 1.123	↑ 2.010	→ 1.290	→ 0.536
FAM159A	698	38	14	52	31	43	19	1.588	0.873	1.916	2.116	1.482	1.072	→ 0.550	→ 1.207	↑ 2.424	→ 0.934	→ 1.228
GH1	376	5	14	4	27	3	25	0.388	1.620	0.274	3.421	0.192	2.619	↑ 4.179	→ 0.706	↑ 2.111	-	→ 1.616
IGSF1	1787	172	55	140	109	165	83	2.807	1.340	2.015	2.906	2.221	1.830	↓ 0.477	→ 0.718	↑ 2.169	→ 0.791	→ 1.366
LIN7B	755	23	19	30	36	35	30	0.888	1.095	1.022	2.272	1.115	1.565	→ 1.233	→ 1.151	↑ 2.074	→ 1.255	→ 1.429
LINC00278	530	21	10	28	26	25	18	1.155	0.821	1.359	2.337	1.135	1.338	→ 0.711	→ 1.176	↑ 2.846	→ 0.982	→ 1.629
RPS27	351	14	9	15	21	14	15	1.163	1.116	1.099	2.850	0.960	1.683	→ 0.959	→ 0.945	↑ 2.554	→ 0.825	→ 1.509
SCARNA17	421	6	12	3	26	12	15	0.416	1.241	0.183	2.942	0.686	1.404	↑ 2.985	-	↑ 2.372	→ 1.650	→ 1.131
TERC	451	2	7	4	19	2	10	0.129	0.676	0.228	2.007	0.107	0.873	↑ 5.224	→ 1.764	↑ 2.971	→ 0.825	→ 1.293
HIST4H4	412	18	4	28	24	25	30	1.274	0.423	1.748	2.775	1.460	2.868	↓ 0.332	→ 1.372	↑ 6.568	→ 1.146	↑ 6.788
SLC38A6	1649	72	18	55	70	84	52	1.273	0.475	0.858	2.022	1.226	1.242	↓ 0.373	→ 0.674	↑ 4.257	→ 0.963	-
GNG8	213	4	7	8	19	7	19	0.548	1.430	0.966	4.249	0.791	3.514	↑ 2.612	→ 1.764	↑ 2.971	→ 1.444	↑ 2.457
SPTLC1	968	154	20	138	50	171	65	4.639	0.899	3.667	2.461	4.250	2.645	↓ 0.194	→ 0.791	↑ 2.737	→ 0.916	↑ 2.942
TAF1A	1796	191	41	209	78	217	128	3.101	0.994	2.994	2.069	2.907	2.808	↓ 0.320	→ 0.965	↑ 2.082	→ 0.937	↑ 2.826
ACPP	3219	351	88	393	113	441	195	3.180	1.190	3.141	1.672	3.296	2.386	↓ 0.374	→ 0.988	→ 1.406	→ 1.037	↑ 2.006
ARL6	1838	92	43	101	47	129	99	1.460	1.018	1.414	1.218	1.689	2.122	→ 0.698	→ 0.968	→ 1.196	→ 1.157	↑ 2.084
C9orf72	1873	181	34	169	58	170	100	2.818	0.790	2.321	1.475	2.184	2.103	↓ 0.280	→ 0.824	↑ 1.867	→ 0.775	↑ 2.662
CASP1	434	37	19	49	25	50	42	2.486	1.905	2.904	2.744	2.772	3.812	→ 0.766	→ 1.168	→ 1.440	→ 1.115	↑ 2.001
LOC100506639	1548	130	36	151	54	149	93	2.449	1.012	2.509	1.662	2.316	2.367	↓ 0.413	→ 1.025	→ 1.642	→ 0.946	↑ 2.338
MRPS18C	1121	247	97	286	115	273	300	6.425	3.766	6.563	4.887	5.859	10.542	→ 0.586	→ 1.021	→ 1.298	→ 0.912	↑ 2.799
NEK1	5541	626	149	615	162	626	336	3.294	1.170	2.855	1.393	2.718	2.389	↓ 0.355	→ 0.867	→ 1.190	→ 0.825	↑ 2.041
PRR4	564	28	17	31	24	36	38	1.448	1.312	1.414	2.027	1.536	2.654	→ 0.906	→ 0.977	→ 1.545	→ 1.061	↑ 2.023
PSMC6	1593	92	43	86	63	118	103	1.684	1.175	1.389	1.884	1.782	2.547	→ 0.698	→ 0.825	→ 1.604	→ 1.058	↑ 2.168
RDM1	545	42	14	71	12	45	37	2.247	1.118	3.351	1.049	1.986	2.674	↓ 0.497	→ 1.491	→ 0.938	→ 0.884	↑ 2.392
SCARNA13	275	9	7	16	11	19	16	0.954	1.108	1.497	1.906	1.662	2.292	→ 1.161	→ 1.568	→ 1.720	→ 1.742	↑ 2.069
UCN	615	18	25	31	27	35	58	0.853	1.769	1.297	2.091	1.369	3.715	↑ 2.073	→ 1.519	→ 1.182	→ 1.604	↑ 2.100
VAMP4	2853	383	69	356	114	384	204	3.915	1.053	3.210	1.904	3.238	2.817	↓ 0.269	→ 0.820	→ 1.808	→ 0.827	↑ 2.676

Table 5.4. RNASeq Experiment 2 Complete Up-regulation Results

Gene Symbol	Length (bp)	Number of Reads						RPKM = (R*1E9)/(LN)						Fold Decrease				
		0Gy 30min	0Gy 6hr	20mGy 30min	20mGy 6hr	1Gy 30min	1Gy 6hr	0Gy 30min	0Gy 6hr	20mGy 30min	20mGy 6hr	1Gy 30min	1Gy 6hr	0Gy 6hr	20mGy 30min	20mGy 6hr	1Gy 30min	1Gy 6hr
HIST1H2BH	425	32	45	17	27	25	29	2.196	4.608	1.029	3.026	1.415	2.688	⇧2.099	⇩0.469	⇨0.657	⇨0.645	⇨0.583
LEPROT	597	42	20	31	11	25	25	2.051	1.458	1.336	0.878	1.007	1.650	⇨0.711	⇨0.651	⇨0.602	⇩0.491	⇨1.131
RPL23AP7	1231	85	5	58	6	6	8	2.014	0.177	1.212	0.232	0.117	0.256	⇩0.088	⇨0.602	⇨1.314	⇩0.058	⇨1.448
C8orf47	596	91	69	144	30	99	95	4.452	5.039	6.215	2.398	3.996	6.279	⇨1.132	⇨1.396	⇩0.476	⇨0.898	⇨1.246
LOC100130275	1304	103	172	124	71	156	161	2.303	5.741	2.446	2.594	2.878	4.864	⇧2.492	⇨1.062	⇩0.452	⇨1.250	⇨0.847
TRAPPC2P1	732	103	57	85	26	108	48	4.103	3.389	2.987	1.692	3.550	2.583	⇨0.826	⇨0.728	⇩0.499	⇨0.865	⇨0.762
SMIM1	546	38	43	49	15	56	29	2.029	3.428	2.309	1.309	2.468	2.092	⇨1.689	⇨1.138	⇩0.382	⇨1.216	⇨0.610
EXD3	2565	164	200	168	90	193	120	1.864	3.394	1.685	1.672	1.810	1.843	⇨1.820	⇨0.904	⇩0.493	⇨0.971	⇨0.543
APOC1	461	12	56	26	19	35	26	0.759	5.287	1.451	1.963	1.827	2.222	⇧6.965	⇨1.911	⇩0.371	-	⇩0.420
RPS4Y2	888	3	363	9	9	27	7	0.099	17.791	0.261	0.483	0.731	0.311	⇧180.592	-	⇩0.027	-	⇩0.017
NNAT	1221	28	60	33	30	35	27	0.669	2.139	0.695	1.170	0.690	0.871	⇧3.198	⇨1.040	⇨0.547	⇨1.031	⇩0.407
MIXL1	699	55	51	93	30	86	19	2.294	3.175	3.423	2.045	2.960	1.071	⇨1.384	⇨1.492	⇨0.644	⇨1.290	⇩0.337
EZR-AS1	350	72	42	101	25	93	21	5.999	5.223	7.424	3.403	6.393	2.364	⇨0.871	⇨1.238	⇨0.652	⇨1.066	⇩0.453
SNORD17	237	18	20	17	13	19	11	2.215	3.673	1.845	2.613	1.929	1.828	⇨1.658	⇨0.833	⇨0.711	⇨0.871	⇩0.498
BRI3	699	52	52	53	43	58	28	2.169	3.238	1.951	2.931	1.996	1.578	⇨1.492	⇨0.899	⇨0.905	⇨0.920	⇩0.487
INSL3	805	13	58	24	48	14	22	0.471	3.136	0.767	2.841	0.418	1.077	⇧6.659	⇨1.629	⇨0.906	⇨0.888	⇩0.343
GPAT2	2824	185	155	128	130	185	78	1.910	2.389	1.166	2.193	1.576	1.088	⇨1.250	⇨0.610	⇨0.918	⇨0.825	⇩0.455
IFITM3	663	36	60	48	53	52	27	1.583	3.939	1.862	3.808	1.887	1.604	⇧2.487	⇨1.176	⇨0.967	⇨1.192	⇩0.407
TMEM238	662	70	110	103	105	105	59	3.083	7.232	4.003	7.556	3.816	3.511	⇧2.345	⇨1.298	⇨1.045	⇨1.238	⇩0.485

In the second experiment, 50 genes met the selection criteria, of which 31 were up-regulated (**Figure 5.7A**) and 19 were down-regulated at 30 min and/or 6 hr (**Figure 5.7B**). Complete results for the second experiment are reported in Table 5.3 (up-regulated) and Table 5.4 (down-regulated). One up-regulated gene is classified as a solely fast response gene as it is up-regulated at 30 min for 20mGy and/or 1Gy. 30 up-regulated genes are classified as solely slow response genes as these are up-regulated at 6hr for 20mGy and/or 1Gy. 4 of these genes are up-regulated at 6 hr for both 20mGy and 1Gy. Three down-regulated genes are classified as solely fast response genes as these are down-regulated at 30 min for 20mGy or 1Gy. 16 down-regulated genes are classified as solely slow response genes as these are down-regulated at 30 min for 20mGy and/or 1Gy. Two of these genes are down-regulated at 6 hr for both 20mGy and 1Gy.

Due to the lack of consistency between experiments, the differences in RPKM values were investigated for the selected genes for each treatment from each experiment. The differences between the RPKM values from probes in the first experiment (2012) compared to the corresponding RPKM values from the second experiment (2013) are summarized in Table 5.5. The differences between the RPKM values from probes in the second experiment (2013) compared to the corresponding RPKM values from the first experiment (2012) are summarized

Table 5.5 Average %difference in baseline RPKM between 2012 and 2013 Experiments

	0Gy 30min	0Gy 6h	20mGy 30min	20mGy 6h	1Gy 30min	1Gy 6h
Average	326.10%	369.43%	173.88%	235.25%	70.61%	95.99%
Stdev	970.05%	2306.08%	361.87%	1218.86%	125.63%	193.72%
Min	1.44%	0.42%	1.98%	5.49%	5.28%	4.24%
Max	4387.49%	18077.86%	1866.84%	9566.05%	999.72%	1524.31%

in Table 5.6. It is clear that there is little similarity in RPKM values between experiments. Additionally, in the second experiment, there was approximately twice the number of total reads (N) for each treatment indicating either a greater amount of RNA extracted, better purification or increased amplification.

Table 5.6 Average %difference in baseline RPKM between 2013 and 2012 Experiments

	0Gy 30min	0Gy 6h	20mGy 30min	20mGy 6h	1Gy 30min	1Gy 6h
Average	184.97%	257.79%	130.58%	203.01%	245.95%	374.68%
Stdev	364.03%	406.20%	316.28%	259.32%	819.49%	993.26%
Min	3.19%	7.40%	0.59%	2.29%	7.56%	2.57%
Max	2472.52%	2619.39%	2450.38%	1303.28%	6611.70%	7861.82%

Despite experimental irreproducibility, differential expression patterns within individual experiments revealed interesting results which may inform future investigation. In the first experiment, five transcripts were selected in which the associated proteins are implicated in either cancer induction or the oxidative stress response. Four and a half LIM domains 2 (FHL2) has both oncoprotein and tumor suppressor functions which are tissue-specific (108, 109). Additionally, FHL2 functions as a scaffolding protein integral to extracellular membrane assembly (110). This transcript is upregulated 2.4 fold after 1Gy at 6 hr and 1.5 fold after 20mGy. Following a similar expression pattern, zinc finger protein 385A (ZNF385A) is unregulated 2.3 fold after 1Gy at 6 hr and 1.4 fold after 20mGy. This protein acts as transcription repressor, functions as a tumor suppressor and its inhibition has been linked to decreased overall survival in ovarian cancer (111, 112). Sestrin 1 (SESN1) is also upregulated after 1Gy at 6 hr by 2.0 fold and is upregulated after 20mGy to a lesser 1.5 fold and at 30 min rather than 6 hr. SESN1 is a p53 induced protein which is important in the DNA damage and

oxidative stress responses through growth inhibition and antioxidant mechanisms (113, 114). Interestingly, NADPH oxidase organizer 1 (NOXO1) presents a reverse dose response with a 2.6 fold upregulation at 30 min after 20mGy but only a 1.6 fold upregulation at 30 min after 1Gy. NOXO1 is an important positive regulator of the NOX1 and NOX3 proteins which modulate the cellular oxidative state (115). Ubiquitin-conjugating enzyme E2S (UBE2S) is downregulated by 2.4 fold after 1Gy at 6 hr and shows now robust downregulation after 20mGy. This protein activates ubiquitin chain linkage and increased expression has been implicated in decreased overall cancer survival (116, 117).

In the second experiment, eight transcripts were investigated in which the associated proteins are involved in cancer induction, cell death, chromatin structure or the DDR. Histone cluster 4, H4 (HIST4H4) had the largest upregulation with a 6.6 and 6.8 fold increase at 6 hr after 20mGy and 1Gy respectively compared to non-irradiated samples. This protein forms the core histone H4, required for chromatin structure (118). Similarly serine palmitoyltransferase, long chain base subunit 1 (SPTLC1) is upregulated to a similar extent for both 20mGy and 1Gy at 6 hr with 2.7 and 2.9 fold increases respectively. Inhibition of SPTLC1 (phosphorylation by the ABL protein) promotes cell survival, while activation promotes apoptosis (119). RAD52 motif 1 (RDM1) presents upregulation at 6 hr of 2 fold after 1Gy and 1.5 fold after 20mGy. This protein contains a motifs found in the HR protein RAD52 and has been shown to recognize DNA distortions from DNA damaging agents like cisplatin. However, ablation of *RDMI* does not promote hypersensitivity to ionization radiation as it does for cisplatin (120). Caspase 1 (CASP1), which is involved in apoptosis, exhibits 2.4 fold upregulation at 6 hr but only after 1Gy. No robust differential regulation is seen for 20mGy (121). Both histone cluster 1, H4b

(HIST1H4B) and CD9-coding transcripts display reverse dose response at 6 hr. HIST1H4B, another core histone protein, is upregulated 3.1 fold following 20mGy but only 1.8 fold after 1Gy. Similarly, CD9 is upregulated 2.1 fold and 1.4 fold after 20mGy and 1Gy respectively at 6 hr. CD9 is a cell surface glycoprotein, which may affect a variety of cellular processes including cancer cell motility and metastasis suppression (122). Interestingly, at 6hr, EGF-like-domain, multiple 7 (EGFL7) is upregulated by 2.0 fold after 20mGy but downregulated by 1.9 fold after 1Gy. EGFL7 may regulate vasculogenesis and promote the proliferation of tumor cells (123-125). Histone cluster 1, H2bh (HIST1H2BH) is downregulated after both 20mGy and 1Gy and at both 30 min and 6 hr. However, it is downregulated most substantially at 30 min after 20mGy, with a 2.1 fold decrease with a drop to 1.5 fold for 1Gy and similar decreases at 6 hr for both doses. HIST1H2BH is another core histone protein.

5.3.3 Irradiation schemes similar to CT protocols alter the DNA damage response

Multiple low dose irradiations separated on the order of minutes alter the biological response compared to single irradiations of the equivalent total dose in both murine tumor infiltrating lymphocytes (TILs) (**Figure 5.8A**), and in the human wild-type lymphocyte cell line ESW-WT3 (**Figure 5.8B**). In both mouse and human cell lines, a linear, dose-dependent response of normalized gammaH2AX signal was observed for single doses of 20-60mGy. However, in cells exposed to multiple exposures of 20mGy, a significant decrease ($P<0.05$) in normalized gammaH2AX signal was observed compared to the signal from the single equivalent total dose. However, these experiments were performed at a single time-point (30 min post irradiation); additional time-points were necessary to determine if the reduction in signal was due to a time shift (delay or advancement) in repair kinetics. Figure 5.9A clearly demonstrates

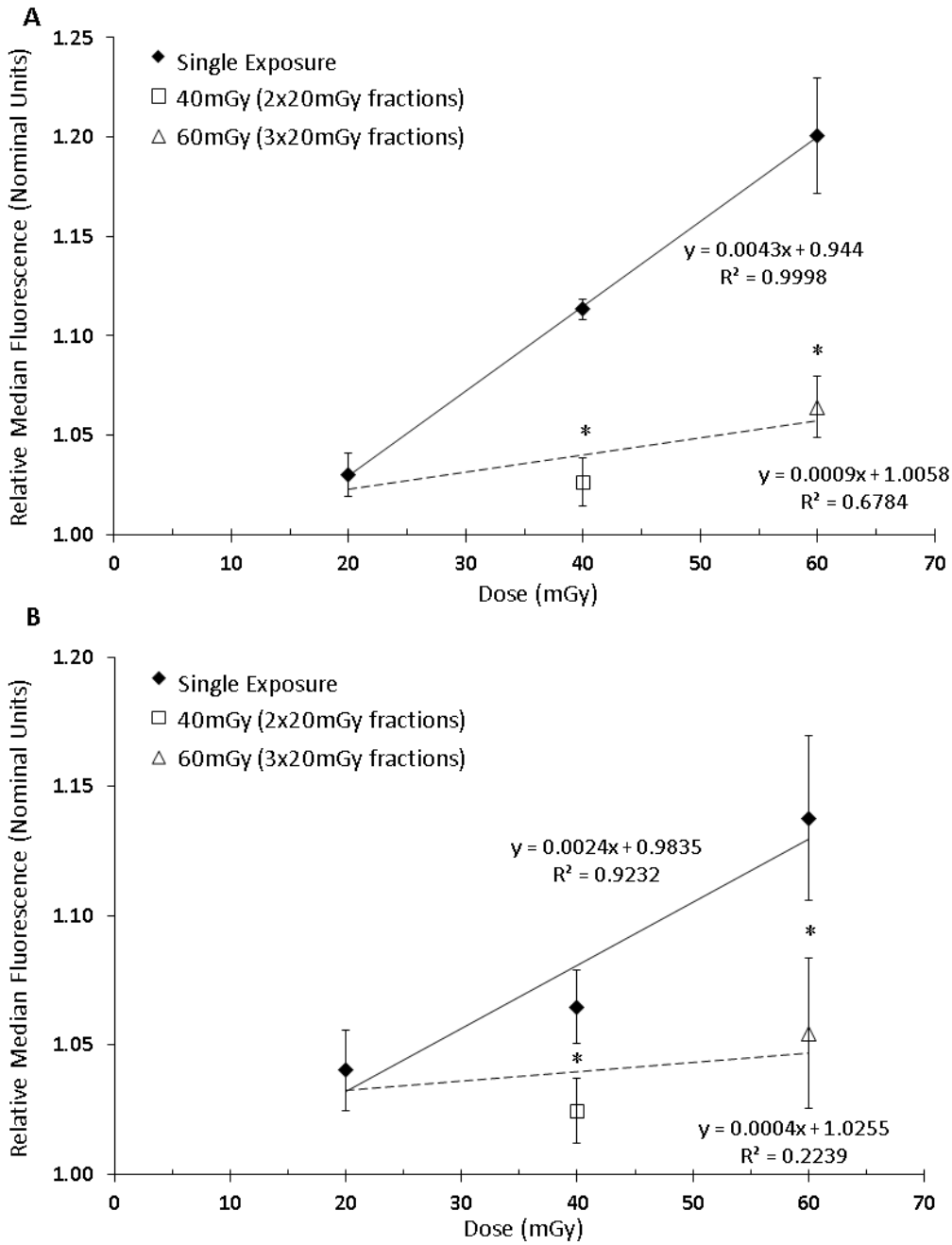

Figure 5.8. Modulation of gammaH2AX response after quickly fractionated low doses (2min apart) mimicking CT protocol schemes in (A) mouse tumor infiltrating lymphocytes (Tils) and (B) cultured human lymphocytes. Cells were irradiated to 20-60mGy in 20mGy fractionated exposures separated by two minutes (open markers) or as a single exposure (closed diamonds). After IR exposure, samples were incubated in the dark at room temperature and analyzed at 30min. A linear, dose-dependent response of normalized gammaH2AX signal was observed for single exposures of 20-60mGy (solid line). In cells exposed to multiple exposures of 20mGy (dashed line), a significant decrease ($P<0.05$) in normalized gammaH2AX signal was observed compared to the single equivalent total dose. Linear

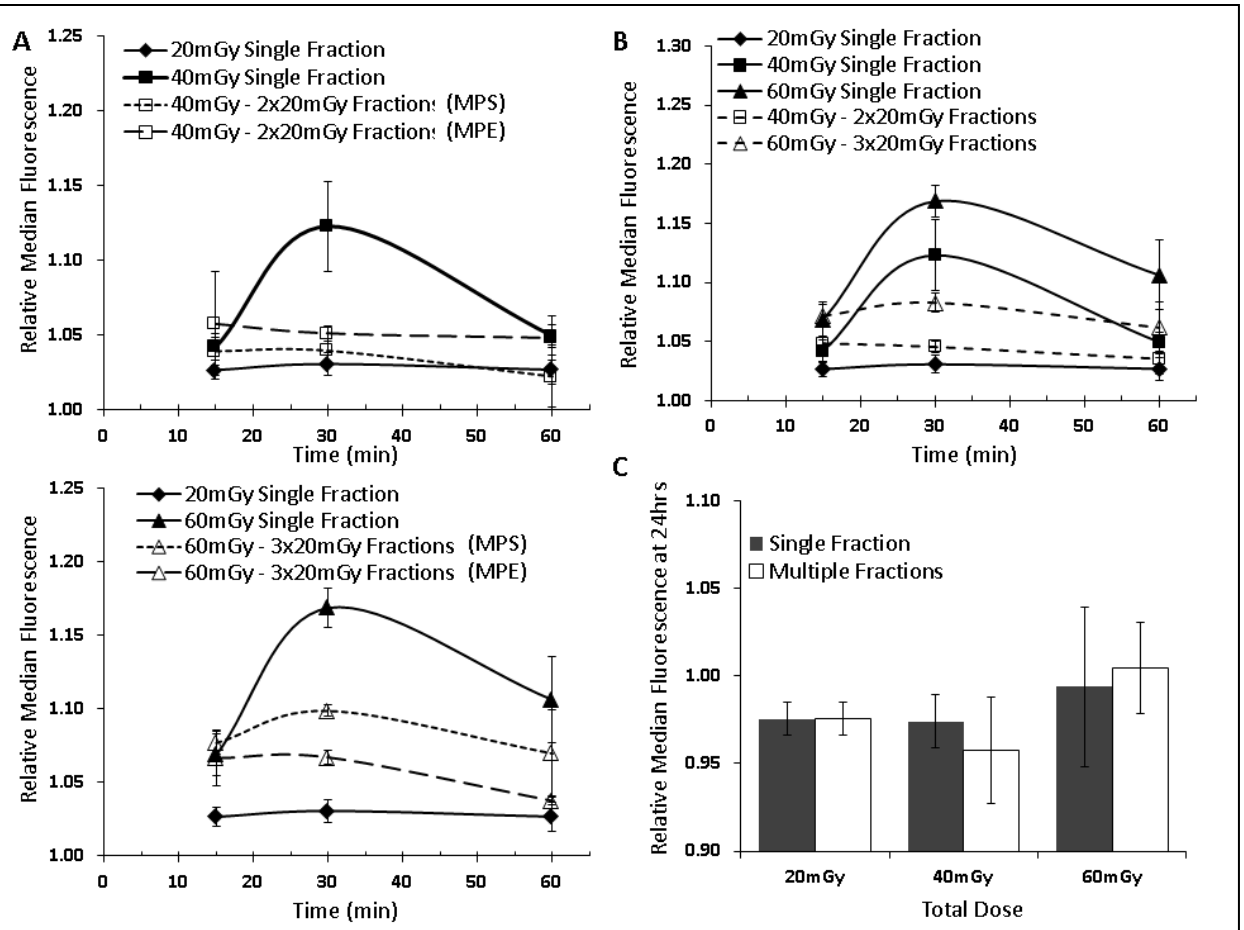

Figure 5.9. Kinetic response to quickly fractionated low doses mimicking CT protocol schemes in cultured human lymphocytes. Cultured lymphocytes were irradiated to 20-60mGy in 20mGy fractionated exposures separated by two minutes (dashed lines) or as a single exposure (solid lines). After IR exposure, samples were incubated at 37°C for t 15-60min and analyzed for gammaH2AX. **A.** To account for possible differences in repair kinetics during the fractionation periods two timing schemes were employed: one where time points were assessed from the start of radiation exposure (MPS) and a second where time points were assessed from the end of radiation exposure (MPE). Reduction in signal is only seen at the 30min for both 40mGy and 60mGy irradiations ($p<0.05$). **B.** Averaged kinetic response to quickly fractionated low doses mimicking CT protocol schemes in cultured human lymphocytes. Due to the limited difference between experiments, MPS and MPE data was averaged to demonstrate the variation in response to single (solid lines) and fractionated doses (dashed lines). **C.** Comparison of relative gammaH2AX signal between multiple (white) and single (grey) fractions 24hr after quickly fractionated low doses of IR mimicking CT protocol schemes. Both single and multiple fractionation schemes return to background levels.

that the reduction in gammaH2AX signal seen after multiple low-dose irradiations is not solely due to a change in repair kinetics. The reduction in signal is only seen at the 30 min time-point, whereas at 15 and 60 min the normalized fluorescence is equivalent for both single and split-

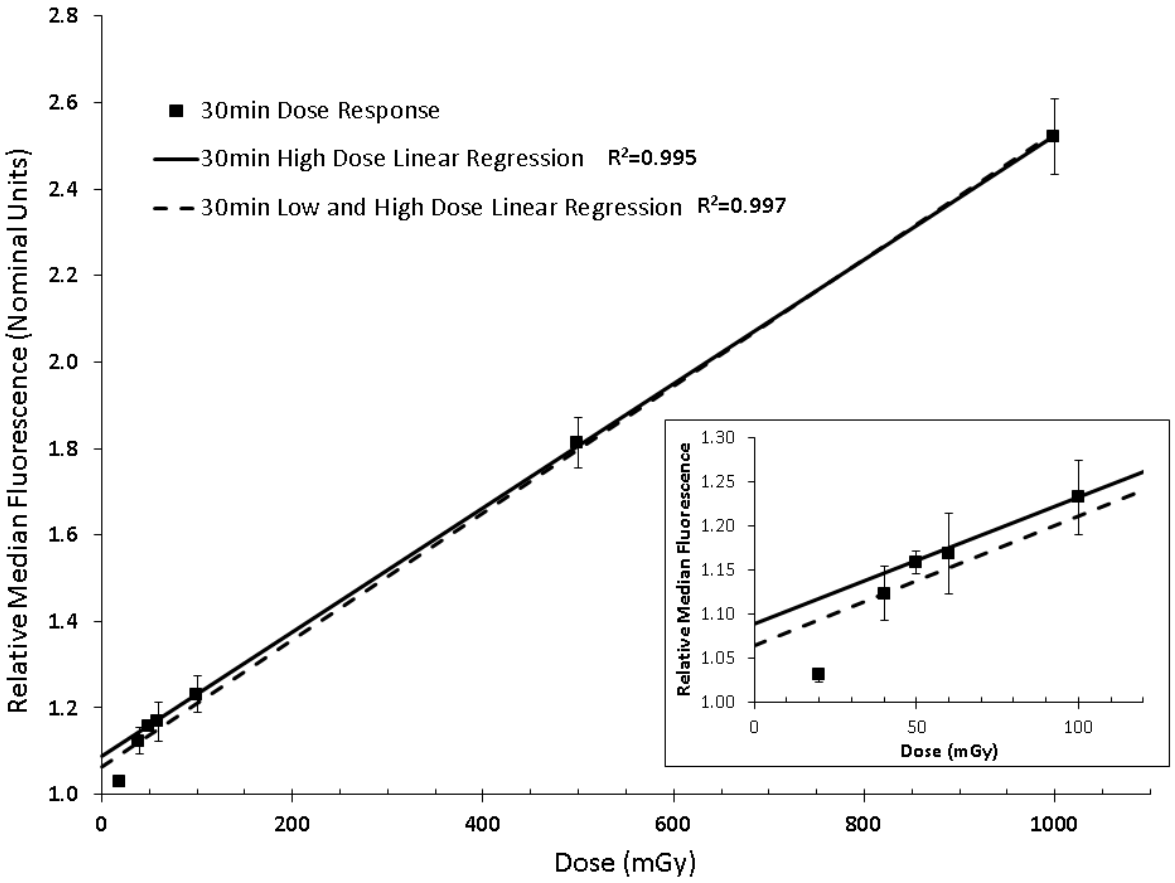

Figure 5.10. Dose response at 30min in cultured human lymphocytes. At 30min, where the dose response is exceptionally linear, low dose data correlates well with the linear regression fitted to the higher dose data (solid line) - R2=0.976 (insert). However, 20mGy falls below this line which may indicate a difference in the biological response to doses below 40mGy. Using both high and low dose data results in a slight change in linear regression (dashed line) - R2=0.997 for all data. R2=0.987 for low dose data.

dose irradiations. Due to the limited difference between experiments, MPS and MPE data was averaged to demonstrate the overall variation in response to single and fractionated doses (**Fig. 5.9B**). At 24 hr, gammaH2AX levels return to background levels for both single- and multiple-fraction experiments (**Fig 5.9C**). Interestingly, at 30 min, where the dose response is exceptionally linear, the 40 and 60mGy data correlates well with the line fitted to the higher dose data (R^2=0.976), while 20mGy falls below this line (**Figure 5.10**).

It has been suggested that there is a threshold dose, below which cells are unable to efficiently repair induced DNA DSB (126, 127). To establish if the phenomena above is observed only below a threshold dose, we conducted higher dose fractionated experiments. As seen in

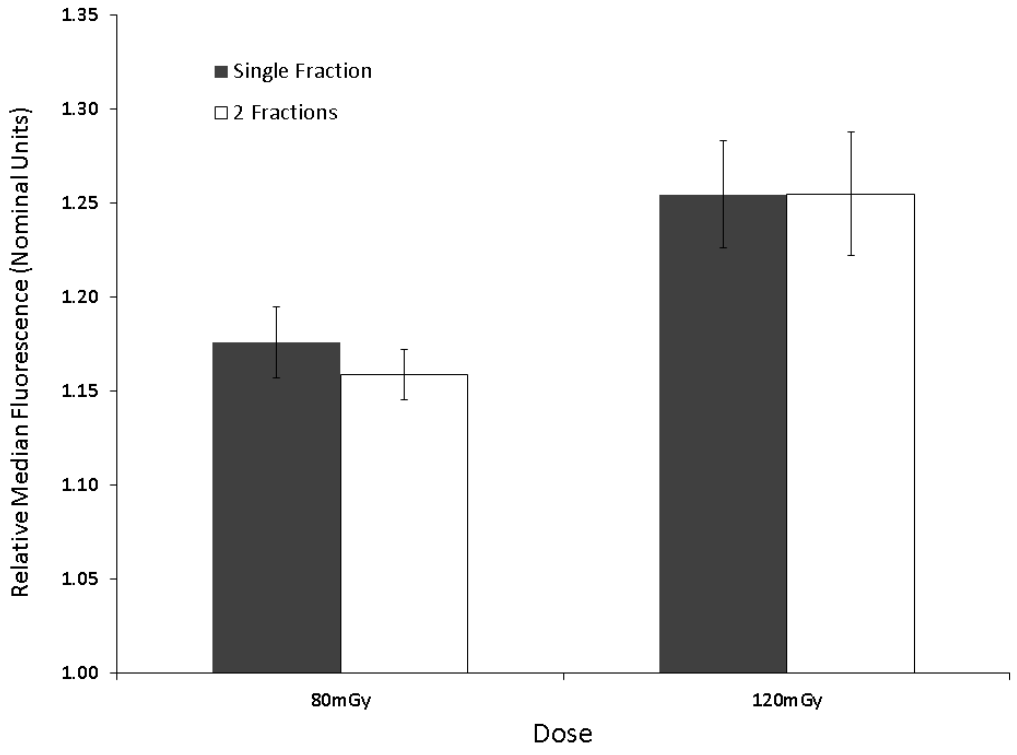

Figure 5.11. Comparison of gammaH2AX relative signal between multiple (white) and single (grey) exposures of higher doses (still within the diagnostic radiology dose region) in cultured human lymphocytes. Samples were irradiated with the following fractionation schemes: two 40mGy doses separated by two minutes with an equivalent 80mGy single dose control or two 60mGy doses separated by two minutes with an equivalent 120mGy single dose control. These samples were evaluated at 30min at 37°C after IR exposure. Multiple fractions of higher doses fail to produce the same reduction in signal compared to their single dose counterparts.

Fig. 5.11, multiple fractions of higher doses (still within the diagnostic radiology dose region) fail to produce the same reduction in signal compared to their single dose counterparts, which suggests that at least the initial dose must fall below a threshold to effect H2AX phosphorylation.

5.3.4 Variable modulation of radio-protective action at different dose levels and dosing schemes

The antioxidant NAC reduces H2AX phosphorylation following 1Gy at 60 min when administered both before (9.0%; **Figure 5.12A**) and after (7.7%; **Figure 5.12C**) irradiation. Because its effect is observed even after irradiation, it is clear that NAC does not act solely by scavenging ROS from the initial IR treatment. Additionally, signal reduction is not seen at the earlier 30 min time point indicating a promotion of repair rather than a reduction in initial damage. Furthermore, signal reduction is only indicated at 60 min after 20mGy when NAC is administered post-IR (4.1%; **Figure 5.12A-C**). Because administration of NAC only affected 20mGy when administered after irradiation at 60 min, it was this treatment that was used for multi-pass experiments. Interestingly, a robust reduction in H2AX phosphorylation is observed following 60mGy when given as a single dose (18.2%), whereas a much smaller, albeit significant, reduction is seen when 60mGy is given as three fractions of 20mGy separated by 2min (5.9%) (**Figure 5.12D**).

The antibiotic tetracycline reduces H2AX phosphorylation following 1Gy for all time points (15min – 6.7%; 30min – 35.6%; 60min – 46.8%; **Figure 5.13A**). Conversely, tetracycline increases H2AX phosphorylation at all time points following 20mGy (15min – 2.4%; 30min – 3.2%; 60min – 1.3%; **Figure 5.13A**). For comparison to NAC treatment only the 60 min time point was investigated for multi-pass exposures. Interestingly, when 60mGy is given in three fractions of 20mGy a reduction in H2AX phosphorylation is observed (2.7%) following tetracycline treatment. Again, when 60mGy is given as three fractions of 20mGy, there is a decrease in H2AX phosphorylation compared to a single exposure as previously observed. However, tetracycline treatment for single exposure 60mGy appears to reduce H2AX phosphorylation to a similar level as the fractionated exposure indicating more effective

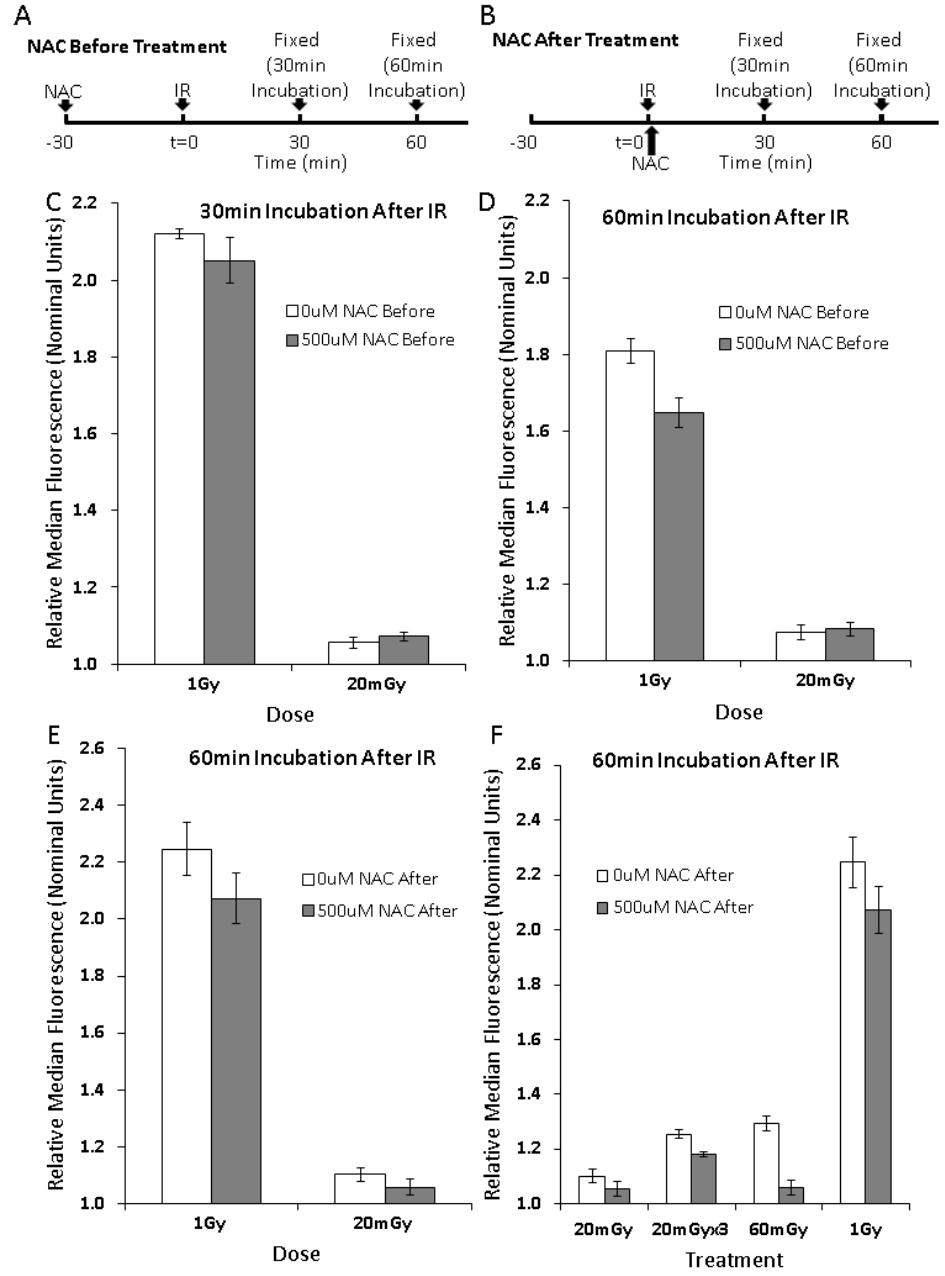

Figure 5.12. Effects of N-acetyl cysteine (NAC) on irradiated lymphocytes. NAC was added either 30min prior to (**A**), or immediately following (**B**) irradiation to a final concentration of 500uM (**C-F**). Samples were irradiated to 20mGy or 1Gy and incubated at 37°C for 30 or 60 minutes as indicated and analyzed for gammaH2AX fluorescence. Additional samples were irradiated to 60mGy in single or three fractioned exposures and assessed at 60min. Control samples were treated with PBS. **C.** NAC has no significant effect at 30min. **D.** NAC reduced H2AX phosphorylation following 1Gy at 60min when administered before (9.0%) and after (7.7%) irradiation. **E.** Reduction is only seen at 20mGy when NAC is given after IR at 60min (4.1%). **F.** A robust reduction in H2AX phosphorylation is observed at 60mGy when given as a single dose (18.2%), whereas a much smaller albeit significant reduction is seen when 60mGy is given as three fractions of 20mGy separated by 2min (5.9%).

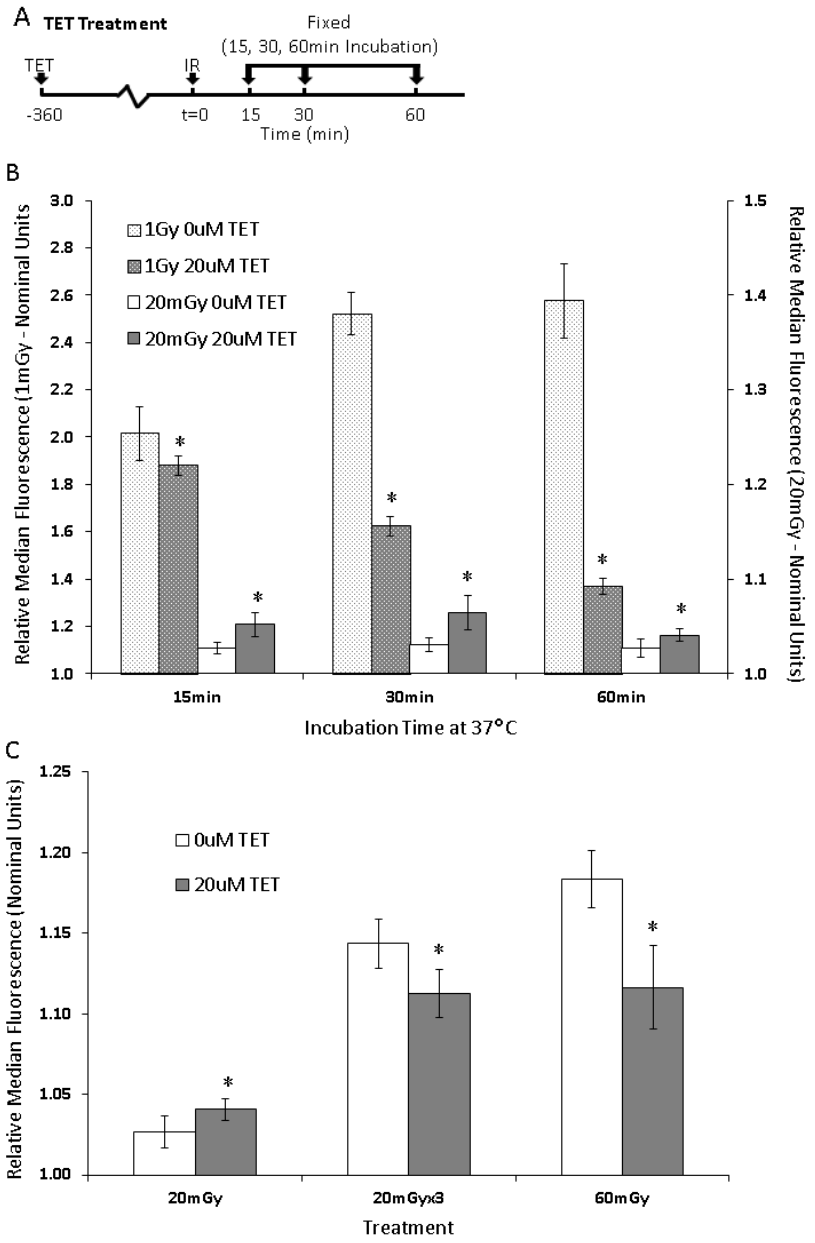

Figure 5.13. Effects of tetracycline (TET) on irradiated lymphocytes. Tetracycline (TET) was added 3hr prior to irradiation to a final concentration of 20uM. **A-B.** Samples were irradiated to 20mGy or 1Gy and incubated at 37°C for 15, 30 or 60 minutes and analyzed for gammaH2AX fluorescence. **B.** Tetracycline reduces H2AX phosphorylation following 1Gy for all time points (15min–6.7%; 30min–35.6%; 60min– 46.8%). Conversely, tetracycline increases H2AX phosphorylation at all time points following 20mGy (15min–2.4%; 30min–3.2%; 60min–1.3%). **C.** Additional samples were irradiated to 60mGy in a single or three fractioned exposures and assessed at 60min. Control samples were treated with PBS. When 60mGy is given in three fractions of 20mGy a reduction in H2AX phosphorylation is seen (2.7%) following tetracycline treatment. Tetracycline treatment for single exposure 60mGy appears to reduce H2AX phosphorylation to a similar level as the fractionated exposure indicating more effective protection following single exposures (5.7%).

protection following single exposures (5.7%) (**Figure 5.13B**). Clearly, these two agents which have been shown to provide radio-protective action have different mechanisms not only of between each other but also at different dose levels.

5.4 Conclusions

For the first time, differences in repair kinetics that depend on the magnitude of doses for both cultured and whole blood lymphocytes are characterized. Samples irradiated with lower doses (≤100mGy) tend to demonstrate their peak response later than those irradiated with higher doses in terms of H2AX phosphorylation. These differences suggest distinct dose-dependent mechanisms of response suggesting that multiple damage detection and repair mechanisms are activated after high doses whereas after low doses, fewer or different mechanisms are activated or the response is slower as the lower number of damaged sites is below what the cellular machinery can detect. It has been shown that H2AX continues to be phosphorylated if DNA DSBs remain unrepaired (128). Thus, it is plausible, according to our data that delay in damage repair leads to continued H2AX phosphorylation, altering the linearity of gammaH2AX signal seen at shorter time-points, making it appear that lower doses induce more damage at later time points. Therefore, the shape of the dose response depends greatly on the time at which it is observed in the repair process and should be taken into account when establishing low dose sensitivity.

The human wild-type cell-line ESW-WT3 models whole blood lymphocytes in the assay developed here. The overall shapes of the curves for cultured and whole blood lymphocytes are similar. Whole blood lymphocytes appear to detect and repair damage faster than cultured lymphocytes as indicated by the steeper initial increase and faster time to peak in gammaH2AX

signal. The relative median fluorescence levels for blood samples are higher than for cultured cell line samples. Fresh whole blood lymphocytes may be more radiation sensitive than cultured lymphocytes, or background levels of gammaH2AX may be higher for cultured immortalized lymphocytes than for blood lymphocytes (128), minimizing the measured effect of radiation on overall gammaH2AX levels. Moreover, it is possible to use this assay to analyze patient samples receiving doses as low as 5mGy.

Of particular interest is the difference in H2AX phosphorylation kinetics between single-exposure and multiple-exposure samples. It appears that multi-pass CT protocols alter the biological response to DNA DSBs *in vitro*, with significantly reduced peak gammaH2AX signal when the same total dose is fractionated over a few minutes, rather than delivered as a single exposure. However, the biological significance of these effects is unclear. This phenomenon is only seen with 20mGy fractionated doses, not with the higher-dose fractions tested. In addition, the gammaH2AX kinetic curves for multiple 20mGy fractions appear similar in shape to the single exposure 20mGy curve which lacks a prominent peak at 30 min. Furthermore, a single dose of 20mGy does not follow the linearity seen at 30 min for doses of 40mGy and above; instead the signal for this dose is lower than expected. These results suggest that at doses up to 20mGy, (and possibly beyond 20, but certainly below 40mGy) a response is initiated for subsequent fractions such that H2AX phosphorylation is sub-additive to that of the individual fractions. Yet, multiple fractions of higher doses are additive, at least over a short time period. A decrease in gammaH2AX signal could indicate either a reduction in damage (i.e., enhanced repair) or a reduction in H2AX phosphorylation capacity. Unlike higher doses where unrepaired breaks continue to be phosphorylated until repair takes place, damage induced at

20mGy may not induce extensive phosphorylation. Factors which effect the phosphorylation H2AX may be activated at different dose levels; for example, TNF-β is fully activated by at least 50mGy and has been shown to control ATM signaling, but ATM is not fully active until 500mGy. Whether this response is beneficial or detrimental in terms of carcinogenesis or other late effects of irradiation remains to be elucidated. Although the exact role of phosphorylation of gammaH2AX in DNA damage repair remains elusive, it is clear that it is an important step for efficient repair (129). Responses that affect repair efficiency have the potential to alter the risk of carcinogenesis and other late effects.

The results presented in Figure 5.1 show the levels of gammaH2AX return to control values by 24 hr after irradiation with single exposure doses equal to or below 100mGy, whereas those for 500mGy and above are still slightly, but not significantly above controls. Similarly, relative gammaH2AX levels returned to control values by 24 hr (Fig. 7C) after both single and split-exposure low dose experiments indicating completion of damage repair on a similar time scale. Although complete repair is indicated by the return of gammaH2AX to background levels at 24 hr, repair is not necessarily faithful. Taken together with the possibility of an altered H2AX phosphorylation response, the effects of split-dose irradiations could have marked implications for clinical CT examinations, especially for protocols that involve multiple scans of the same anatomic area. Examples would include scans such as pre- and post-contrast scans, 2- or 3-phase liver exams and others which use a time delay between scans to investigate different contrast enhancement phases. Future research is necessary to determine the consequences of this split-low-dose phenomenon, which would lead to a better understanding of the effects of these protocols on risk and may ultimately be exploited to mitigate patient risk.

The results from radio-protective agents reveal differential modulation of the DDR. Because NAC has the capacity to decrease H2AX when administered before and after IR, scavenging of initial radiation-induced ROS near DNA is unlikely to be the sole contributor to radio-protective effects. In order to scavenge ROS, which are directly detrimental to DNA, NAC would need to be within the nucleus. Transport from the cytoplasm to inside the nuclear envelop is highly regulated making it improbable that NAC would be available for large-scale scavenging. Taken together these results indicate another mechanism of action by NAC besides ROS scavenging at the site of potential DNA breaks. ROS scavenging in extracellular or cytoplasmic spaces however, could potentially modulate the activation of other response factors along with other mechanisms. Alternatively, NAC has been shown to induce regeneration of the endogenous scavenger glutathione by providing an essential cysteine residue and regulate apoptosis through the formation of inactive adducts, independent of antioxidant activity (130). The decrease in H2AX phosphorylation after 20mGy only when NAC is administered following IR is surprising. However, if NAC has the ability to form inactive adducts the addition of NAC before IR may keep some pathway from being initiated, whereas if administered after IR would allow mechanisms to be initiated and downstream events to occur leading to a reduction of H2AX phosphorylation. At 20mGy, administration of NAC before irradiation could be inhibiting one of the few pathways available but after 1Gy mechanisms are not so limited.

To explore how the radio-protective potential may be modulated by the split-dose phenomenon described earlier, samples were exposed to radio-protectors and assessed for H2AX phosphorylation. Because the NAC-induced effect was only observed when administered

following exposure to low doses of IR at 60min, it was this treatment and time point that was investigated. Clearly, the action of NAC is more dramatic when 60mGy is given as a single dose. Reduction in H2AX phosphorylation after 20mGy appears not to be as robust and when 60mGy is given as multiple doses of 20mGy, the final reduction in signal is similar that of 20mGy alone and that seen after 1Gy. It is possible that the response to lower doses of IR is more dependent on ROS regulation as suggested by the differential expression of NOXO1 from our RNAseq data but that below a certain dose, the activation of repair factors may not be as robust to effectively repair damage. Because multiple exposures of 20mGy fail to show the dramatic reduction in H2AX phosphorylation seen for a single dose of 60mGy and exhibit a response which is more similar to a repetition of the 20mGy response, it is clear that there are distinct responses at these different dose levels. At 60mGy (delivered as a single dose), repair factors not available at 20mGy may be activated and in combination with the effects of NAC and because the amount of damage is relatively small, repair capacity and efficiency is greatly enhanced. However, at 1Gy where DNA damage is more significant, repair factors are active but have an excess of repair to perform, possibly of greater complexity. Addition of NAC may aid in promoting repair but have a significantly reduced effect due to the more overwhelming effect of DNA damage.

The gammaH2AX profiles for tetracycline treatment were unexpected, namely the increase in signal following 20mGy rather than a decrease. Tetracycline has been shown to activate both ATM and DNA-dependent protein kinase catalytic subunit (DNA-PKcs) (131) which are responsible for H2AX phosphorylation (132). Tetracycline may promote enhanced H2AX phosphorylation at 20mGy but, as suggested in the response to NAC, activation of other repair

factors involved in completion of break repair may lag and thus H2AX remains phosphorylated even at later time points. An increase in H2AX levels, especially if found to be deficient at low doses, could induce more efficient repair. Tetracycline activation of Tip60 promotes chromatin relaxation at the site of damage as well as repair factor activation (131, 133), which may also allow access to repair factors and further promote increased phosphorylation of H2AX to levels more consistent with higher dose levels. The similarity in H2AX phosphorylation following 60mGy given as both a single dose and as multiple doses of 20mGy, suggests that tetracycline promotes the resolution of damage to a similar extent regardless of the exposure scheme. Taken together with the increase in H2AX phosphorylation observed at 20mGy alone, these results indicate that tetracycline not only promotes more efficient phosphorylation of H2AX but also the modulation of some repair mechanism which is unavailable at 20mGy but becomes so at higher doses regardless of the dosing scheme. Thus the mechanism(s) modulated by tetracycline differ from those affected by NAC. The incredible decrease in H2AX phosphorylation after 1Gy with tetracycline treatment substantiates a multi-potent mechanism of action as the response is not nearly as limited when the amount of damage is more severe as seen with NAC treatment.

The different responses to these two classes of radio-protectors suggest important roles of ROS signaling (not only scavenging) and chromatin structure following IR exposure. The role of ROS signaling seems to be dose-dependent but may also be affected by DDR factor activation. Chromatin structure appears to be a critical element in DNA repair, which may be deficient at lower doses. Importantly, these experiments provide further evidence of

differential modulation of the biological response to low doses and dosing schemes similar to those experienced in CT examinations demonstrated previously in this study.

Unfortunately, RNASeq analysis results indicate irreproducibility between replicate experiments. Because transformed cells were used, rather than primary cell line samples, it is possible that replication of data is difficult due to changes over the life time of different cultures. These two experiments were conducted over six months apart, and while lymphocyte samples were both healthy at the time of treatment, they were at different passage numbers which could affect expression outcomes. Moreover, these cells were actively progressing through the cell cycle, giving a population of cells in variable cell cycle stages. Additionally, appreciable changes in gene expression may be minimal at the doses investigated here and thus difficult to assess with the current selection criteria. However, despite the lack of reproducibility, each experiment indicated a few genes which warrant further investigation into their effects at different dose levels.

In light of the discussed effects of antioxidants as radio-protectors, the differential expression of NOXO1 is of particular interest. NOXO1 is a membrane protein associated with the regulation of basal and stimulated levels of superoxide within the cellular and extracellular environment. ROS regulation has been implicated in cellular processes including signal transduction, cell proliferation and apoptosis. NOXO1 is upregulated early in both 20mGy and 1Gy irradiated samples, but to a greater extent after 20mGy. Although future investigations are required to confirm this differential expression, it indicates an increased dependency on ROS regulation in the response to lower dose irradiations. The use of antioxidants as radio-

protectors for low doses of IR may not be as straight forward as previously thought due to the possibility of disrupting critical cell signaling processes (134-137).

Although SESN1 did not meet selection criteria for the second experiment, it was selected in the first experiment and presented a similar trend in the second at least for 1Gy treatment. SESN1 is a p53-induced protein implicated in antioxidant defense as well as the inhibition of cell growth in response to DNA damage. Upregulation of this gene is observed at 6 hr after 1Gy irradiation. A less robust upregulation is seen at 30 min after 20mGy irradiation indicating a possible dose and kinetic differential in cell cycle modulation and ROS response between low and high doses. It is possible that due to the multiple actions of SESN1, that each dose activates a distinct mechanism. If cells are more dependent of ROS regulation following low dose irradiations, SESN1 regulation of ROS may be the more important than cell cycle modulation. NOXO1 is also upregulated at the short time point, suggesting that the induction of an ROS response is initiated early in the response to DNA damage.

CASP1 met the selection criteria in the second experiment, but was not one of the probes available for the first experiment. After both doses of IR, CASP1 was upregulated in a dose dependent manner. CASP1 has a role in apoptosis and activates interleukin-1 which is involved in inflammation, and wound healing. Although only after 1Gy did upregulation exceed the 2fold selection criteria, it was upregulated by a modest 1.4fold following 20mGy indicating that low doses of IR can still induce apoptotic signaling as well as other danger signals. Similar to SESN1, it is possible that different dose levels could promote differential effects of CASP1 actions. For example, for low dose, inflammation and wound healing signaling may be promoted while at high doses apoptosis is the dominant mechanism.

Histone proteins take the brunt of damage under oxidative conditions surrounding DNA with approximately 50% of ROS quenched by histone proteins (115). Thus, the histone turnover presented in the differential expression of histone proteins following both doses of IR in the second RNASeq experiment suggests a DNA damage-independent response. In fact, HIST4H4 shows a robust increase in expression at 6 hr following IR, where it is upregulated by over 6fold after both 20mGy and 1Gy demonstrating and independence from dose in the response to IR. It is possible that even low doses of IR trigger histone replacement in large swaths of the genome in response to partial histone oxidation and other forms of damage including single strand breaks, and base and nucleotide damage, regardless of the amount of DNA DSBs. As other forms of DNA still require highly orchestrated repair mechanisms involving chromatin restructuring, histone turnover may be an essential part of that repair process.

By investigating the dose response to IR in conjunction with kinetic analysis, it is possible to discern differences in the biological response. The major difference between single and multiple low dose irradiations only occurs during a short window which could be overlooked if only a single time point was assessed. As the split-dose irradiations investigated here are more similar to those experienced during a CT examination, it is essential to understand why and how these differences occur. It is clear that ROS signaling and chromatin structure play and important role in the repair response but their relative importance at different dose levels must be more thoroughly investigated. Additionally, the modulation of radiation protective action at different dose levels requires further investigation to determine the potential usefulness of these agents for diagnostic, therapeutic, occupational or un-planned emergency exposures.

5.5 References

100. Hall EJ, Giaccia AJ. Radiobiology for the Radiologist. Philadelphia, PA USA: Lippincott Williams & Wilkins, 2006.

101. Geisel D, Zimmermann E, Rief M, et al. DNA double-strand breaks as potential indicators for the biological effects of ionising radiation exposure from cardiac CT and conventional coronary angiography: a randomised, controlled study. European Radiology 2012; 22:1641-1650.

102. Brand M, Sommer M, Achenbach S, et al. X-ray induced DNA double-strand breaks in coronary CT angiography: Comparison of sequential, low-pitch helical and high-pitch helical data acquisition. European journal of radiology 2012; 81:e357-e362.

103. Kuefner MA, Grudzenski S, Hamann J, et al. Effect of CT scan protocols on x-ray-induced DNA double strand breaks in blood lymphocytes of patients undergoing coronary CT angiography. Eur Radiol 2010; 20:2917 - 2924.

104. Kuefner MA, Hinkmann FM, Alibek S, et al. Reduction of X-Ray Induced DNA Double-Strand Breaks in Blood Lymphocytes During Coronary CT Angiography Using High-Pitch Spiral Data Acquisition With Prospective ECG-Triggering. Investigative Radiology 2010; 45:182-187 110.1097/RLI.1090b1013e3181d1093eddf.

105. Elgart SR, Bostani M, Adibi A, et al. Evaluation of a rapid protocol for time sensitive kinetic assessment of DNA damage response following ionization radiation using whole blood samples. PLoS ONE: Submitted May 7, 2014.

106. Kuefner MA, Grudzenski S, Schwab SA, et al. DNA Double-Strand Breaks and Their Repair in Blood Lymphocytes of Patients Undergoing Angiographic Procedures. Investigative Radiology 2009; 44:440-446.

107. Schmidt B, Saltybaeva N, Kolditz D, Kalender WA. Assessment of patient dose from CT localizer radiographs. Medical Physics 2013; 40:-.

108. Verset L, Tommelein J, Moles Lopez X, et al. Epithelial expression of FHL2 is negatively associated with metastasis-free and overall survival in colorectal cancer. Br J Cancer 2013; 109:114-120.

109. Ng C-F, Xu J-Y, Li M-S, Tsui SK-W. Identification of FHL2-Regulated Genes in Liver by Microarray and Bioinformatics Analysis. Journal of Cellular Biochemistry 2014; 115:744-753.

110. Park J, Will C, Martin B, et al. Deficiency in the LIM-only protein FHL2 impairs assembly of extracellular matrix proteins. The FASEB Journal 2008; 22:2508-2520.

111. Elgaaen BV, Olstad OK, Sandvik L, et al. *ZNF385B* and *VEGFA* Are Strongly Differentially Expressed in Serous Ovarian Carcinomas and Correlate with Survival. PLoS ONE 2012; 7:e46317.

112. Das S, Raj L, Zhao B, et al. Hzf Determines Cell Survival upon Genotoxic Stress by Modulating p53 Transactivation. Cell 2007; 130:624-637.

113. Lee JH, Budanov AV, Park EJ, et al. Sestrin as a Feedback Inhibitor of TOR That Prevents Age-Related Pathologies. Science 2010; 327:1223-1228.

114. Budanov AV, Karin M. p53 Target Genes Sestrin1 and Sestrin2 Connect Genotoxic Stress and mTOR Signaling. Cell 2008; 134:451-460.

115. Villamena FA. Molecular Basis of Oxidative Stress: Chemistry, Mechanisms, and Disease Pathogenesis: John Wiley & Sons, 2013.

116. Garnett MJ, Mansfeld J, Godwin C, et al. UBE2S elongates ubiquitin chains on APC/C substrates to promote mitotic exit. Nat Cell Biol 2009; 11:1363-1369.

117. Clarke C, Madden SF, Doolan P, et al. Correlating transcriptional networks to breast cancer survival: a large-scale coexpression analysis. Carcinogenesis 2013; 34:2300-2308.

118. Pauli U, Chrysogelos S, Stein G, Stein J, Nick H. Protein-DNA interactions in vivo upstream of a cell cycle-regulated human H4 histone gene. Science 1987; 236:1308-1311.

119. Taouji Sd, Higa A, Delom Fdr, et al. Phosphorylation of Serine Palmitoyltransferase Long Chain-1 (SPTLC1) on Tyrosine 164 Inhibits Its Activity and Promotes Cell Survival. Journal of Biological Chemistry 2013; 288:17190-17201.

120. Hamimes S, Arakawa H, Stasiak AZ, et al. RDM1, a Novel RNA Recognition Motif (RRM)-containing Protein Involved in the Cell Response to Cisplatin in Vertebrates. Journal of Biological Chemistry 2005; 280:9225-9235.

121. Zitvogel L, Kepp O, Galluzzi L, Kroemer G. Inflammasomes in carcinogenesis and anticancer immune responses. Nat Immunol 2012; 13:343-351.

122. Maecker HT, Todd SC, Levy S. The tetraspanin superfamily: molecular facilitators. The FASEB Journal 1997; 11:428-442.

123. Parker LH, Schmidt M, Jin S-W, et al. The endothelial-cell-derived secreted factor Egfl7 regulates vascular tube formation. Nature 2004; 428:754-758.

124. Nichol D, Shawber C, Fitch MJ, et al. Impaired angiogenesis and altered Notch signaling in mice overexpressing endothelial Egfl7. Blood 2010; 116:6133-6143.

125. Sun Y, Bai Y, Zhang F, Wang Y, Guo Y, Guo L. miR-126 inhibits non-small cell lung cancer cells proliferation by targeting EGFL7. Biochemical and Biophysical Research Communications 2010; 391:1483-1489.

126. Fernandez-Capetillo O, Chen H-T, Celeste A, et al. DNA damage-induced G2-M checkpoint activation by histone H2AX and 53BP1. Nat Cell Biol 2002; 4:993-997.

127. Rothkamm K, Lobrich M. Evidence for a lack of DNA double-strand break repair in human cells exposed to very low x-ray doses. Proc Natl Acad Sci USA 2003; 100:5057 - 5062.

128. Rothkamm K, Horn S. gamma-H2AX as protein biomarker for radiation exposure. Annali dell'Istituto superiore di sanità 2009; 45:265-271.

129. Celeste A, Fernandez-Capetillo O, Kruhlak MJ, et al. Histone H2AX phosphorylation is dispensable for the initial recognition of DNA breaks. Nature Cell Biology 2003; 5:675-U651.

130. Sun S-Y. N-acetylcysteine, reactive oxygen species and beyond. Cancer Biol Ther 2010; 9:109-110.

131. Squatrito M, Gorrini C, Amati B. Tip60 in DNA damage response and growth control: many tricks in one HAT. Trends in Cell Biology 2006; 16:433-442.

132. Yano K, Morotomi-Yano K, Adachi N, Akiyama H. Molecular Mechanism of Protein Assembly on DNA Double-strand Breaks in the Non-homologous End-joining Pathway. Journal of Radiation Research 2009; 50:97-108.

133. Kim K, Pollard JM, Norris AJ, et al. High-throughput screening identifies two classes of antibiotics as radioprotectors: tetracyclines and fluoroquinolones. Clinical Cancer Research 2009; 15:7238-7245.

134. Kuefner MA, Brand M, Ehrlich J, Braga L, Uder M, Semelka RC. Effect of Antioxidants on X-ray-induced gH2AX Foci in Human Blood Lymphocytes: Preliminary Observations. Radiology 2012; 264:59-67.

135. Reliene R, Pollard JM, Sobol Z, Trouiller B, Gatti RA, Schiestl RH. N-acetyl cysteine protects against ionizing radiation-induced DNA damage but not against cell killing in yeast and mammals. Mutation Research/Fundamental and Molecular Mechanisms of Mutagenesis 2009; 665:37-43.

136. Sedelnikova OA, Redon CE, Dickey JS, Nakamura AJ, Georgakilas AG, Bonner WM. Role of oxidatively induced DNA lesions in human pathogenesis. Mutation Research/Reviews in Mutation Research 2010; 704:152-159.

137. Bjelakovic G, Nikolova D, Gluud L, Simonetti RG, Gluud C. Mortality in randomized trials of antioxidant supplements for primary and secondary prevention: Systematic review and meta-analysis. JAMA 2007; 297:842-857.

Chapter 6: Patient Analysis

6.1 Introduction

As shown previously, the biological response to irradiation schemes similar to CT protocols with multiple exposures differs when the same total dose is delivered as a single exposure (138). Though the consequences on late effects and other related risks are unclear, these findings suggest that risk may be a function of not only total dose delivered, but also other contributing factors such as scan and patient parameters.

Because it is impossible to directly measure the absorbed dose to a patient, the radiology community must rely on dose estimates such as the Computed Tomography Dose Index (CTDI) and Dose Length Product (DLP) (139-141). Many scanners report both the $CTDI_{vol}$ and DLP values for each scan within a single CT exam as well as the total values. $CTDI_{vol}$ represents the average radiation dose within a scan volume for a standardized phantom, while DLP is the $CTDI_{vol}$ multiplied by the scan length (142). These values are useful in comparing different CT protocols and for quality control purposes. However, a representation of scanner output with no consideration of patient parameters or dose delivery may not adequately describe the complex biological response to CT protocols (140).

In an effort to better understand consequences of CT examinations at the cellular level, the previously developed rapid protocol is used for gammaH2AX analysis in whole blood to assess the biological response in patients after CT exams (143). Here, the complexity of the biological response to a variety of CT protocols and the relation to patient and CT exam parameters is described. While others have investigated gammaH2AX under similar circumstance, many have used techniques that question the validity of results (143). Without

the need for blood separation, our protocol allows for virtually immediate fixation of patient samples and thus precise kinetic analysis of the damage response.

It is imperative that risk estimates be based not solely on epidemiological assumptions, but also on empirical evidence of biological repercussions, especially in the light of increasing radiation exposure due to medical examinations especially CT (144-146).

6.2 Materials and Methods

6.2.1 Patients, CT scan protocols and blood samples

21 adult patients (11 male, 10 female, median age: 61 years, range: 32-79 years) undergoing a variety of clinically-indicated CT exams including contrast-enhanced cardiac CTA (CCTA) (n=6), or abdomen and pelvis (AP) (n=15) who met the inclusion/exclusion criteria (after signing the consent and HIPAA forms) were included. Exclusion criteria were allergy/anaphylactic reaction to iodinated contrast agents or previously experienced adverse reactions to non-ionic iodinated contrast material, patients with history of lymphoma or leukemia, radiation therapy or systemic chemotherapy within the last 6 months, and x-ray examination within the last 3 days, subjects unable to undergo clinically-indicated imaging study for any reason (i.e. renal failure, hyperthyroidism, etc.), unable to give informed consent.

Three separate blood samples were collected under IRB approval for biological analysis. Antecubital vein blood was collected into K2 EDTA containing vials: 4mL of blood was taken before the CT exam (“pre”) and 2ml of blood was collected at 2 min and 30 min after the CT exam. For each patient, two samples of pre-exam blood were transferred into 1.5mL plastic tubes; one was positioned on the patient within the exam region and the second was kept at room temperature outside the examination room for *ex vivo* comparative analysis.

Four patient samples were excluded due to technical issues during collection and analysis (all AP patients). Samples from the remaining 17 patients (8 male, 9 female, median age: 62 years, range: 32-79 years) were analyzed for gammaH2AX fluorescence.

6.2.2 Immunofluorescent Analysis for gammaH2AX

Triplicate *in vivo* and *ex vivo* whole blood samples for each patient were fixed immediately after blood draw and stained for gammaH2AX as described previously and in the Materials and Methods chapter. Samples were analyzed on a BD FACSCaliber flow cytometer with CellQuestPro software package (Becton, Dickinson and Company, Franklin Lakes, New Jersey, USA). Forward and side scatter gating was used to segregate the lymphocyte cell population for analysis and 20,000 events were collected for each sample. Average median fluorescence was recorded for each time point and normalized to unirradiated control values.

6.2.3 CT Dose Values

For each patient, total DLP and $CTDI_{vol}$ values were obtained from the scanner digital output. Additionally, average values were calculated for these dose metrics. Total and average size specific dose estimate (SSDE) values were also calculated as described in the AAMP task group 204 report (147). Briefly, region/anatomy-specific $CTDI_{vol}$ values are multiplied by TG 204 conversion factors (CF) to calculate SSDE. CF are based on a patient's effective diameter (ED) calculated for each specific region/anatomy (separate ED was calculated for chest, abdomen, and pelvic for multi-scan examinations). ED = √(AP*LAT) where AP is the anterior-posterior distance of the patient and LAT is the lateral distance. For each calculated ED, a tabulated CF value was extracted from the AAPM Task Group 204 documentation. Total and average values

for $CTDI_{vol}$ for the *ex vivo* sample tube were calculated by summing the $CTDI_{vol}$ values for each image series for which the sample tube was visible in the corresponding images.

6.2.4 CT protocol timing and average dose rate

For each patient, the time each scan was performed within an exam was collected from the digital record of the exam in the Digital Imaging and Communications in Medicine (DICOM) image collected from the work station following an exam. Total exam time was calculated by subtracting the time of the last scan from the time of the first scan. To estimate how dose was delivered over the length of the exam, dose values were normalized to total scan time to give an averaged dose rate in dose/sec. This value does not represent true dose rate of the individual scans within an exam and is referred to as a quasi-dose rate.

6.3 Results

6.3.1 Varying biological responses after irradiation in vivo

As a population, no clear dose response in gammaH2AX phosphorylation is observed at 2 min or 30 min after CT examination regardless of the dose metric used (**Figure 6.1**). It is possible that 2 min is insufficient time to observe any change in H2AX phosphorylation. However, it is unexpected that no dose response was observed at 30 min. To minimize variation in exam parameters, patients were grouped by exam type: Abdomen-Pelvis (AP) or Coronary CT Angiography (CCTA) exams. While total DLP values are significantly greater for AP than for CCTA exams ($p<0.0001$) (**Figure 6.2A**), this relationship is not reflected in relative H2AX phosphorylation levels. No significant difference in relative fluorescence at 2 or 30 min between exam types was observed. Individuals who received AP exams show an improved but mild dose response in relative gammaH2AX signal at 30 min (**Figure 6.2B**), indicating an

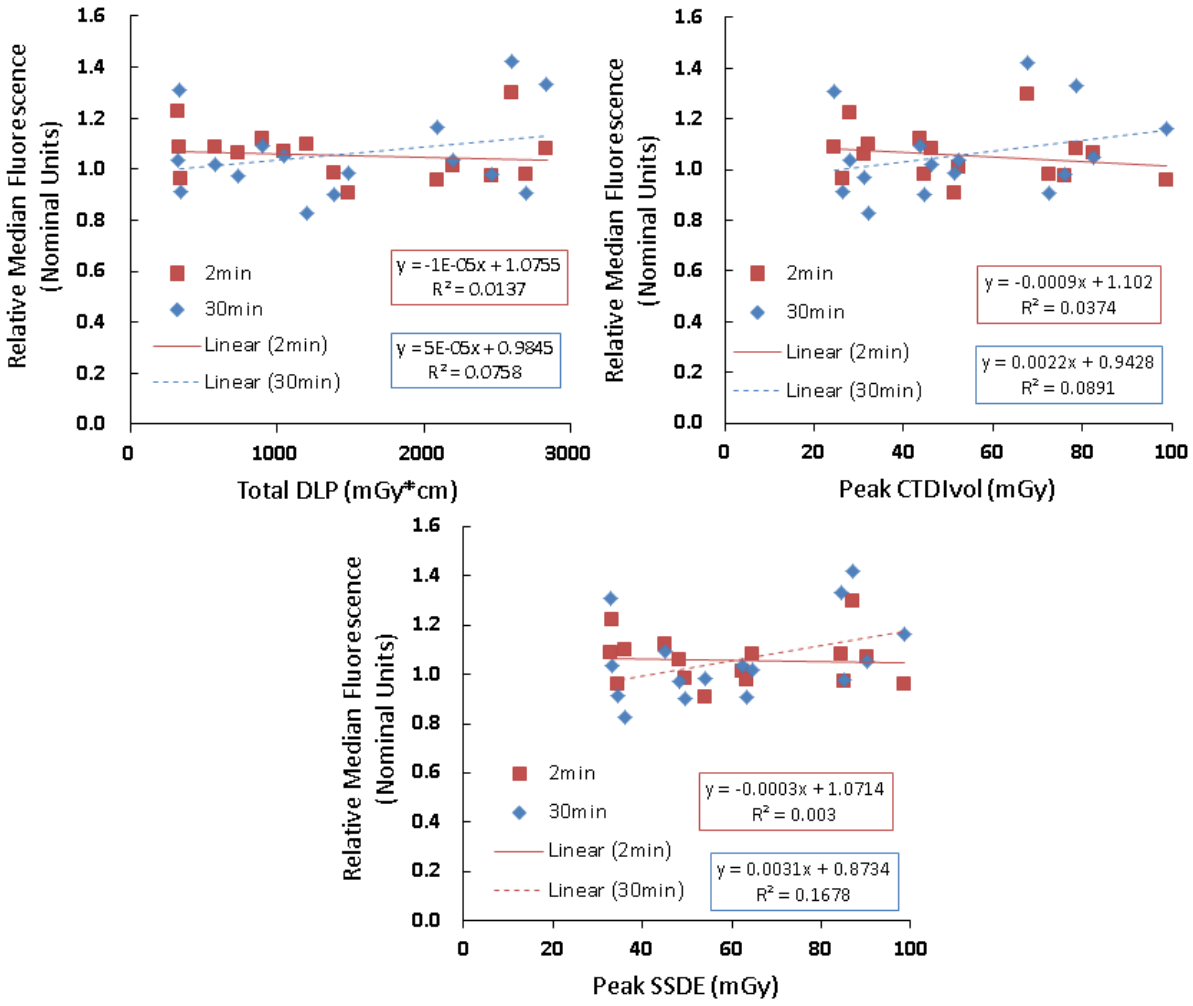

Figure 6.1. Individual responses following CT examinations compare to dose metrics. Whole blood samples were collected under IRB approval for each patient before the CT exam, at 2 min and 30 min after the CT exam, fixed immediately after blood draw and stained for gammaH2AX. Average median fluorescence was recorded for each time point and normalized to unirradiated control values and reported. No clear dose response in gammaH2AX phosphorylation is observed at 2min or 30min after CT exam regardless of the dose metric – dose length product (DLP), CT dose index (CTDIvol), size specific dose estimate (SSDE).

improved dose response with higher dose examinations. Again, no dose response was observed for either population at 2 min. To investigate the possibility of a dose-modulated response further, patients were categorized into lower and higher dose exams based on the median total DLP, regardless of protocol. The dose response for higher dose exams was again improved compared to the overall dose response and to a similar extent when patients were categorized

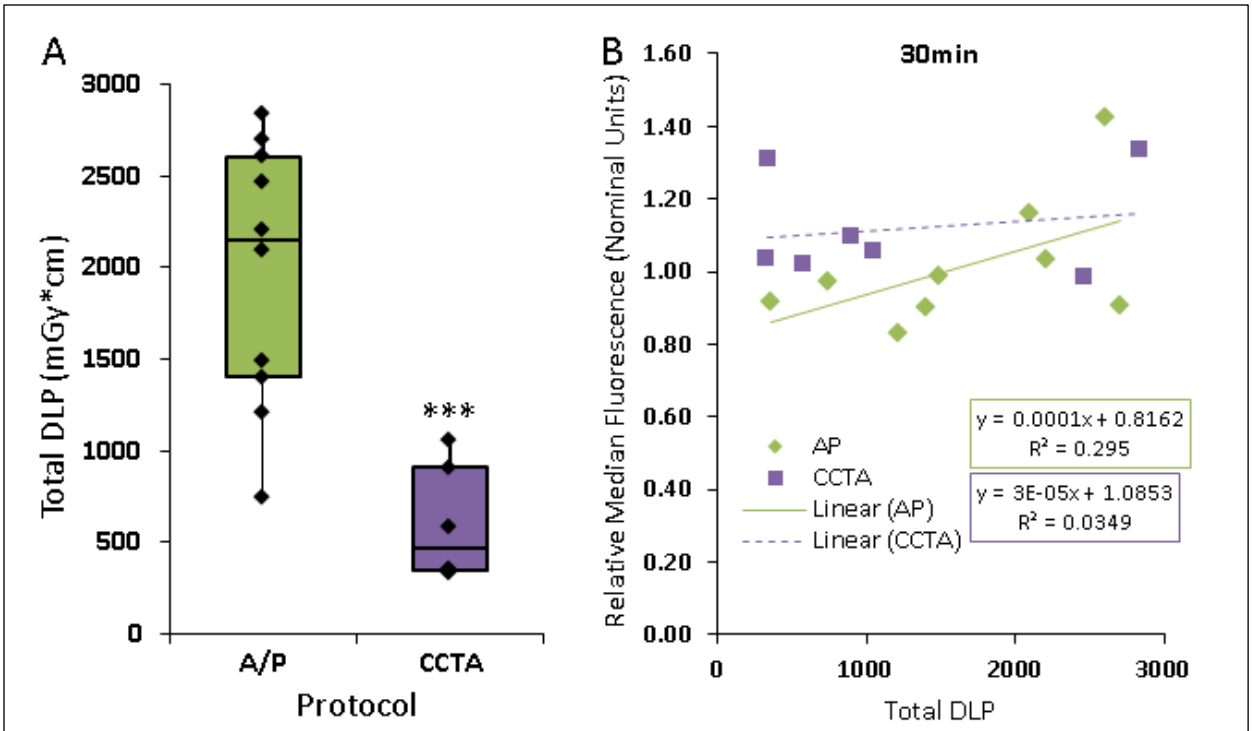

Figure 6.2. Effect of examination protocol on patient response. To minimize variation in exam parameters, patients were grouped by exam type: Abdomen-Pelvis (A/P) or Coronary CT Angiography (CCTA) exams. **A.** Total DLP values are significantly greater for A/P than for CCTA exams ($p<0.0001$). **B.** Individuals who received AP exams show an improved but mild dose response in relative gammaH2AX signal at 30min compared to the total population. No dose response was observed for either population at 2min.

by protocol alone (**Figure 6.3A**). Upon inspection of the individual scan dose magnitude and timing for the lower dose exams, it appears that they share similar protocols: many multiple exposures near or below 20mGy each. As illustrated in figure 6.3B, lower dose exams not only have significantly lower individual scan doses but also have significantly more scans within an exam. As described previously in Chapter 5, multiple-exposure irradiations have an altered repair response compared to single exposure irradiations. Furthermore, this phenomenon is only observed for exposures near 20mGy. Thus, the lower multi-scan examinations may be promoting a similar response to that demonstrated *in vitro*.

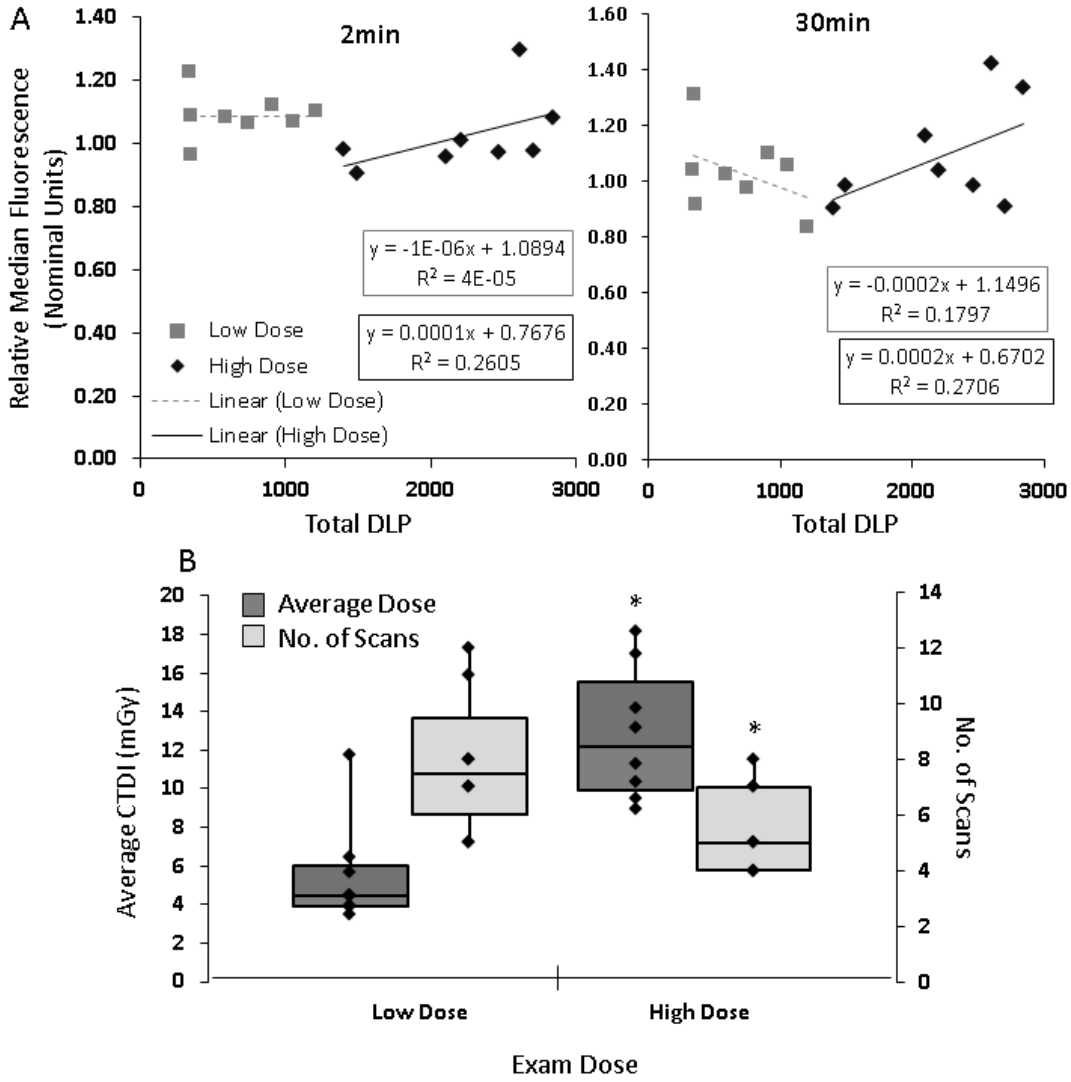

Figure 6.3. Effect of examination dose on patient response. Patients were categorized into lower and higher dose exams based on the median total DLP. **A.** The dose response for higher dose exams was improved compared to the overall dose response and to a similar extent when patients were categorized by protocol alone. **B.** Upon inspection of the individual scan dose magnitude and timing for the lower dose exams, it appears that they share similar protocols: many multiple exposures near or below 20mGy. Lower dose exams not only have significantly lower individual scan doses but also have significantly more scans within an exam.

When patient responses were examined individually, three biological response patterns are observed: (a) fast – gammaH2AX phosphorylation increased by 2 min and fell by 3 0min, (b) slow – gammaH2AX phosphorylation continued to increase to 30 min and (c) none – little change was observed or irradiated samples fell below controls (**Figure 6.4A**). Total DLP values

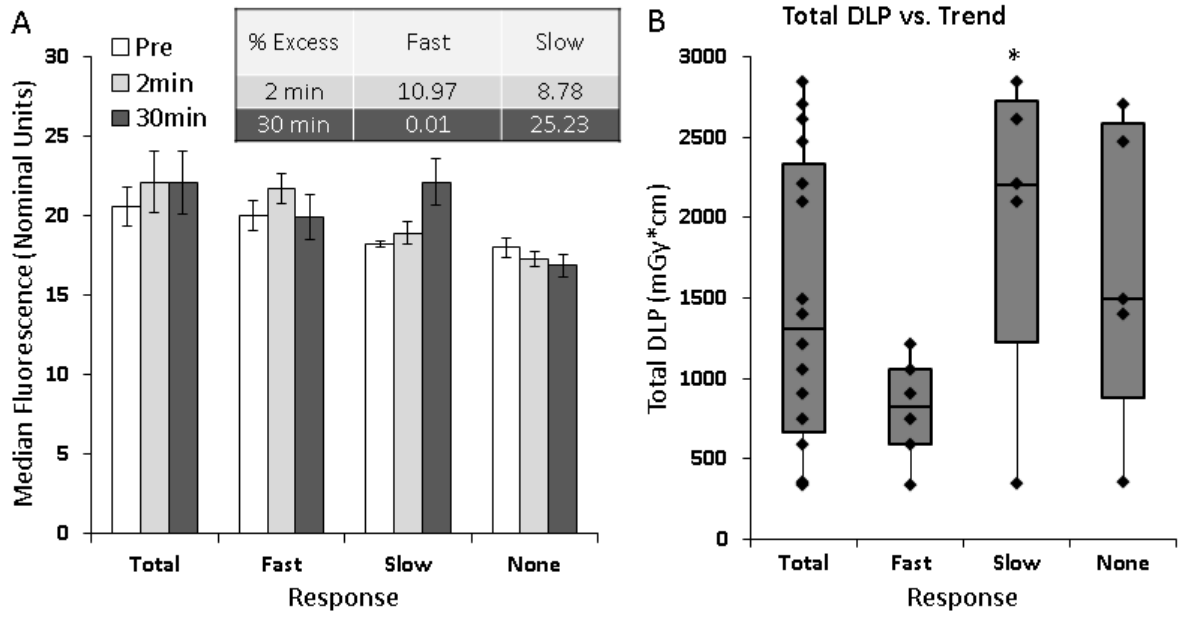

Figure 6.4. Biological responses following CT examinations. **A.** Three biological response patterns are observed: (a) fast – gammaH2AX phosphorylation increased by 2min and fell by 30min, (b) slow – gammaH2AX phosphorylation continued to increase to 30min and (c) none – little change was observed or irradiated samples fell below controls. **B.** Total DLP values were significantly higher for individuals exhibiting a slow response compared to those presenting a fast response ($p<0.05$).

were significantly higher for individuals exhibiting a slow response compared to those presenting a fast response ($p<0.05$) (**Figure 6.4B**), suggesting again, a dose-dependent modulation of the biological response to CT exams. This effect suggests distinct DNA damage responses depending on exam conditions that may not necessarily be reflected solely by dose metrics like DLP but rather how dose is delivered during an examination.

6.3.2 Age is a significant factor in the biological response

Multiple patient parameters were examined to determine which might affect the biological response to CT exams including patient size, age and gender. As depicted in Figure 6.5A, fast responding individuals are significantly younger than slow responding patients ($p<0.05$). If individuals who show no biological response are excluded from the population, a much clearer dose response is observed for young patients (≤61 years) at 30 min ($R^2=0.5$), while

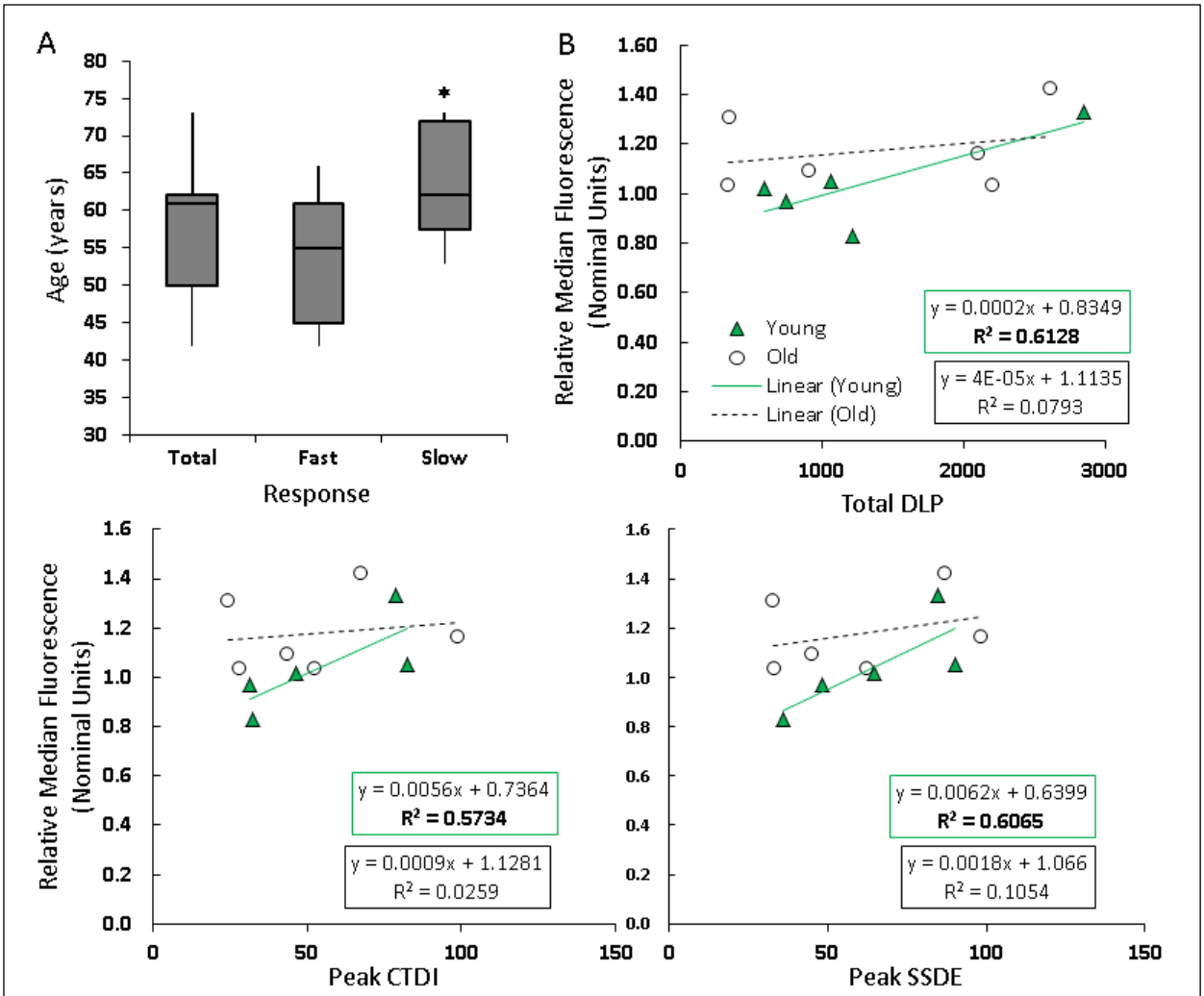

Figure 6.5. Age-related response to CT examinations. **A.** Fast responding individuals are significantly younger than slow responding patients ($p<0.05$). **B.** If individuals who show no biological response are excluded from the population, a clearer dose response is observed for young patients at 30min ($R^2=0.5$), while the older population shows no dose response.

the older (>61 years) population still shows no dose response (**Figure 6.5B**). No dose response is observed for either population at 2 min. The young and old populations were defined based on the median age of the responding population (61 years). This age-related response suggests that the repair of DNA damage may be more rapid in a younger population and slower and more varied as the population ages.

6.3.3 Dose rate affects the biological response

Examination times vary considerably both between and within exam types. Total exam time from the first scout projection image to completion of the exam ranged from 3-38 min in our population (**Figure 6.6A**). Due to the dynamic nature of DNA damage repair, the time over

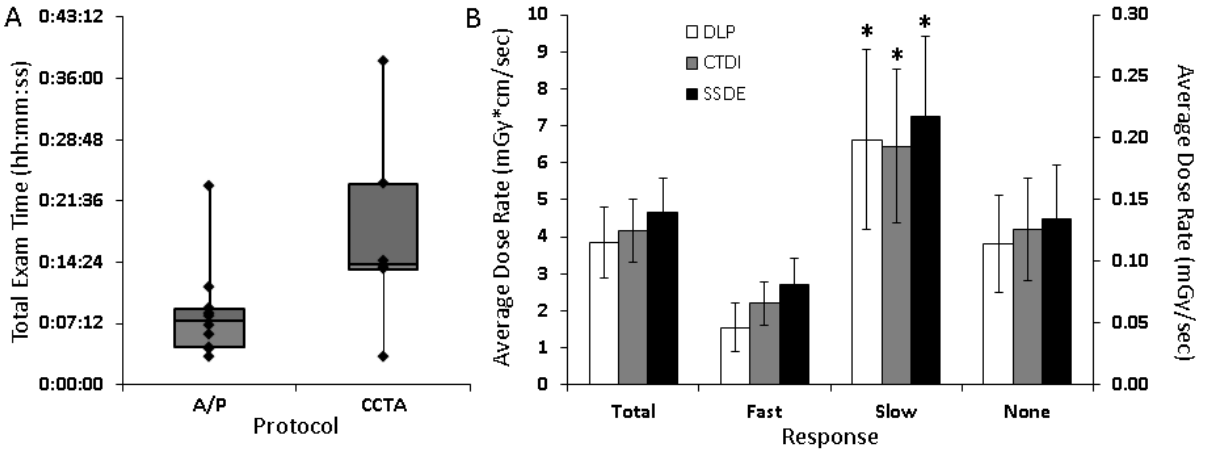

Figure 6.6. Dose delivery effects on the biological response to ionizing radiation. Total exam time was calculated by subtracting the time of the last scan from the time of the first scan. To estimate how dose was delivered over the length of the exam, dose values were normalized to total exam time to give an averaged dose rate in dose/sec. This value does not represent true dose rate of the individual scans within an exam. **A.** Total exam time from the first scout projection image to completion of the exam ranged from 3-38min. **B.** Patient response was compared to dose values normalized to total exam time (dose/sec). Patients exhibiting a fast response received exams with significantly smaller dose rate than patients presenting a slow response ($p<0.05$).

which a certain dose was delivered was investigated for effects on the biological response to radiation. Patient response was compared to dose values normalized to total exam time (dose/sec). This value, quasi-dose rate, does not represent true dose rate of the individual scans within an exam, but rather an average value of how dose is delivered over the length of the exam. Patients exhibiting a fast response received exams with significantly smaller quasi-dose rate than patients presenting a slow response ($p<0.05$) (**Figure 6.6B**), suggesting that patient response may be related to scan timing within an exam protocol.

6.3.4 Ex vivo and in vivo samples differ in biological response

An aliquot of pre-exam patient blood was placed on each patient and irradiated simultaneously to provide a comparison of the response between *ex vivo* and *in vivo* samples. Interestingly, ex *vivo* samples differed in biological response in 4 out of 11 patients (36.4%) that

Table 6.1. *In vivo* and *ex vivo* responses

Patient No.	CT Protocol	*In Vivo* Response	*Ex Vivo* Response
8	AP	Slow	None
5	CCTA	Fast	None
20	AP	None	Fast
18	CCTA	Fast	Fast
14	AP	Fast	Fast
7	CCTA	Slow	Fast
10	CCTA	Slow	Slow
15	CCTA	None	Slow
11	AP	Slow	Slow
21	AP	None	Slow
9	CCTA	Fast	Slow
19	AP	None	Slow
16	AP	None	Slow
13	CCTA	Fast	Slow
6	AP	Fast	Slow
17	AP	Slow	Slow

exhibited a response *in vivo.* Furthermore, all 5 individuals that presented with no response *in vivo* exhibited either a slow (n=4) or fast (n=1) response *ex vivo* (**Table 6.1**). We compared calculated tube dose to patient dose (**Figure 6.7A**) (either $CTDI_{vol}$ or SSDE) and found that fast response patients have a significantly greater correlation between tube and patient dose than slow responders ($CTDI_{vol}$ $p<0.05$, SSDE $p<0.01$; **Figure 6.7B**). Receiving a smaller tube dose seems to shift the response to a slow response. It is interesting that this result is accentuated when a comparison is made to SSDE, which includes a consideration of patient size, signifying the importance of patient parameters in the individual biological response.

Interestingly, unlike *in vivo* samples, age does not significantly affect the patient response *ex vivo*, suggesting an age-related systemic response to radiation that is not present if samples are irradiated outside the body.

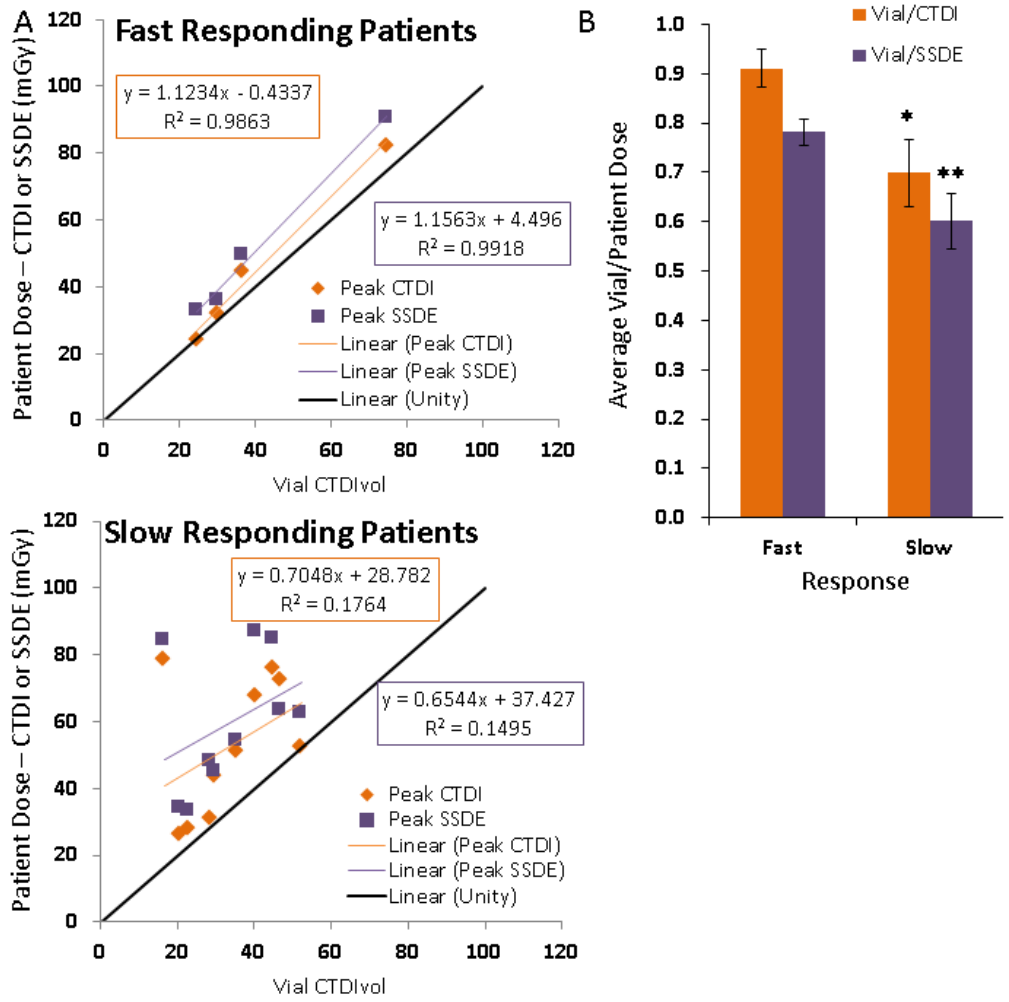

Figure 6.7. Relationship between *ex vivo* irradiated sample and biological response. **A.** Calculated tube dose was compared to patient dose (either $CTDI_{vol}$ or SSDE). **B.** Fast response patients have a significantly greater correlation between tube and patient dose than slow responders ($CTDI_{vol}$ $p<0.05$, SSDE $p<0.01$). Receiving a smaller tube dose seems to shift the response to a slow response. This result is accentuated when a comparison is made to SSDE, which includes a consideration of patient size, signifying the importance of patient parameters in the individual biological response.

6.3.5 Putative radiosensitivity detection

Upon examination of individual levels of H2AX phosphorylation in pre-exam samples, two patients presented significantly higher basal gammaH2AX signal compared to the population average ($p<0.05$; **Figure 6.8A**). Both patients exhibited large increases in H2AX phosphorylation after CT examination but showed different responses. Patient #11 presents a

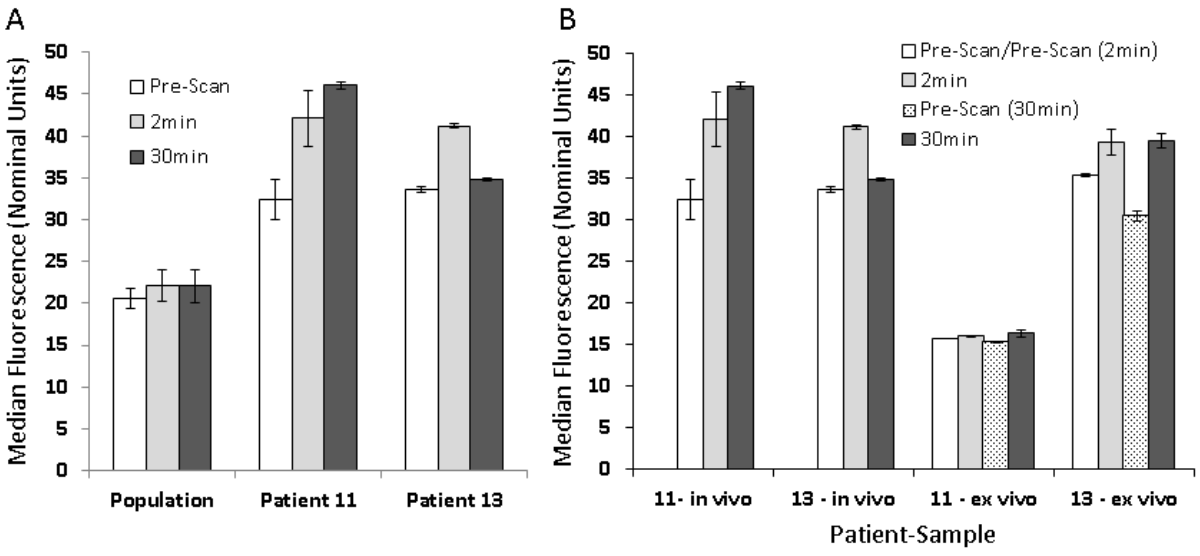

% Excess	Average Population	#11	#13
2 min	5.51	**29.9**	**22.4**
30 min	5.94	**42.2**	3.5

% Excess	#11 in vivo	#11 ex vivo	#13 in vivo	#13 ex vivo
2 min	**29.9**	3.4	**22.4**	**19.5**
30 min	**42.2**	6.7	3.5	**29.8**

Figure 6.8. Putative radiation sensitive patient analysis. **A.** Two patients presented significantly higher basal gammaH2AX signal compared to the population average ($p<0.05$). Both patients exhibited large increases in H2AX phosphorylation after CT examination but showed different responses. Patient #11 presents a slow response, while patient #13 shows a fast response in vivo. **B.** For patient #11, the high background signal *in vivo* is diminished *ex vivo* as well as the increased response to irradiation indicating a systemic effect. Conversely, patient #13 continues to show an increased response to radiation *ex vivo*, but rather than a fast response as observed *in vivo*, exhibits a slow response.

slow response, while patient #13 shows a fast response *in vivo*. Interestingly, for patient #11, the high background signal *in vivo* is diminished *ex vivo* as well as the increased response to irradiation indicating that this response may be modulated by a systemic response to radiation rather than a purely cellular response (**Figure 6.8B**). Conversely, patient #13 continues to show an increased response to radiation *ex vivo*, but rather than a fast response as observed *in vivo*,

exhibits a slow response. Based on these results, these two patients may represent appropriate candidates for further radiation sensitivity testing.

6.4 Conclusions

Instead of examining DNA repair at a single point in time, the short-term kinetics were evaluated to better understand the effects of exam and patient parameters on the biological response to CT examinations. It is interesting that no clear dose response following irradiation was observed as others have. Other studies investigated specific protocols with relatively standard parameters. Because of the wide range in CT protocols used in this study, it is possible that parameters other than dose are altering the biological response. When separated, higher dose exams show an improved dose response over lower dose exams. Furthermore, examinations in the lower dose region may be exhibiting a response characterized previously *in vitro*, resulting in a reduction of gammaH2AX signal and thus affecting the response in this dose region. Although these results indicate substantial variation in repair kinetics across a small sample of patients, categorizing individuals based on exam and patient parameters highlighted possible factors affecting the biological response.

Three distinct biological responses to CT examinations: fast, slow and none are suggested. Although we have not been able to establish why five patients did not exhibit any response, this study is the first to use the originally developed protocol in a patient population and suggests that blood processing and assessment can confound interpretation. Slow responding patients received exams with significantly higher total DLP values compared to fast responding patients, indicating that exams with higher total DLP shift the biological response to a slower response, possibly due to repair requiring more time. Additionally, AP exams have

significantly higher total DLP values than CCTA exams. It would follow that a slow response following radiation correlates to receiving an AP exam, which the data suggests, but significance could not be reached possibly due to the small sample size. This effect suggests distinct DNA damage responses depending on exam conditions that may not necessarily be reflected solely by dose metrics like DLP. The differences in response may be related to not only magnitude of dose, but also dose rate, timing (e.g. scan-phase time intervals) as well as individual patient parameters.

For the first time, non-dose related effects on the biological response to CT examinations have been established. Age is indicated as a significant factor in modulation of the biological response to radiation. Younger patients tend to have a faster repair response compared to older patients. Thus, comparing values from patients at the same time may confound damage kinetics results due to age differences. As biological processes can slow or change with age (148-150), it follows that the same may be true for the DNA damage repair response to radiation. Additionally, the average quasi-dose rate of an exam has been shown to significantly affect the biological response. Patients who receive smaller quasi-dose rate exams tend to exhibit a faster repair response. Taken together with the *in vitro* dose-timing study, it appears that repeated doses – near or below 20mGy – alter the repair response the patient population in a similar manner to what has been observed *in vitro*. These results demonstrate that dose alone may not adequately describe or predict the biological response of an individual patient.

Although *ex vivo* samples were irradiated identically to each patient, the responses were markedly different from their *in vivo* counterparts. Samples were incubated outside the

body at ambient room temperature, which may alter damage kinetics toward a slower response. Additionally, *ex vivo* samples were stationary during irradiation and contained blood which was free of contrast media, while *in vivo* blood samples continue to circulate during the exam. Thus, *ex vivo* samples may more accurately represent the physiological response of stationary organs rather than blood, although oxygen levels may differ and confound results.

Notably, two patients out of the sample population were detected that exhibited both increased background gammaH2AX signal and higher than average responses to radiation. High basal levels of gammaH2AX are indicative of radiation sensitivity but not necessarily directly related to DNA repair pathways (151). Possible explanations could be a constitutively active cellular damage mechanism such as ROS generation or a disrupted protection mechanism such as radical scavenging. It is interesting to note that one of the phenotypes only presents *in vivo*, suggesting a required extracellular component to modulate the radiation response. These results show that the developed protocol can be used to potentially screen patients for altered responses to radiation. This application could provide a useful tool for the oncology field since most patients undergoing radiation therapy for cancer treatment receive a CT examination for diagnosis and treatment planning. This assay may provide valuable analysis for individuals who may require further testing to ensure the least risk to the patient.

6.5 References

138. Elgart SR, Bostani M, Mok KC, et al. Investigation of DNA damage dose-response kinetics after ionizing radiation schemes similar to CT protocols. Radiation Research: Submitted April 3, 2014.

139. Seibert JA, Boone JM, Wootton-Gorges SL, Lamba R. Dose Is Not Always What It Seems: Where Very Misleading Values Can Result From Volume CT Dose Index and Dose Length Product. Journal of the American College of Radiology: JACR 2014; 11:233-237.

140. McCollough CH, Leng S, Yu L, Cody DD, Boone JM, McNitt-Gray MF. CT Dose Index and Patient Dose: They Are Not the Same Thing. Radiology 2011; 259:311-316.

141. American Association of Physicists in M. AAPM Report No. 96. The measurement, reporting, and management of radiation dose in CT. College Park, MD: AAPM 2008.

142. McCollough CH. Patient Dose in Cardiac Computed Tomography. Herz 2003; 28:1-6.

143. Elgart SR, Bostani M, Adibi A, et al. Evaluation of a rapid protocol for time sensitive kinetic assessment of DNA damage response following ionization radiation using whole blood samples. PLoS ONE: Submitted May 7, 2014.

144. Thurston J. NCRP Report No. 160: Ionizing Radiation Exposure of the Population of the United States. Physics in Medicine and Biology 2010; 55:6327.

145. Mettler FA, Huda W, Yoshizumi TT, Mahesh M. Effective Doses in Radiology and Diagnostic Nuclear Medicine: A Catalog. Radiology 2008; 248:254-263.

146. Mettler FA, Jr., Thomadsen BR, Bhargavan M, et al. Medical Radiation Exposure in the U.S. in 2006: Preliminary Results. Health Physics 2008; 95:502-507.

147. Boone JM, Strauss KJ, Cody DD, et al. Size-specific dose estimates (SSDE) in pediatric and adult body CT examinations. Report of AAPM Task Group 2011; 204.

148. Swaab DF, Bao A-M. (Re-)activation of neurons in aging and dementia: Lessons from the hypothalamus. Experimental Gerontology 2011; 46:178-184.

149. Rube CE, Fricke A, Widmann TA, et al. Accumulation of DNA Damage in Hematopoietic Stem and Progenitor Cells during Human Aging. PLoS ONE 2011; 6:e17487.

150. Halicka HD, Zhao H, Li J, et al. Potential anti-aging agents suppress the level of constitutive mTOR-and DNA damage-signaling. Aging (Albany NY) 2012; 4:952.

151. Nahas SA, Gatti RA. DNA double strand break repair defects, primary immunodeficiency disorders, and 'radiosensitivity'. Current Opinion in Allergy and Clinical Immunology 2009; 9:510-516 510.1097/ACI.1090b1013e328332be328317.

Chapter 7: Conclusions

7.1 Pre-Analytical Techniques Should be Used with Caution

As demonstrated here, current sample handling practices are problematic when dynamic processes such as DNA damage repair are investigated. The unknown effects on biological endpoints and outcomes associated with these techniques only contribute to the uncertainty in risk assessment for diagnostic imaging, making their use counterproductive. Moreover, the lack of standardization between and within experiments further confounds results and increases uncertainty. Until the effects of these handling practices are better understood, they should be used with caution, especially when analyzing patient samples and clinical protocols. The RFP developed and evaluated here is superior for clinical applications as it provides effective and precise fixation as close to physiological conditions as possible, eliminating pre-analytical techniques and their contributions to risk uncertainties all together. Additionally, it provides valuable time savings and sample requirements are reduced from 6mL to 300uL both of which provide necessary steps toward finger prick technology. Development of a hand-held device could provide rapid analysis of radiation exposure and/or sensitivity in a clinical or emergent setting. Furthermore, such a device could be used to monitor radiation exposure for manned space missions where both space and resources are limited. Thus, the significance of this innovative protocol reaches beyond diagnostic imaging.

7.2 Atomic Bombs and CT Exams are Not the Same Thing

This work provides compelling evidence supporting differential biological responses not only between high and low doses, but also between single- and multiple-exposures of low doses of ionizing radiation. These differences indicate a multifaceted biological response that is

not only dose-dependent but also dose-delivery-dependent. CT doses and schemes appear to alter the biological response to IR and these changes are apparent *in vitro* and are also reflected in patient outcomes. Therefore, current risk estimates based on the LSS may be less accurate due to heterogeneity in dosing and timing. Although seemingly obvious, IR doses received by atomic bomb survivors differ from those delivered by a CT examination even though the absolute amount may be similar. Moreover, individual patient factors may further modulate the response to radiographic procedures. Patient parameters include both cellular and systemic factors that may have wide inter-individual variation. Whether the differences characterized here are beneficial or detrimental remains to be clarified. Delayed repair could induce apoptosis of damaged cells leading to decreased risk of carcinogenesis but increased risk of tissue damage, which may increase other IR-related risks. Conversely, delayed repair could promote accumulation of damage increasing the risk of carcinogenesis. On the other hand, accelerated repair could provide faster damage recovery or decreased repair fidelity. Thus, the detection of early markers for DNA damage and repair demands to be put into the greater context of late effects and survival benefit for more accurate risk assessment.

7.3 Future Directions

Future work needs to further probe the responsible mechanisms involved in the damage response at different dose levels and schemes as well as those involved in carcinogenesis and other late effects. Assays for sensitive *in vitro* and *in vivo* analysis of doses and dosing schemes relevant to CT exams must be developed that do not rely on surrogate markers such as gammaH2AX to provide greater context for damage repair systems. Although the radio-protector and RNASeq experiments provide interesting insight into the possible mechanisms by

which these responses are controlled, it is clear that this work has instigated more questions than it has answered. In addition to understanding the response at a cellular level, it is imperative to examine the systemic response. Furthermore, how repeated exposures over an individual's lifetime may affect lifetime risk remains to be elucidated. Once it is possible to integrate both cellular and systemic knowledge then it may be possible to accurately extrapolate and forecast individual risk.